Reviews in Mineralogy & Geochemistry
Vol. 56, pp. 1-82, 2004

Physical and Chemical Properties of the Epidote Minerals – An Introduction –

Gerhard Franz

Technische Universität Berlin
Fachgebiet Petrologie
D 10623 Berlin, Germany
gerhard.franz@tu-berlin.de

Axel Liebscher

Department 4, Chemistry of the Earth
GeoForschungsZentrum Potsdam
Telegraphenberg
D 14473 Potsdam, Germany
alieb@gfz-potsdam.de

INTRODUCTION

Epidote minerals are known since the 18th century, but at that time the greenish to dark colored varieties were termed actinolite or schorl and not distinguished from the minerals to which these names apply today. Haüy defined the mineral species and introduced the name "epidote" in 1801, whereas Werner in 1805 used the term pistacite (quoted from Hintze 1897). Epidote is derived from greek *epidosis* = to increase, because the base of the rhombohedral prism has one side larger than the other and pistacite refers to its green color (all references for names after Lüschen 1979; Blackburn and Dennen 1997). Weinschenk (1896) proposed the name clinozoisite from its monoclinic symmetry and zoisite-like composition for those monoclinic members of the epidote family that are Fe poor, optically positive and have low refractive indices and birefringence.

Zoisite was probably confused with tremolite until the beginning of the 19th century. In 1804, Siegmund Zois, Baron von Edelstein 1747–1819, an Austrian sponsor of mineral collections, found and described a new mineral in a handspecimen from the Saualpe Mountains in Carinthia that was named zoisite by Werner.

Haüy (1822) interpreted zoisite as a variety of epidote and included it in his "epidote spezies." Weiss (1820) presented a theory of the epidote system and also discussed crystal morphological features of the epidote minerals (Weiss 1828). Rammelsberg (1856) studied the relationship between epidote and zoisite and presented a compilation of chemical analyses of zoisite. He already noticed that the relative concentrations of di-, tri- and tetravalent cations are identical in zoisite and epidote but that the Fe content in zoisite (about 2–3.5 wt% Fe_2O_3) is generally less than in epidote (about 9–12 wt% Fe_2O_3). Piemontite (see Bonazzi and Menchetti 2004) was probably first described in 1758 by Cronstedt as "röd Magnesia" and later termed "Manganèse rouge" by Chevalier Napione in 1790. Cordier (1803) first recognized the mineral as an "Èpidote manganésifere" a name, which was adopted by Haüy (1822) who

1529-6466/04/0056-0001$10.00

included this mineral as a variety in his "Epidote spezies." Finally the name "piedmontite" (today transformed into piemontite) was proposed according to the type locality Piemont in Northern Italy. The first Cr rich epidote occurrence was described by Bleek (1907) who also introduced the term tawmawite according to the type locality Tawmaw in Burma. Brooke in 1828 (quoted by Hintze 1897) gave the name "thulite" to the pink colored Mn-minerals of the epidote group, named after Thule, the ancient name for Norway.

Allanite, the rare earth element epidote, was already described by Thomson (1810) and named after Thomas Allan, 1777–1833, a Scottish mineralogist, who noticed it in alkaline rocks of Greenland. The name was used for unaltered crystals with a tabular habit parallel to the orthopinacoid. Berzelius (1818, quoted in Hintze 1897) found a similar mineral, however altered and hydrated and with a prismatic habit, and named it "orthit," but this name was abandoned later (Hutton 1951). The rare earth element epidote minerals developed into a complex group (see Gieré and Sorensen 2004), and the newly discovered species are androsite-(La) (Bonazzi et al. 1996), named after its locality Andros Island/Greece; dissakisite-(Ce) (Grew et al. 1991), named from Greek *dissakis* twice over, alluding to the fact that this Mg analogue has been described twice; dollaseite-(Ce) (Peacor and Dunn 1988), named after W. A. Dollase, who carried out definitive research on the epidote minerals; khristovite-(Ce) (Pautov et al. 1993), named after the Russian geologist E. V. Khristov.

Among the rare epidote minerals, hancockite, with Pb and Sr (named after E. P. Hancock, a mineral collector from Franklin/USA) was also already known in the 19th century (Penfield and Warren 1899). All others, mukhinite, the V^{3+} epidote, named after A. S. Mukhin, a geologist who worked in Western Siberia (Shepel and Karpenko 1969) and the Sr epidotes twedillite, named after S. M. Twedill, the first curator of the geological museum in Pretoria/RSA (Armbruster et al. 2002); strontiopiemontite (Bonazzi et al. 1990); and niigataite (Miyajima et al. 2003), named after its locality, were discovered late in the 20th century or recently.

The sum formula $Ca_2(Al,Fe^{3+})_3Si_3O_{13}H$ for epidote was presented as early as 1872 by Ludwig and was since then generally accepted. Finally Ito (1950) gave the structural interpretation of the sum formula as $Ca_2(Al,Fe)_3SiO_4Si_2O_7(O/OH)$. Since that time, our knowledge of occurrence, structure, and crystal chemistry of the epidote minerals increased considerably. X-ray diffraction studies with structure refinements established the structural relationships within and between the monoclinic and orthorhombic solid solution series, spectroscopic studies addressed and partly resolved the problems of site occupancies, and microanalytical techniques allowed to study chemical variations within the epidote minerals. What used to be rather simple has turned into a quite complex mineral group.

This chapter intends to serve as an introduction to the different mineralogical and geochemical aspects of epidote mineralogy addressed in the individual chapters. After nomenclatural aspects it reviews the structural, crystal chemical, and optical properties of the epidote minerals. Finally, it addresses some aspects of epidote mineralogy that are not covered by own chapters e.g., morphology, twinning, deformation behavior, and use as gemstones.

NOMENCLATURE

Epidote group minerals are monoclinic sorosilicates with mixed SiO_4 tetrahedra and Si_2O_7 groups with the general formula A1A2M1M2M3[O/OH/SiO_4/Si_2O_7], the M cations in octahedral and the A cations in larger coordination (group 9.BG 05 of Strunz and Nickel 2001). The orthorhombic mineral zoisite (group 9.BG 10 of Strunz and Nickel 2001), structurally very similar, is a polymorph of clinozoisite, and therefore also included here. The epidote minerals are structurally related to the pumpellyite-sursassite group minerals (Table 1). Besides their common silica building units, they all have the M position (filled predominantly with M^{3+} but

Table 1. General formulae of epidote and structurally related minerals

epidote, zoisite	A1A2	M1M2M3	[O/OH/	SiO_4/Si_2O_7]
pumpellyite	A1A2	M1M2M3	$[(OH)_2$/(O,OH)/	SiO_4/Si_2O_6(O,OH)]
sursassite	A1A2	M1M2M3	$[(OH)_3$/	SiO_4/Si_2O_7]
ilvaite	A	M1M2M3	$[O/(OH)_2$/	Si_2O_7]
gatelite-(Ce)	A1A(2,3,4)	M1M2a,bM3	$[O/(OH)_2$/	$(SiO_4)_3/Si_2O_7$]
lawsonite	A	M1M2	$[(OH)_2$/	Si_2O_7]•H_2O

also M^{2+}) in edge sharing chains. In ilvaite the octahedra form double chains, and in lawsonite the single octahedral chains have very similar M positions as in epidote. All minerals listed in Table 1 have (OH) bonded to the octahedra; lawsonite is the only mineral, which also has molecular water in the structure. In the newly described mineral gatelite-(Ce) (Bonazzi et al. 2003), modules of the epidote-type structure alternate with modules of another hydrous REE nesosilicate törnebohmite. These mineral groups are also chemically related because they can basically be regarded as hydrous Ca-Al-silicates, where Ca can be exchanged against REE and Sr, and Al against Fe^{3+} and Mn^{3+}.

For a description of the nomenclature we use the concept of additive and exchange components. As the additive component we choose the composition $Ca_2Al_3[O/OH/SiO_4/Si_2O_7]$, or written as a sum formula $Ca_2Al_3Si_3O_{12}(OH)$, for both the monoclinic and orthorhombic forms, and we distinguish simple and combined exchange vectors (Table 2). There has been considerable confusion in the literature how to name the monoclinic end members and the different monoclinic solid solutions and how to express their respective compositions, especially with respect to the monoclinic Al-Fe^{3+} solid solution series. Pistacite has been either used to describe Fe rich crystals with a composition near to $Ca_2Al_2Fe^{3+}Si_3O_{12}(OH)$ or to describe the hypothetical end member $Ca_2Fe^{3+}{}_3Si_3O_{12}(OH)$. Epidote has also been used for the composition $Ca_2Al_2Fe^{3+}Si_3O_{12}(OH)$. Some authors used epidote for the optically negative and clinozoisite for the optically positive solid solutions thus following Weinschenk (1896), while others reserved epidote for the whole mineral group and termed all monoclinic Al-Fe^{3+} solid solutions as clinozoisite. Consequently, the composition of solid solutions was expressed as mol% or mol fraction of the $Ca_2Fe^{3+}{}_3Si_3O_{12}(OH)$ component, as Fe^{3+} per formula unit, or as mol% or mol fraction of the $Ca_2Al_2Fe^{3+}Si_3O_{12}(OH)$ component. In case of Cr^{3+} bearing monoclinic solid solutions the term tawmawite has been used for the end member composition $Ca_2Al_2Cr^{3+}Si_3O_{12}(OH)$ but was also applied generally to Cr rich solid solutions. For a discussion of the problems with the nomenclature of Mn bearing epidote minerals and of allanite see Bonazzi and Menchetti (2004) and Gieré and Sorensen (2004), respectively.

The confusion and problems with the nomenclature of epidote minerals are partly historically determined (different nomenclatural traditions in North America and Europe) and partly due to the structural and crystal chemical characteristics of the epidote minerals (see below). According to the standard guidelines for mineral nomenclature, end member names should be reserved to those members that have the respective element dominant at one crystallographic site. Applying this rule to epidote minerals with three octahedral and two A-sites (see below) will obviously lead to an uncomfortable number of possible end members, even if one considers only the major elements Ca, Sr, Pb, REE^{3+}, Al, Fe^{3+}, Mn^{3+}, Cr^{3+}, and V that constitutes most of the epidote minerals (see below). Another problem arises because some of these possible end members have not yet been found in nature and are thus only hypothetic and not minerals in the strict sense. To overcome at least partly the confusion with the nomenclature of epidote minerals, the CNMMN subcommittee of the International Mineralogical Association on the nomenclature of epidote minerals has set up some

Table 2. Exchange vectors and nomenclature for orthorhombic and monoclinic epidote minerals.

EXCHANGE VECTORS	FORMULA	NAME
Orthorhombic Pnma, additive component zoisite $Ca_2Al_3Si_3O_{12}(OH)$		
simple in A-position		
$Ca_{-1}Sr$	$CaSrAl_3Si_3O_{12}(OH)$	no separate name
$Ca_{-1}Pb$	$CaPbAl_3Si_3O_{12}(OH)$	no separate name
simple in M-positions		
$Al_{-1}Fe^{3+}$	$Ca_2Al_2Fe^{3+}Si_3O_{12}(OH)$	no separate name
$Al_{-1}Mn^{3+}$	$Ca_2Al_2Mn^{3+}Si_3O_{12}(OH)$	no separate name (var. “thulite”)
$Al_{-1}V^{3+}$	$Ca_2Al_2V^{3+}Si_3O_{12}(OH)$	no separate name (var. “tanzanite”)
$Al_{-1}Cr^{3+}$	$Ca_2Al_2Cr^{3+}Si_3O_{12}(OH)$	no separate name
combined in AM-positions		
$Ca_{-1}Al_{-1}REE^{*}(Mg,Fe^{2+})$	$CaREEAl_2(Mg, Fe^{2+})Si_3O_{12}(OH)$	no separate name
Monoclinic $P2_1/m$*, additive component clinozoisite* $Ca_2Al_3Si_3O_{12}(OH)$		
simple in A-position		
$Ca_{-1}Sr$	$CaSrAl_3Si_3O_{12}(OH)$	niigataite
$Ca_{-1}Pb$	$CaPbAl_3Si_3O_{12}(OH)$	hancockite
$Ca_{-1}Mn^{2+}$	$CaMn^{2+}Al_3Si_3O_{12}(OH)$	(manganoan clinozoisite)
simple in M-positions		
$Al_{-1}Fe^{3+}$	$Ca_2Al_2Fe^{3+}Si_3O_{12}(OH)$	epidote
$Al_{-3}Fe^{3+}{}_3$	$Ca_2Fe^{3+}{}_3Si_3O_{12}(OH)$	(“pistazite”, theor. endmember)
$Al_{-1}Mn^{3+}$	$Ca_2Al_2Mn^{3+}Si_3O_{12}(OH)$	piemontite
$Al_{-1}V^{3+}$	$Ca_2Al_2V^{3+}Si_3O_{12}(OH)$	mukhinite
$Al_{-1}Cr^{3+}$	$Ca_2Al_2Cr^{3+}Si_3O_{12}(OH)$	“tawmawite”
combined in AM-positions		
$Ca_{-1}Al_{-1}SrMn^{3+}$	$CaSrAl_2Mn^{3+}Si_3O_{12}(OH)$	strontiopiemontite
$Ca_{-1}Al_{-2}SrMn^{3+}{}_2$	$CaSrAlMn^{3+}{}_2Si_3O_{12}(OH)$	twedillite
$Ca_{-2}Al_{-2}REEMn^{2+}Mn^{3+}Mn^{2+}$	$Mn^{2+}REEAlMn^{3+}Mn^{2+}Si_3O_{12}(OH)$	androsite
$Ca_{-1}Al_{-1}REEMg$	$CaREEAl_2MgSi_3O_{12}(OH)$	dissakisite
$Ca_{-1}Al_{-1}REEFe^{2+}$	$CaREEAl_2Fe^{2+}Si_3O_{12}(OH)$	allanite (syn.: “orthite”)
$Ca_{-1}Al_{-2}REEFe^{3}Fe^{2+}$	$CaREEAlFe^{3}Fe^{2+}Si_3O_{12}(OH)$	Fe^{3+}-analogue of allanite-(Ce)
combined in AMO-positions		
$Ca_{-1}Al_{-1}O_{-1}REE\ Mg_2F$	$CaREEAlMg_2Si_3O_{11}F(OH)$	dollaseite
$Ca_{-2}Al_{-3}O_{-1}REE_2MgMn^{2+}F$	$REE_2Mn_2MgSi_3O_{11}F(OH)$	krishtovite

* includes all trivalent rare earth elements and Y; the corresponding monoclinic endmembers and minerals are then named, for example, allanite-(Ce) according to the dominantly present REE

preliminary guidelines for the nomenclature of epidote minerals (Armbruster, pers. com.). According to these guidelines the term epidote refers to the whole mineral group but also to the composition $Ca_2Al_2Fe^{3+}Si_3O_{12}(OH)$. The Al end member $Ca_2Al_3Si_3O_{12}(OH)$ is termed clinozoisite and tawmawite refers to the Cr^{3+} end member $Ca_2Al_2Cr^{3+}Si_3O_{12}(OH)$. The term pistacite should generally be avoided. Consequently, the composition of binary or ternary solid solutions is given as mol fraction (X) of the respective end members:

$$X_{\mathrm{Taw}} = \frac{\mathrm{Cr}^{3+}}{\mathrm{Fe}^{3+} + \mathrm{Al} + \mathrm{Cr}^{3+} - 2}$$

$$X_{\mathrm{Czo}} = \frac{\mathrm{Al} - 2}{\mathrm{Fe}^{3+} + \mathrm{Al} + \mathrm{Cr}^{3+} - 2} \qquad X_{\mathrm{Ep}} = \frac{\mathrm{Fe}^{3+}}{\mathrm{Fe}^{3+} + \mathrm{Al} + \mathrm{Cr}^{3+} - 2}$$

For the nomenclature of intermediate members the 50% rule applies (Fig. 1). Although these preliminary guidelines have some severe shortcomings, they are adopted in Table 2. These short comings are that the term epidote not only denotes the whole mineral group but also an end member as well as specific solid solutions, and that Al-M^{3+} solid solutions with more than 1 M^{3+} = Fe^{3+} + Cr^{3+} per formula unit (pfu) will have negative mole fractions of clinozoisite if one uses only the end members mentioned above. Unfortunately, the preliminary guidelines have been set up during the preparation of this volume and it was therefore impossible with respect to editorial deadlines to make all chapters consistent with the recommended nomenclature. The reader should therefore be aware that different chapters use different nomenclature.

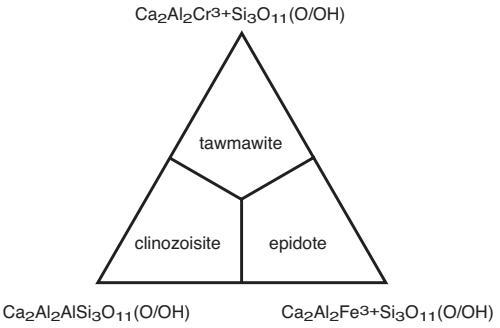

Figure 1. Nomenclature of monoclinic ternary Al-Fe-Cr epidote minerals. Analogue diagrams for other solid solutions (e.g., with V = mukhinite as an endmember) can be used.

Because the orthorhombic polymorph zoisite displays a much more restricted chemical variation and any substitution is restricted to small values far below mol fractions of $X = 0.5$ (see below), the nomenclature is much more consistent in the literature. The variety names "thulite" for Mn^{3+} bearing and "tanzanite" for V bearing solid solutions should be avoided, although with regard to petrographic purposes these names are convenient and helpful as they refer to zoisite crystals with distinct optical properties (see below). Furthermore, the only epidote mineral that is a significant gem stone is the blue colored vanadium bearing zoisite, which in this context is generally termed tanzanite. We therefore recommend using the terms "thulite" and "tanzanite" only for petrographic or gemological purposes. The composition of orthorhombic solid solutions should be expressed as the mole fractions X_{Fe}, X_{Mn} and X_{V} of the respective theoretical end members, which are $Ca_2Al_2Fe^{3+}Si_3O_{12}(OH)$, $Ca_2Al_2Mn^{3+}Si_3O_{12}(OH)$, and $Ca_2Al_2V^{3+}Si_3O_{12}(OH)$. Very often it is difficult to distinguish optically between orthorhombic and monoclinic, because of small grain size and inappropriate orientation of the crystals, and many authors have used "zoisite/clinozoisite." We recommend using instead "epidote minerals" which comprises both.

Recommended abbreviations for the common epidote minerals are:

Aln = allanite	Ps = pistacite (note, however, that it will not be a recommended name by the IMA)
Cz = clinozoisite	
Ep = epidote	Taw = tawmawite
Pie = piemontite	Zo = zoisite

For the other only rarely occurring epidote minerals with exotic composition we recommend not to use abbreviations.

CRYSTAL STRUCTURE

The monoclinic epidote minerals

Principal features and lattice constants. The monoclinic structure was first determined by Ito (1950) and subsequently confirmed by Ito et al. (1954) and Belov and Rumanova (1953, 1954). Based on the similarities in diffraction pattern and by comparing the X-ray spectra intensities of Fe poor and Fe rich clinozoisite-epidote, Gottardi (1954) established the isomorphous relationship along the Al-Fe solid solution join. Ueda (1955) and later Rumanova and Nikolaeva (1960) refined the structure of allanite and found a structural topology similar to clinozoisite. In detailed studies, Dollase (1968, 1969, 1971) fully refined the structures of two crystals with X_{Ep} = 0.03 and X_{Ep} = 0.81, respectively, and those of hanckokite, allanite, and piemontite. Intermediate crystals (X_{Ep} = 0.22, 0.40, 0.60, 0.81, 0.84) were later refined by Gabe et al. (1973), Stergiou et al. (1987), Kvick et al. (1988), and Comodi and Zanazzi (1997). By means of single crystal X-ray diffraction with structure refinements, Carbonin and Molin (1980) systematically studied the geometrical and structural variations accompanying the Al-Fe^{3+} substitution in natural crystals spanning the compositional range X_{Ep} = 0.30 to 0.86. Bonazzi and Menchetti (1995) extended this work by refining natural Al-Fe^{3+} crystals of the compositional range X_{Ep} = 0.24 to 1.14 and natural REE and Fe^{2+} bearing crystals to study the effects of the Fe^{3+} and Fe^{2+} substitution and the entry of REE. The only systematic structural study on synthetic Al-Fe^{3+} crystals is from Giuli et al. (1999) on seven samples spanning the compositional range X_{Ep} = 0.66 to 1.09.

The monoclinic epidote minerals all have space group $P2_1/m$ (for a discussion of a possible symmetry reduction to Pm, $P\bar{1}$, or $P2_1$ as response to cation ordering see below). The monoclinic structure (Fig. 2) is built up by two types of endless octahedral chains that run parallel [010] and consist of three non-equivalent octahedra M1, M2, and M3. The M1 octahedra form endless, edge sharing single chains to which individual M3 octahedra are attached on alternate sides forming a zigzag pattern. The second type of octahedral chain is made up exclusively by edge sharing M2 octahedra. The octahedral chains are cross linked in [100] and [001] by isolated T3 tetrahedra and $T1T2O_7$ groups with two non-equivalent large A1 and A2 positions in between (Fig. 2). Depending on composition and study cited, the lattice parameters of natural and synthetic Al-Fe^{3+} dominated solid solutions are a = 8.861–8.922 Å, b = 5.577–5.663 Å, c = 10.140–10.200 Å, β = 115.31–115.93°, and the cell volume is V = 452.3–463.9 $Å^3$ (Table 3), which correlate positively with Fe content, except for β which shows a slightly negative correlation (Figs. 3, 4). Linear regression equations of the data are compiled in Table 3.

The correlation trends of individual structural parameters with increasing Fe content display changes in slope at X_{Ep} = 0.6 to 0.7 and suggest a change in the Al–Fe^{3+} substitution mechanism from exclusive substitution on M3 for X_{Ep} < 0.6 to 0.7 to a combined substitution on M3 and M1 for X_{Ep} > 0.6 to 0.7 (see below). Such a change in the Al–Fe^{3+} substitution mechanism should also appear in the correlation trends between lattice constants and Fe content. Unfortunately, due to the different techniques applied by the different authors and the problems inherent in studying natural samples (impurities, minor amounts of other elements, zoning etc.) the data scatter and mask this change (Fig. 3). To overcome this problem we plotted only the data for almost pure Al-Fe^{3+} solid solutions (Fig. 4) from the systematic studies on Fe incorporation in clinozoisite-epidote from Carbonin and Molin (1980), Bonazzi and Menchetti (1995), and Giuli et al. (1999). Although the data still scatter, there appear subtle changes in the slopes of the correlation trends between lattice parameters a, b, c, and β and Fe content in the compositional range X_{Ep} = 0.5 to 0.7. Linear regression equations of the data for X_{Ep} < 0.6 and X_{Ep} > 0.6 are compiled in Table 3.

The changes in slope are opposite for a and c. Therefore, they largely cancel out and there appears no change in slope for V within the quality of the data (Fig. 4e). The observed changes

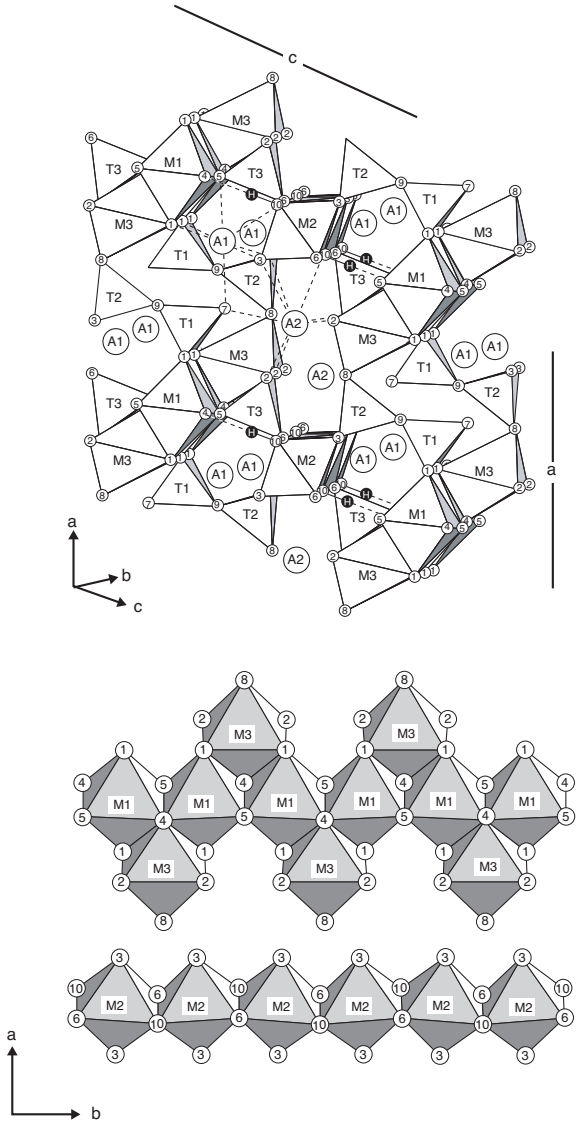

Figure 2. Coordination polyhedra of epidote (upper part) and notation of the M positions in the octahedral chains (lower part), with numbers for oxygen (adopted from Dollase 1968).

in slope of the lattice parameters at about $X_{Ep} = 0.6$ are in good accordance with the optical parameters that show discontinuities in this compositional range (Hörmann and Raith 1971; see below), with Mössbauer spectroscopic work that indicate Fe substitution exclusively on M3 for $X_{Ep} < 0.6$ and a combined substitution on M3 and M1 for $X_{Ep} > 0.6$ (Fehr and Heuss-Aßbichler 1997), and with the theoretical model for the intracrystalline Al–Fe^{3+} distribution of Bird and Helgeson (1980) that indicates an increasingly important contribution of M1 to the overall Fe incorporation for Fe contents above $X_{Ep} = 0.6$ to 0.7 (see Gottschalk 2004).

Table 3. Linear regression equation for lattice constants as a function of composition of monoclinic and orthorhombic epidote minerals; data sources for the monoclinic epidote minerals see text.

MONOCLINIC

	$0<X_{Ep}<1$	$X_{Ep} < 0.6$	$X_{Ep} > 0.6$
a [Å]	$(3.59\times10^{-2})X_{Ep} + 8.868$	$(4.75\times10^{-2})X_{Ep} + 8.861$	$(3.30\times10^{-2})X_{Ep} + 8.869$
b [Å]	$(6.34\times10^{-2})X_{Ep} + 5.583$	$(7.83\times10^{-2})X_{Ep} + 5.576$	$(6.78\times10^{-2})X_{Ep} + 5.580$
c [Å]	$(2.81\times10^{-2})X_{Ep} + 10.143$	$(2.61\times10^{-2})X_{Ep} + 10.142$	$(3.20\times10^{-2})X_{Ep} + 10.137$
β [°]	$(-7.76\times10^{-2})X_{Ep} + 115.48$	$(-1.55\times10^{-1})X_{Ep} + 115.51$	$(-1.04\times10^{-1})X_{Ep} + 115.49$
V [Å^3]	$(8.70)X_{Ep} + 452.98$	—	—

ORTHORHOMBIC

	Myer (1966)	Liebscher et al. (2002)	
		zoisite I	zoisite II
a [Å]	$(1.35\times10^{-1})X_{Fe} + 16.201$	$(-3.72\times10^{-2})X_{Fe} + 16.1913$	$(-8.26\times10^{-2})X_{Fe} + 16.2061$
b [Å]	$(7.84\times10^{-2})X_{Fe} + 5.550$	$(6.43\times10^{-2})X_{Fe} + 5.5488$	$(8.14\times10^{-2})X_{Fe} + 5.5486$
c [Å]	$(4.32\times10^{-2})X_{Fe} + 10.035$	$(3.43\times10^{-2})X_{Fe} + 10.0320$	$(1.18\times10^{-1})X_{Fe} + 10.0263$
V [Å^3]	$(24.2)X_{Fe} + 902.2$	$(11.4)X_{Fe} + 901.3$	$(19.3)X_{Fe} + 901.6$

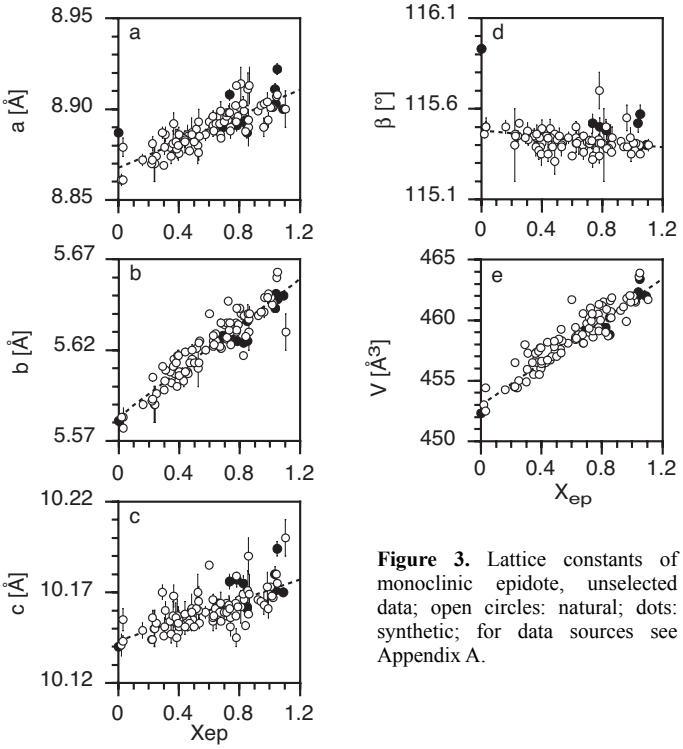

Figure 3. Lattice constants of monoclinic epidote, unselected data; open circles: natural; dots: synthetic; for data sources see Appendix A.

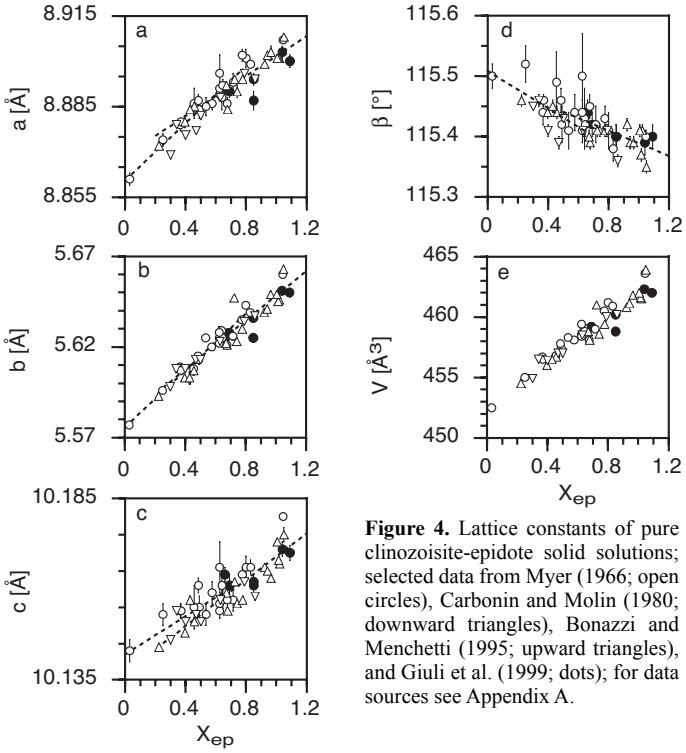

Figure 4. Lattice constants of pure clinozoisite-epidote solid solutions; selected data from Myer (1966; open circles), Carbonin and Molin (1980; downward triangles), Bonazzi and Menchetti (1995; upward triangles), and Giuli et al. (1999; dots); for data sources see Appendix A.

A detailed description and discussion of the structural changes accompanying the Al-Fe^{3+} substitution is given below.

A comparable change in substitution mechanism is also seen in the lattice parameters of synthetic Al-Mn^{3+} solid solutions (Anastasiou and Langer 1977, Langer et al. 2002; Fig. 5). Although some of the reported compositions of the synthetic Al-Mn^{3+} solid solutions might be questionable because Anastasiou and Langer (1977) could not analyze the run products, but assumed synthesis on the bulk composition based on mass balance considerations, the data indicate a change in substitution mechanism at about 1 Mn^{3+} pfu. The data also show that the substitution by Mn^{3+} changes the lattice parameters differently than the substitution by Fe^{3+} (Figs. 4, 5). For the same degree of Al–M^{3+} substitution (with M^{3+} = Fe^{3+} or Mn^{3+}) *a* is generally shorter (it actually correlates negatively with Mn content for Mn^{3+} < 1 cat. pfu) whereas *b*, *c*, and *V* are slightly larger in Al-Mn^{3+} than in Al-Fe^{3+} solid solutions. In contrast to Al-Fe^{3+} solid solutions in which β correlates negatively with Fe content it correlates positively with Mn contents in Al-Mn^{3+} solid solutions (Figs. 4d, 5d). The changes in slopes of the lattice parameters at about 1 Mn^{3+} pfu indicate the change in substitution mechanism from incorporation of Mn^{3+} on M3 to incorporation on M1 (for a detailed description of Mn bearing monoclinic epidote minerals see Bonazzi and Menchetti 2004).

To study the structural changes accompanying the Al–Fe^{3+} substitution in monoclinic epidote minerals, we took the structure refinements of natural and synthetic samples for which precise chemical analyses are presented and which represent almost pure Ca-Al-Fe^{3+} solid solutions (Dollase 1968, 1971; Gabe et al. 1973; Carbonin and Molin 1980; Stergiou et al. 1987; Kvick et al. 1988; Bonazzi and Menchetti 1995; Comodi and Zanazzi 1997;

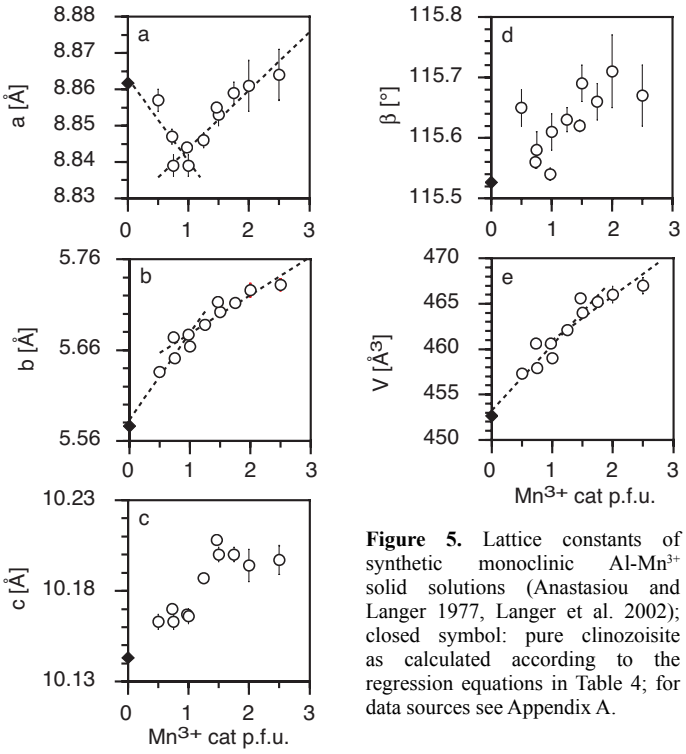

Figure 5. Lattice constants of synthetic monoclinic Al-Mn^{3+} solid solutions (Anastasiou and Langer 1977, Langer et al. 2002); closed symbol: pure clinozoisite as calculated according to the regression equations in Table 4; for data sources see Appendix A.

Giuli et al. 1999). We started from the refined fractional atom coordinates and recalculated the structural parameters. Below we briefly review the results for the individual polyhedra with special emphasis on the structural changes accompanying the Al–Fe^{3+} substitution.

Octahedra. The M1 octahedron lies on a symmetry centre and links the oxygen atoms O1, O4, and O5. The individual M1 octahedra share a common O4–O5 edge forming endless octahedral chains to which the individual M3 octahedra are attached. M1 and M3 share a common O1–O4 edge (Fig. 2). The M1 octahedron is fairly regular with a bond angle variance (Robinson 1971) s^2 = 15 to 20 (Fig. 6, Appendix B). Its mean bond length is about 1.90 to 1.94 Å and its volume 9.0 to 9.5 $Å^3$ (Figs. 6a, b). Up to about X_{Ep} = 0.6 the M1 octahedron shows only minor structural changes with increasing Fe content: the mean bond length, the volume, and the distance between the two apical O1 atoms slightly increase (Fig. 6) as response to the expansion of the attached M3 (see below) due to increased Fe content on M3 (Bonazzi and Menchetti 1995). For X_{Ep} > 0.6 the structural changes are slightly more pronounced suggesting Fe^{3+} incorporation also on M1. With increasing Fe content, the bond angle variance s^2 generally decreases and M1 becomes more regular (Fig. 6d). The inclination of M1 to [001] calculated as the angle between O1–O1´ and [001] decreases only slightly with increasing Fe^{3+} content (Appendix B).

Like M1 the M2 octahedron lies on a symmetry centre. It links the oxygen atoms O3, O6, and O10. The M2 octahedra share a common O6–O10 edge and form endless, edge sharing single chains that are interconnected with the other structural units by the isolated $T3O_4$ tetrahedra, which are attached alternately on both sides of the M2 chains (Fig. 2). It is the smallest and most regular of all three octahedra and shows the smallest changes with

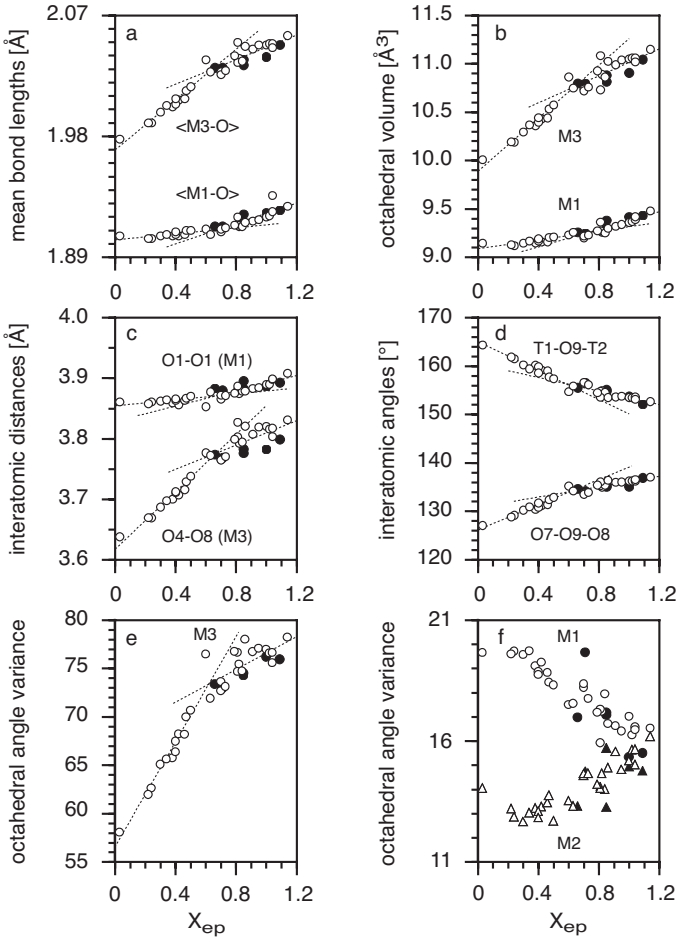

Figure 6. Bond length, volume and interatomic angles of monoclinic epidote minerals; open circles: natural; dots: synthetic; for data sources see Appendix B.

increasing Fe content. Its mean bond length is 1.88 to 1.89 Å and the volume 8.8 to 8.9 Å^3 (Appendix B). The bond angle variance s^2 is between 12 and 16 and indicates that M2 becomes more distorted with increasing Fe content (Fig. 6d). The inclination of M2 to [001] calculated as the angle between O3–O3´ and [001] decreases continuously with increasing Fe^{3+} content indicating a rotation of M2 (Appendix B). The structural changes in M2 are due to the changes occurring in the other structural units especially in M1 and M3 and to the overall expansion of the structure with increasing Fe content (Bonazzi and Menchetti 1995). The structural data give no hints for Fe^{3+} incorporation in M2, although Bonazzi and Menchetti (1995) found evidence for very small amounts of Fe in M2 for $X_{Ep} > 1.0$ and Giuli et al. (1999) found up to 0.08 Fe^{3+} pfu in M2 in their synthetic samples. Incorporation of small amounts of Fe^{3+} in M2 is also supported by Mössbauer spectroscopy (see Liebscher 2004).

The M3 octahedron is located on the mirror plane and coordinates the oxygen atoms O1, O2, O4, and O8. It is the largest and most distorted octahedron in the structure. Increasing

Fe content increases its mean bond length from 1.98 to 2.06 Å and enlarges its volume from 10.0 to 11.2 Å^3 (Figs. 6a,b; Appendix A). The distance between the two apical oxygen atoms O4 and O8 is considerable smaller than the comparable O1–O1 distance in M1, but increases significantly with increasing Fe content (Fig. 6c). Because M3 shares O4 with two M1 octahedra (Fig. 2), which therefore has a relatively fixed position, the increase in the O4–O8 distance primarily results from a significant shift of O8 perpendicular to the M1 octahedral chain. The general short O4–O8 distance points to a strong tetragonal distortion of M3. The strong distortion of M3 is also supported by its bond angle variance s^2, which is very large compared to M1 and M2 and increases from 58 to 79 with increasing Fe content (Fig. 6d). All structural changes of M3 are most pronounced for $X_{Ep} < 0.6$ and display a clear linear relationship with Fe content. For $X_{Ep} > 0.6$ the structural changes are less pronounced and the linear trend is partly masked by a considerable scatter of the data (Fig. 6). This different behavior for $X_{Ep} < 0.6$ and $X_{Ep} > 0.6$ is consistent with Fe^{3+} substitution exclusively in M3 for $X_{Ep} < 0.6$ and a combined Fe^{3+} substitution in M1 and M3 for $X_{Ep} > 0.6$. The scatter of the data for $X_{Ep} > 0.6$ most probably reflects different degrees of intracrystalline order-disorder at M1 and M3 due to different P and T of crystallization or metastable persistence of an ordered or disordered state (see below).

Tetrahedra and Si_2O_7 group. The tetrahedra are the most rigid units of the structure. Mean bond lengths and tetrahedral volumes are 1.626 (2) Å and 2.197 (9) Å^3 for T1, 1.614 (2) Å and 2.157 (8) Å^3 for T2, and 1.640 (2) Å and 2.248 (8) Å^3 for T3 (Appendix B). None of these parameters shows significant changes, which indicates no substantial substitution of Si by other cations, in accordance with the findings of Bonazzi and Menchetti (1995). The most evident and important feature is the rotation of T1 and T2 of the $T1T2O_7$ group relative to each other to compensate the structural changes in M3 accompanying the incorporation of Fe^{3+}. Fe substitution in M3 enlarges the M3 octahedron and results in a significant shift of O8 (see above). Because O8 is shared by M3 and T2, its shift leads to a rotation of T2. This rotation is mirrored by an increase of the O7–O9–O8 angle and a decrease of the T1–O9–T2 angle of the $T1T2O_7$ group (Fig. 6d). Like the other structural parameters the changes of both angles are most pronounced for $X_{Ep} < 0.6$, which gives further evidence that the substitution mechanisms change at about $X_{Ep} = 0.6$ from Fe incorporation purely in M3 to a combined incorporation in M1 and M3.

A-positions. In Al-Fe^{3+} solid solutions A1 is mostly described as nine-fold coordinated whereas A2 is described as ten-fold coordinated. Only in an almost Fe free clinozoisite, Dollase (1968) described A1 as seven-fold and A2 as eight-fold coordinated. From a purely charge balance point of view A1 should best be described as seven-fold coordinated whereas A2 is generally under-bonded even in ten-fold coordination (Appendix B) according to charge balance calculations using the refined bond lengths and the bond valence parameters from Brese and O´Keefe (1991). In allanite A1 is nine-fold coordinated whereas A2 is most probably eleven-fold coordinated (Dollase 1971). The A positions show only minor changes with increasing Fe content. These changes depend mostly on structural changes occurring on other sites and on the overall expansion of the structure (Bonazzi and Menchetti 1995).

Proton. Based on crystal chemical considerations, Ito et al. (1954) proposed bonding of the proton to O10 of the M2 octahedron with a hydrogen bridge to O4 of the neighboring M1 octahedron (Fig. 2). This was later confirmed by X-ray diffraction with bond valence calculations (Dollase 1968; Gabe et al. 1973; Carbonin and Molin 1980), infrared spectroscopy (Hanisch and Zemann 1966; Langer and Raith 1974; see also Liebscher 2004), and neutron diffraction (Nozik et al. 1978; Kvick et al. 1988). With increasing Fe content the length of the hydrogen bridge as well as the O10–O4 distance increase (Fig. 7a; Appendix B). But independent from Fe content the length of the O10–H … O4 hydrogen bridge is about 0.02 Å longer than the O10–O4 distance. This is due to bending of the hydrogen bridge with

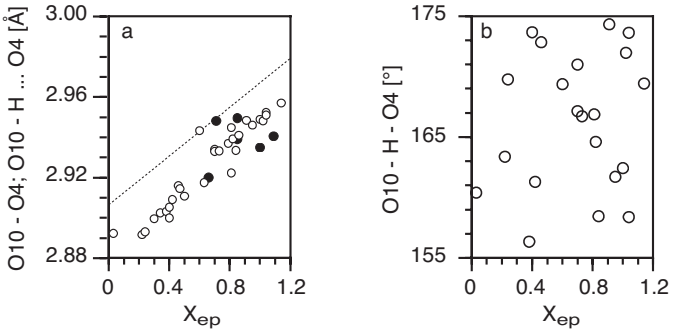

Figure 7. Interatomic distances and angles of the proton environment in monoclinic epidote; (a) O10 – O4 interatomic distance (symbols) and length of the O10 – H … O4 hydrogen bridge (dotted line). The hydrogen bridge is generally about 0.02 Å longer than the O10 – O4 distance due to its bent nature; (b) Bending of the hydrogen bridge with angles between 155 and 175°; open circles: natural; dots: synthetic; for data sources see Appendix B.

angles between 155 and 175° (Fig 7b) as response to the electrostatic repulsions from the M3 octahedron and the A2 position (Kvick et al. 1988). The lengthening of the hydrogen bridge with increasing Fe content was also found by Langer and Raith (1974) by means of infrared spectroscopy. These authors compared the length of the hydrogen bridge for different Fe contents, as calculated from the corresponding IR band, with published O10–O4 distances. Both values seem to converge with increasing Fe content and the authors therefore concluded, that the hydrogen bridge becomes more linear with increasing Fe content (Langer and Raith 1974). Contrary, the more recent diffraction data give no evidence for a change of the bending angle with increasing Fe content (Fig. 7b).

Zoisite (the orthorhombic epidote minerals)

Principal features and lattice constants. The structure of zoisite was first determined by Fesenko et al. (1955, 1956) for an Fe-free zoisite and later refined and fully determined by Dollase (1968) for a zoisite with X_{Fe} = 0.08–0.11. It is orthorhombic with space group Pnma. The structural features resemble those of the monoclinic epidote minerals, but zoisite has only one type of octahedral chain that consists of two non-equivalent octahedra M1,2 and M3. The M1,2 octahedra form endless, edge sharing single-chains parallel [010] to which individual M3 octahedra are attached exclusively on one side (Fig. 8a). As in the monoclinic forms, the octahedral chains are cross linked in [100] and [001] by isolated T3 tetrahedra and $T1T2O_7$ groups with two non equivalent large A1 and A2 positions in between (Fig. 8b). Depending on composition and study cited, the lattice constants of zoisite are a = 16.15–16.23 Å, b = 5.51–5.581 Å, c = 10.0229–10.16 Å, and the cell volume (V) is 900.0–909 Å^3 (Appendix C). The data suggest a positive correlation between b, V, and Fe content whereas for a and c the data scatter and show no clear dependence on Fe content (Fig. 9). The data of Myer (1966) on five natural zoisite crystals with Fe contents ranging from 0.016 to 0.15 X_{Fe} suggest a positive correlation between Fe content and lattice constants. Linear regression equations of his data are compiled in Table 3.

In contrast, in a study on five synthetic zoisite crystals with Fe contents from X_{Fe} = 0 to 0.113, Liebscher et al. (2002) found discontinuities in refined lattice parameters at ~ 0.05 X_{Fe} and attributed them to two orthorhombic modifications labeled zoisite I (< 0.05 X_{Fe}) and zoisite II (> 0.05 X_{Fe}). The correlation between lattice parameters and Fe content was derived for zoisite I and II (Fig. 9; dotted lines). Linear regression equations of the data are compiled in Table 3.

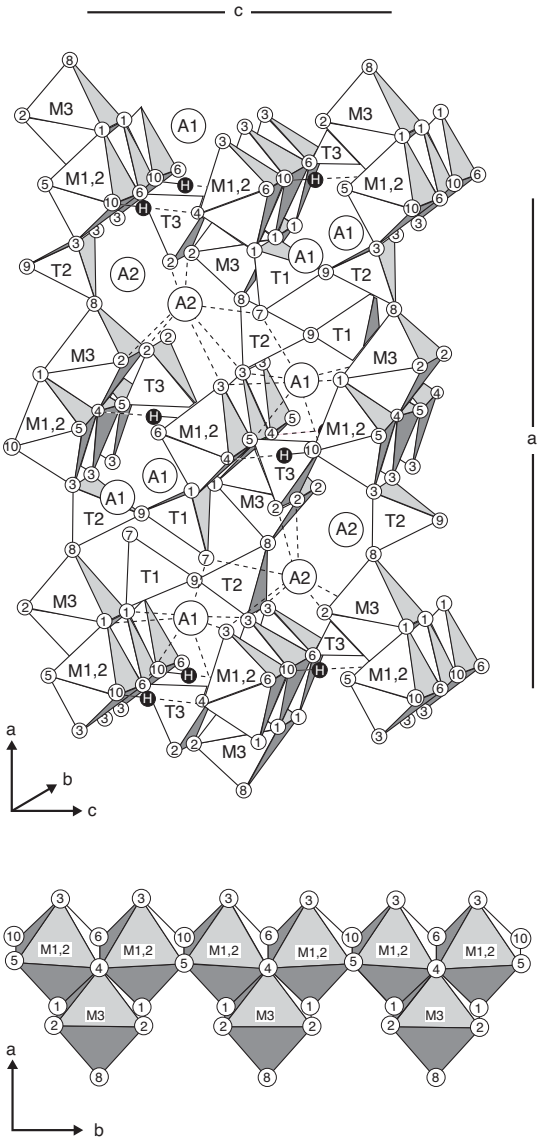

Figure 8. Coordination polyhedra of zoisite and notation of the M positions in the octahedral chains; adopted from Dollase (1968). Compare Figure 2.

Contrary to the data from Myer (1966) *a* is negatively correlated with Fe content and only *b*, *c*, and *V* show a positive correlation. At the transition from zoisite I to zoisite II *a* and *V* show positive, *b* and *c* negative offsets (Fig. 9). Independent on Fe content, zoisite II has the larger cell volume compared to zoisite I. The reason for the discrepancy between the results on synthetic zoisite from Liebscher et al. (2002) and those on natural zoisite is not clear but probably is due to small amounts of other elements like Mn, Mg, Ti, Fe^{2+}, and Sr in the natural

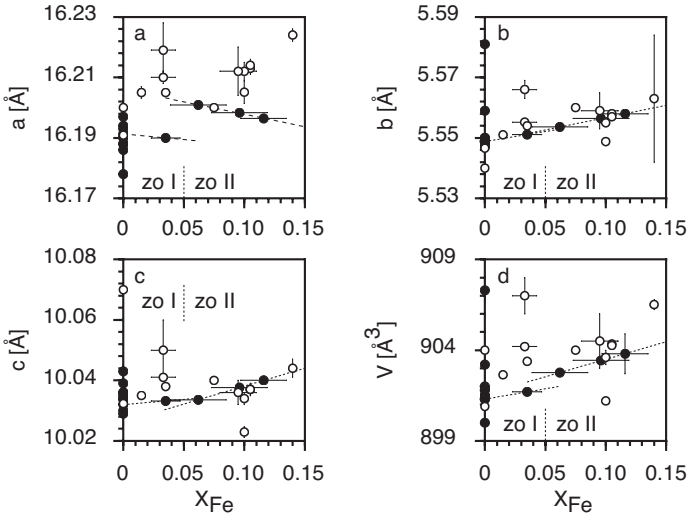

Figure 9. Lattice constants of natural (open circles) and synthetic (dots) zoisite; dotted lines are linear regressions of the data of Liebscher et al. (2002) for zoisite I and zoisite II (corresponding equations see Table 4); for data sources see Appendix C.

zoisite samples that mask the influence of increasing Fe content on the lattice constants. Below we give a brief description of the individual polyhedra with special emphasis on the structural changes accompanying the Al–Fe^{3+} substitution.

Octahedra. Independent upon Fe content the M1,2 octahedron is relatively undistorted. Its minimum and maximum bond lengths deviate by less than 0.1 Å from the mean M1,2–O bond length of about 1.89 Å (Appendix D) and the interatomic angles are within ± 8° of the ideal octahedral values. Its edges show the typical feature of edge shearing octahedra. The mean M1,2 edge length is 2.67 Å, but the shared edges (O4–O6 and O5–O10 between M1,2 octahedra and O1–O4 between M1, 2 and M3 octahedra, Fig. 8) are only 2.47–2,60 Å whereas the edges parallel to the Al–Al vector (O4–O5 and O6–O10) are 2.78–2.79 Å (Appendix D). This length of the Al–Al vector is considerable larger than the mean edge length of the tetrahedra (~2.63 Å; Appendix D), which bridge between the O1 and O3, respectively, of the individual M1, 2 octahedra in [010]. To account for this misfit, the M1,2 octahedral chain is slightly undulated (Fig. 8). The structural features of M1,2 show only minor changes with increasing Fe content. Only O1–O6 and O1–O3 clearly correlate negatively with Fe content, displaying discontinuities at the transition from zoisite I to zoisite II (Fig. 10 b,c).

In contrast to M1,2 the M3 octahedron is strongly distorted. Its minimum and maximum bond lengths deviate up to 0.22 Å from the mean M3–O bond lengths of 1.96–1.97 Å and its interatomic angles deviate up to 18° from the ideal octahedral values (Appendix D). With 2.76 to 2.77 Å its mean edge length is about 0.1 Å larger than that of M1,2. The edges shared with M1,2 (O1–O4, Fig. 10d) are significantly shorter (2.48–2.56 Å) whereas O1–O8 which points away from M1,2 is significantly longer (up to 3.16 Å) than the mean edge length. As indicated by the larger mean bond lengths and mean edge lengths the volume of M3 (9.7 to 9.8 $Å^3$) is about 1 $Å^3$ larger than that of M1, 2 (8.8 to 9.0 $Å^3$). Almost all structural features of M3 show significant changes with increasing Fe content. Especially the O1–O1 distance decreases whereas the O4–O8 distance significantly increases with increasing Fe content and both show discontinuities at the transition from zoisite I to zoisite II (Fig. 10 c,d).

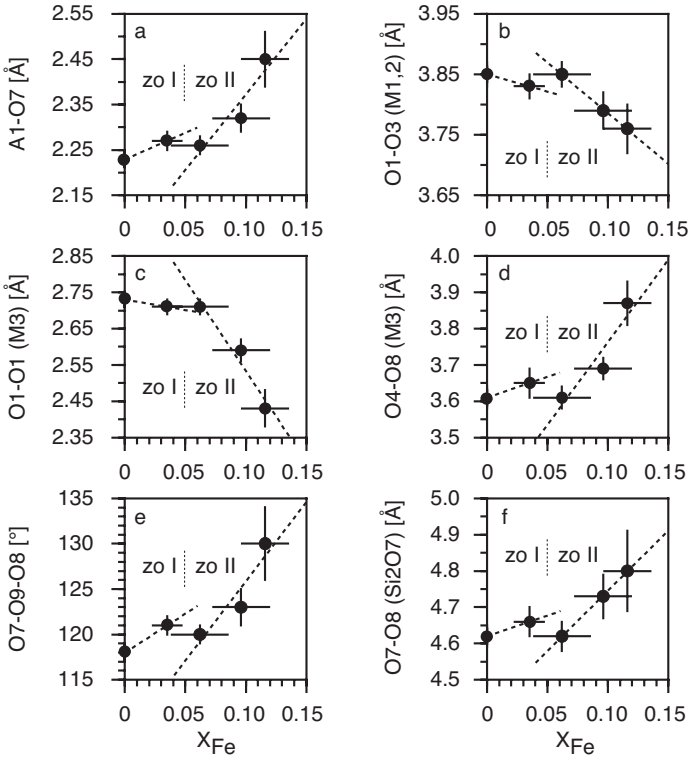

Figure 10. Interatomic distances and bond angles of synthetic zoisite (Liebscher et al. 2002); zo I and zo II refer to iron-poor and iron-rich zoisite in Figure 11; see Appendix D.

Tetrahedra and Si_2O_7 group. The T3 tetrahedron and the $T1T2O_7$ group connect the octahedral chains in [100] and [001] (Fig. 8). T1 and T2 vary significantly and get more distorted with increasing Fe content whereas T3 shows only minor changes. The mean T1–O bond length increases from 1.64 to 1.73 Å mostly due to a significant increase of the T1–O1 bond length whereas the mean T2–O bond length decreases from 1.62 to 1.57 Å (Appendix D). The O–T–O angles in T1 and T2 partly deviate more than 13° from the ideal tetrahedral value of 109°. In T1 the mean O–O distance as well as the volume increase whereas in T2 they decrease. In T3 only O2–O2´ slightly increase with increasing Fe content; all other structural values are, within errors, approximately constant (Appendix D). The geometry of the $T1T2O_7$ group significantly changes with increasing Fe content, due to an opposite rotation of the T1 and T2 tetrahedra (Liebscher et al. 2002). The T1–O9–T2 and O1–O9–O3 angles slightly tighten whereas O7–O9–O8 opens significantly (Fig. 11). Consequently, the O7–O8 distance strongly increases (Appendix D).

A-positions. Including all neighbors up to 2.85 Å, A1 and A2 are seven-fold coordinated independent on Fe content and are best described as trigonal prisms with a seventh and closer oxygen ligand lying outside of one of the equatorial prism faces (Dollase 1968; Appendix D). The mean A1–O bond length is generally shorter by about 0.1 Å than the mean A2–O bond length and both show almost no variation with Fe content. Only A1–O7 significantly increases with increasing Fe content (Appendix D) reflecting the rotation of T1 (see above).

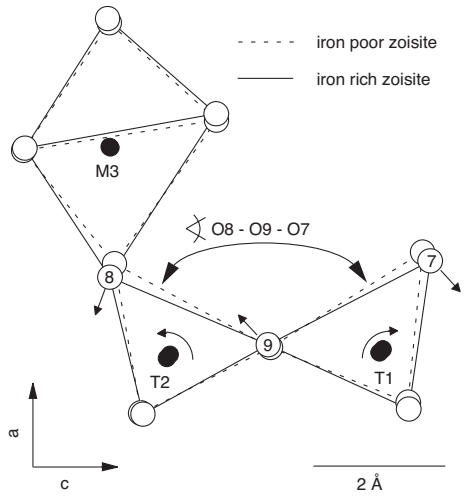

Figure 11. Rotation of tetrahedra T1 and T2 and of the M3 octahedron with increasing Fe content in zoisite.

Proton. The proton in zoisite is bonded to O10 (Fig. 8; Ito et al. 1954; Hanisch and Zemann 1966; Dollase 1968; Linke 1970; Gabe et al. 1973; Smith et al. 1987; Liebscher et al. 2002), which has the lowest bond strength (= 1.02 to 1.25 without hydrogen; Dollase 1968; Liebscher et al. 2002) of all oxygen atoms. The length of the hydrogen bond is 1.2 (2) Å (Dollase 1968). Based on the approximate position of the proton, the O10–O4 separation length and the fact that O4 is slightly under-bonded, Dollase (1968) concluded that the proton forms a hydrogen bridge with O4 of the neighboring octahedral chain. IR spectroscopic work proved this conclusion but also showed evidence for a second hydrogen bridge (Linke 1970; Langer and Raith 1974; Langer and Lattard 1980; Liebscher et al. 2002). Langer and Raith (1974) and Langer and Lattard (1980) speculated about an additional proton position in the structure with a corresponding second hydrogen bridge. However, the results of pressure dependent (Winkler et al. 1989) and temperature dependent (Liebscher et al. 2002) IR spectroscopy indicate that the proton is exclusively bonded to O10 but forms two hydrogen bridges with O4 and O2 of the neighboring octahedral chain. The hydrogen bridge to O2 must be bifurcated (for a review of spectroscopic work done on zoisite see Liebscher 2004). The O10–O4 hydrogen bridge has a length of 2.63 to 2.76 Å and slightly shortens with increasing Fe content (Liebscher et al. 2002; Appendix D).

Monoclinic - orthorhombic structural relationship

Ito (1950) was the first to study the structural relationship between epidote and zoisite. He proposed a unit cell twinning model with $2a_{mcl}\sin\beta = a_{orth}$ that satisfactorily relates unit cell sizes and space group symmetries of the two structures (Fig. 12a). Later structural refinements showed that a simple *n*-glide unit cell twinning does not reproduce the relative atomic movements that occur during the monoclinic–orthorhombic transformation (Dollase 1968). Especially the M1,2 octahedron, that would be produced by this operation and which is formed by joining half the M1 and half the M2 octahedron of clinozoisite, would be distorted due to the different inclination of M1 and M2 to the twin plane (100) (see above). In the orthorhombic structure, however, the M1,2 octahedron is nearly regular (Dollase 1968). This regularity arises from shifts of O3, O6, and O10 that can be viewed as a rotation of half of the M1,2 octahedron. This rotation is responsible for the main difference between zoisite and the monoclinic structure, i.e. the larger A2–O10 bond length and therefore reduced coordination number of A2 in zoisite (sevenfold versus eightfold in clinozoisite) and the larger T1–O9–T2 angle in zoisite (173° versus 164° in clinozoisite) due to a rotation of the T2 tetrahedron (Dollase 1968). Therefore the simple model of unit cell-twinning (Ito 1950) is qualitatively useful for descriptive purposes but does not strictly hold in a quantitative manner (Dollase 1968).

Ray et al. (1986) discussed the polytypic relationship between the monoclinic and orthorhombic structure in terms of different stacking sequences of layers or modules of monoclinic unit cells in [100]. The authors, somewhat arbitrarily, choose the stacking module

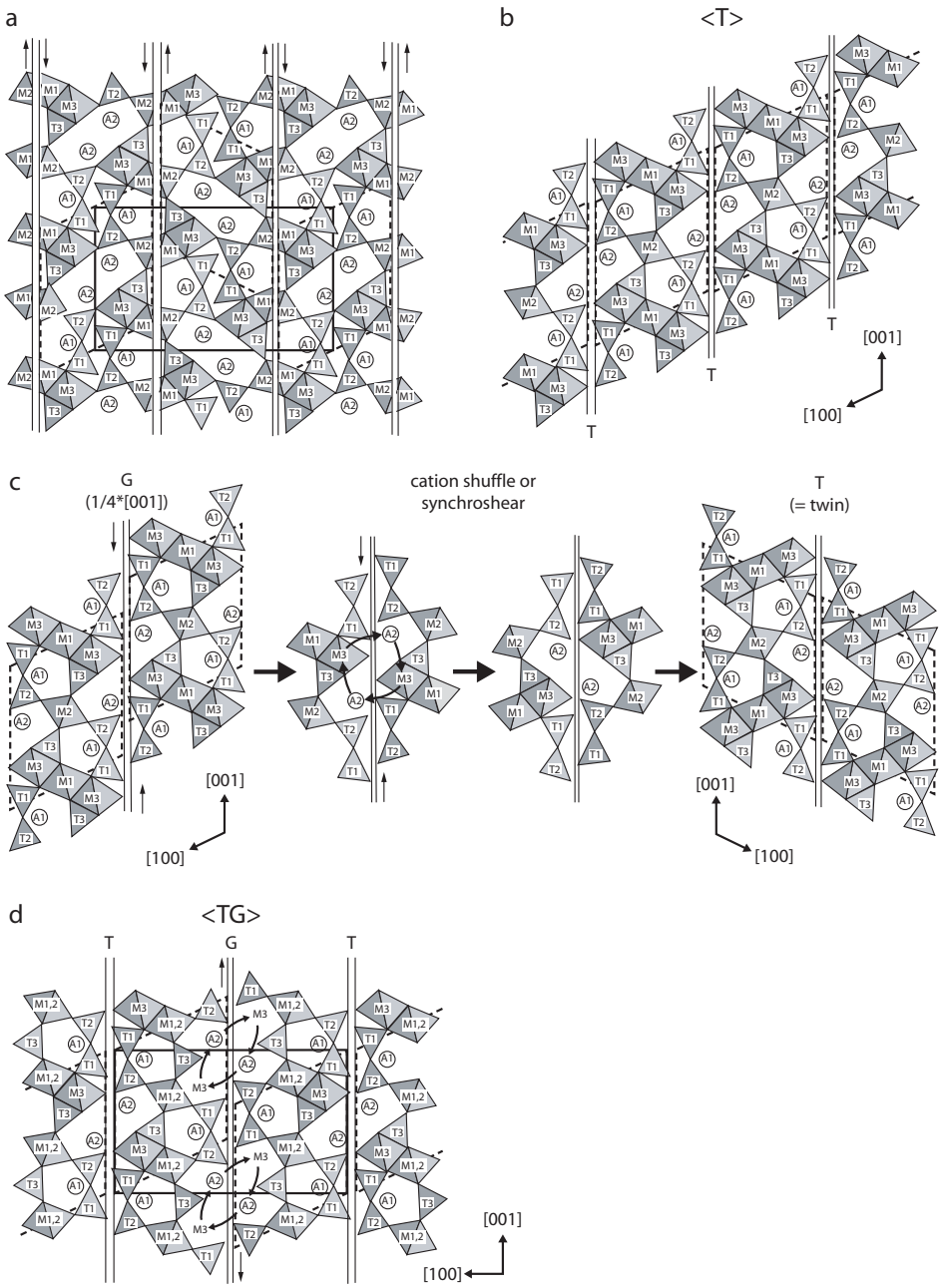

Figure 12. Relationship between clinozoisite and zoisite. (a) Model of Ito (1950) with a simple shearing. (b,c,d) Model of Ray et al. (1986); note the different position of the shearing planes. Monoclinic and orthorhombic unit cells are outlined (for detailed explanation see text).

in that way that its boundary coincides with a (*h*00) plane in the structure with minimal links between the structural framework (Fig. 12b). They show with high resolution TEM images that this plane corresponds well with the position of stacking faults in natural crystals. Each successive module might either be stacked by simple translation without any displacement between the modules (operator T = translation) or by translation with a glide component that introduces a shear displacement between the modules (operator G = gliding). Repeated stacking sequences can then be described by the respective operators in angular brackets, i.e. TTTT becomes <T>, GGGG becomes <G>, and TGTG becomes <TG> (Ray et al. 1986). A simple <T> stacking sequence results in the monoclinic structure (Fig. 12b). Introducing a glide component of 1/4 [001] between each module (<G> stacking sequence) results in the twin of <T> although a "cation shuffle" or "synchroshear" has to take place in order to reproduce a cation arrangement that resembles the original structure (Fig. 12c). If the glide operation together with the "cation shuffle" or "synchroshear" is only introduced every other stacking module a <TG> stacking sequence is produced which results in the orthorhombic structure (Fig. 12d; Ray et al. 1986).

The difference between the real orthorhombic structure and the theoretical structure produced by simple unit cell twinning also sheds some light on the monoclinic to orthorhombic transition as a function of composition. The main structural difference between the monoclinic and the orthorhombic structure, i.e. reduced coordination number of A2 and larger T1–O9–T2 angle in the latter, are due to the rotation of half of the M1,2 octahedron (see above). The data on the Fe^{3+} incorporation in zoisite presented above show that increasing Fe^{3+} content in zoisite enlarges M3, rotates T1 and T2, and decreases the T1–O9–T2 angle. The rotation of T2 also leads to a slight rotation of M1,2 in just the opposite sense to the rotation that occurs at the monoclinic to orthorhombic transition. Therefore, the effects of increasing Fe^{3+} content on the orthorhombic structure are opposite to those of the monoclinic–orthorhombic transition and Fe^{3+} stabilizes the monoclinic with respect to the orthorhombic structure. A structural stabilization of the monoclinic over the orthorhombic form with increasing Fe^{3+} content, or generally speaking with increasing substitution of a larger cation for Al, is also supported by the inclination to (100) of the M1 and M2 octahedra of the monoclinic structure. With increasing Fe^{3+} substitution for Al the inclination to (100) of the M2 octahedron continuously decreases from 66.5° to 61.7° whereas the inclination to (100) of the M1 octahedron only decreases from 76.9° to 75.7° (Appendix B). The structural misfit between M1 and M2 to produce a regular, orthorhombic M1, 2 octahedron therefore continuously increases and prohibits the monoclinic–orthorhombic transition.

TEM investigations

Only very few TEM studies on epidote minerals have been carried out. Our own experience with ion thinning of zoisite, especially when the crystals are embedded in a soft matrix such as carbonate can be problematic, because it is often difficult to obtain a thin edge. Ray et al. (1986) and Heuss-Aßbichler (2000) mentioned that epidote is not stable under the electron beam and easily transforms into amorphous material, which may start along stacking faults. Allanite, in contrast, is quite stable and does not show electron-beam radiation damage (Janeczek and Eby 1993). TEM investigations turned out to be a very useful tool to study the degree of metamictization in allanite and the process of crystallization during heating experiments.

The best orientation to study planar defects on (100) is viewing down the [010] zone axis. Ray et al. (1986) showed lamellar twins on (100) to be common in euhedral clinozoisite vein crystals, and they propose that most of the twins occur as a result of stacking mistakes during growth. However, Müller (pers. comm.) did observe mechanical twinning in epidote (see below Fig. 25k). Stacking faults on (100) are observed sporadically and some of them are terminated by partial dislocations. Investigations on zoisite (from the Eclogite Zone, Tauern Window,

Austria; Ray et al. 1986) showed occasional isolated stacking faults in crystals, which do not show obvious signs of deformation in thin section. In crystals from deformed veins, stacking faults spaced at approximately 250 Å and terminated by partial dislocations are numerous. The stacking faults can produce the clinozoisite sequence TTT in zoisite, interpreted as the result of deformation. Another type of stacking faults on (100) was observed as lamellar intergrowths of iron rich clinozoisite in iron poor zoisite on a scale of 20–200 μm. In zoisite crystals from deformed high-pressure pegmatites, Franz and Smelik (1995) also observed lamellae of clinozoisite in areas of anomalously high Fe content (own unpublished data), which can be interpreted from the textures as a late stage transition from zoisite into clinozoisite. Heuss-Aßbichler (2000) investigated two epidote crystals with X_{Ep} = 0.6 and 0.39, respectively. Generally these crystals lack interesting features of realbau such as stacking faults. However, in *a*-*c* sections the crystal with X_{Ep} = 0.6 shows a slight bending of the planes parallel to the *c*-axis, whereas the planes parallel to *a* are perfectly straight. Oriented parallel to the [100] zone axis the crystal shows a mosaic microstructure caused by twisting of the octahedral chains, which results in stacking faults and dislocations. The other crystal with X_{Ep} = 0.39 is also rather perfect, only in one case modulations were observed, interpreted as the indication for a tweed structure, and additional reflections were interpreted as a superstructure.

CRYSTAL CHEMISTRY

The crystal chemistry of the epidote minerals is especially interesting because they form solid solutions with end members, which are composed of the abundant components CaO-Al_2O_3-Fe_2O_3-SiO_2 and with end members whose components are present in a rock normally only at a subordinate level (Mn_2O_3) or at the trace element level (Sr, Pb, REE, Ba). We will restrict this review to the general features of the crystal chemistry of those elements that normally occur as major or minor constituents in epidote minerals. The trace element crystal chemistry of epidote minerals is presented by Frei et al. (2004), that of Mn bearing monoclinic epidote minerals by Bonazzi and Menchetti (2004), and that of allanite by Gieré and Sorensen (2004). The stable and radiogenic isotope geochemistry of epidote minerals is reviewed by Morrison (2004). For a detailed review of the compositional variation of the epidote minerals in different geological environments, the reader is referred to Bird and Spieler (2004), Grapes and Hoskin (2004), Enami et al. (2004), and Schmidt and Poli (2004). Compilations of analyses of epidote minerals can be found in Kepezhinskas and Khlestov (1971) and Deer et al. (1986).

The monoclinic epidote minerals

Compositional range. Despite their comparable simple crystal structure, the monoclinic epidote minerals display a wide and diverse range of composition. The vast majority belongs to the Al-Fe^{3+} solid solution series with Fe^{3+} contents between about X_{Ep} = 0.2 and X_{Ep} = 1.0. Clinozoisite with Fe^{3+} content below X_{Ep} = 0.2 is only rarely reported, examples include clinozoisite from Willsboro, New York, with about X_{Ep} = 0.03 (DeRudder and Beck 1964; this clinozoisite was used by Dollase 1968 for his structural refinement), and clinozoisite with about X_{Ep} = 0.09 from Alpe Arami, Western Alps (Ernst 1977), although the latter is questionable as Ernst (1977) did not mention how the monoclinic symmetry has been determined. More widespread are examples of epidote with X_{Ep} > 1.0, although these compositions are normally restricted to low-grade metamorphism and alteration or to hydrothermal systems. To the authors knowledge, the highest Fe^{3+} content so far reported for epidote is X_{Ep} = 1.48 from a secondary epidote that occurs in granitoid rocks from New Zealand (Tullock 1979).

Natural binary Al-Mn^{3+} solid solutions along the clinozoisite-piemontite join are rare as most samples also contain Fe^{3+}. Synthetic Al-Mn^{3+} solid solutions suggest about 1.5 Mn^{3+} pfu as the maximum Mn^{3+} content in Fe^{3+} free piemontite (Langer et al. 2002). In addition,

they indicate an orthorhombic to monoclinic transition along the Al-Mn^{3+} binary comparable to the Al-Fe^{3+} binary but at considerable higher degrees of Al substitution; Mn^{3+} content in zoisite is as high as 0.53 Mn^{3+} pfu (Langer et al. 2002; Fig. 13). Natural ternary Al-Fe^{3+}-Mn^{3+} epidote minerals mostly display Al contents between 1.5 and 2.5 Al pfu with a complete Fe^{3+}-Mn^{3+} substitution (see Bonazzi and Menchetti 2004). The highest degree of Al substitution in ternary Al-Fe^{3+}-Mn^{3+} epidote minerals (Al = 0.74 pfu, Fe^{3+} = 0.81 pfu, and Mn^{3+} = 1.42 pfu) is reported from the Sanbagawa belt, Japan (Enami and Banno 2001). This sample also contains considerable amounts of Sr, Pb, and Ba substituting for Ca.

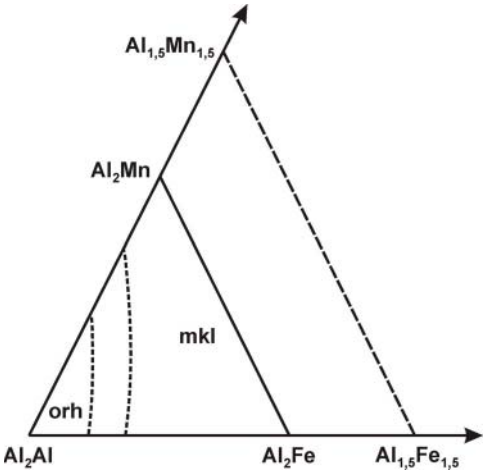

Figure 13. Schematic phase relations for monoclinic and orthorhombic epidote minerals in the ternary system Al-Fe-Mn; the majority of natural crystals lies within the composition Al_2Al-Al_2Fe-Al_2Mn and near to the Al_2Al-Al_2Fe and Al_2Fe-Al_2Mn sides. The maximum amount of substitution for Al is in both cases near to 1.5, and solid solution on the join Al_2Fe-Al_2Mn is continuous (see text). The position of the two-phase area along the Al_2Al-Al_2Mn side was estimated from the data by Langer et al. (2002). Note that the position of the two-phase area is a projection from P and T, and varies strongly.

Epidote minerals containing Cr^{3+} as major element have so far only been reported from few localities (e.g., from Burma by Bleek 1907; Finland by Eskola 1933 and Treolar 1987a, b; New Zealand and Australia by Ashley and Martin 1987; Grapes 1981; Cooper 1980; Challis et al. 1995; India by Devaraju et al. 1999; Spain by Sánchez-Viscaíno et al. 1995). The data suggest a complete solid solution series along the Al-Cr^{3+} join towards tawmawite $Ca_2Al_2Cr^{3+}Si_3O_{12}(OH)$ but indicate a composition gap along the Cr^{3+}-Fe^{3+} substitution (see Grapes and Hoskin 2004). The highest V^{3+} content found so far is 11.29 wt% V_2O_3 (0.80 V^{3+} pfu) in mukhinite from a marble associated with an iron deposit (Tashelginskoye deposit, Russia, Shepel and Karpenko 1969). The concentration of divalent cations Fe^{2+}, Mn^{2+}, and Mg on the octahedral sites is generally very low. Only in case of REE bearing epidote minerals it can reach significant values to charge balance the REE^{3+} substitution on the normally divalent A sites. As the REE^{3+} content in epidote minerals can be $\sum REE^{3+} > 1$ pfu, the amount of divalent cations can also be likewise high in REE bearing epidote minerals (see Gieré and Sorensen 2004). It is still an open question if there is complete miscibility along the join $Ca_{-1}M^{3+}{}_{-1}REE^{3+}{}_{+1}M^{2+}{}_{+1}$ or if there are compositional gaps (Gieré and Sorensen 2004).

Important homovalent substitutions on the divalent A sites include $Ca_{-1}Sr_{+1}$, $Ca_{-1}Pb_{+1}$, and $Ca_{-1}Ba_{+1}$. Sr bearing to Sr rich epidote minerals are reported from several localities (e.g., Grapes and Watanabe 1984; Brastad 1985; Mottana 1986; Akasaka et al. 1988; Harlow 1994; Perseil 1990; Enami and Banno 2001) and the highest Sr content so far reported is 16.3 wt% SrO from Itoigawa-Ohmi, Japan, which corresponds to 0.8 Sr pfu and thus almost represents niigataite endmember composition $CaSrAl_2(Al,Fe^{3+})Si_3O_{12}(OH)$ (Miyajima et al. 2003). The data suggest a complete miscibility of Ca and Sr in epidote minerals (see Grapes and Hoskin 2004). Epidote minerals that contain Pb as trace or minor constituent are widespread but Pb as major element is

only reported from few localities (e.g., Penfield and Warren 1899; Dunn 1985; Neumann 1985; Holtstam and Langhof 1994; Jancev and Bermanec 1998; Enami and Banno 2001). Holtstam and Langhof (1994) described almost pure hancockite ($CaPbAl_2(Al,Fe^{3+})Si_3O_{12}(OH)$) with 32–33 wt% PbO (= 0.95 Pb pfu) from Jacobsberg, Sweden. In rocks from Nezilovo, Macedonia, Jancev and Bermanec (1998) found epidote with ~10 wt% PbO (= 0.23 Pb pfu) and hancockite with 26–27 wt% PbO (= 0.69–0.72 Pb pfu) reflecting different parageneses with different bulk chemistry. From the same locality also piemontite with Pb content up to 23 wt% PbO (~0.6 Pb pfu) is described (Bermanec et al. 1994; Jancev and Bermanec 1998). With its large cation radius Ba normally substitutes for Ca only in trace or minor amounts. The Ba content can only reach noticeable values with concomitant high degrees of (Mn^{3+}, Fe^{3+}) substitution for Al on M1 and M3, as incorporation of Mn^{3+} and Fe^{3+} on M1 and M3 expands the A2 site (Smyth and Bish 1988). Consequently, the highest Ba contents reported so far with 2.7–6.7 wt% BaO (= 0.1–0.25 Ba pfu) occur in Sr piemontite from the Sanbagawa belt, Japan, that also shows $Mn^{3+} + Fe^{3+}$ = 1.68–2.23 pfu (Enami and Banno 2001).

Site occupancy. The sites in which the different major and minor elements substitute in the monoclinic epidote structure are comparably well known. X-ray diffraction and spectroscopic data show that Fe^{3+} strongly favors the largest and most distorted M3 site (e.g., Dollase 1971, 1973; Gabe et al. 1973; Kvick et al. 1988). At high total Fe^{3+} content, it also substitutes on M1 (e.g., Dollase 1973), as increasing Fe^{3+} on M3 enlarges the edge-sheared M1 octahedron (Bonazzi and Menchetti 1995). The ability of M1 to house Fe^{3+} therefore correlates with the volume of M3 and Bonazzi and Menchetti (1995) claimed a critical volume for M3 of about 11 $Å^3$ for the incorporation of significant amounts of Fe^{3+} in M1. This volume corresponds to a total Fe^{3+} content of about 0.8 pfu (Bonazzi and Menchetti 1995) in good accordance with the data of Dollase (1973) that only show Fe^{3+} in M1 for a total Fe^{3+} content of > 0.8 pfu. Contrary, the structural data presented above suggest a substitution in M1 already at a total Fe^{3+} content of about 0.6 pfu. In case of REE bearing epidote minerals in which divalent cations like Fe^{2+} or Mg allow for a greater expansion of M3 (see below) significant amounts of Fe^{3+} may be present in M1 at even lower total Fe^{3+} content (Bonazzi and Menchetti 1995). As M2 is the smallest octahedron of the structure it is generally free of Fe^{3+} (e.g., Dollase 1971, 1973; Gabe et al. 1973; Kvick et al. 1988). Only at very high degrees of substitution and/or high temperature it may contain small but considerable amounts of Fe^{3+}. Giuli et al. (1999) report up to 0.08 Fe^{3+} pfu in M2 in synthetic Al-Fe^{3+} epidote with Fe^{3+}_{tot} = 1.08 pfu, synthesized at 0.5 GPa/700°C, and found a positive correlation between Fe^{3+}_{tot} and Fe^{3+} on M2.

Structural refinements of piemontite by e.g., Dollase (1969), Catti et al. (1988, 1989), and Ferraris et al. (1989) show that Mn^{3+} also has a strong preference for the M3 site and a less pronounced preference for M1 and that M2 is exclusively occupied by Al. Burns and Strens (1967) also interpreted their spectroscopic data on piemontite with a strong preference of Mn^{3+} for M3 but contrary to the structural refinements postulated an only slightly less pronounced preference of Mn^{3+} for M2 compared to M3 and only a very minor preference of Mn^{3+} for M1. In contrast to Fe^{3+} and Mn^{3+}, Cr^{3+} has a strong preference for the M1 site and comparable but significantly minor preferences for M3 and M2 (Burns and Strens 1967). Octahedrally coordinated divalent cations as Fe^{2+}, Mn^{2+}, and Mg have a strong preference for the large M3 site although Mössbauer spectroscopy (Dollase 1971, 1973) and structural refinements (Bonazzi et al. 1992) indicate small amounts of Fe^{2+} and Mg also on M1.

Stoichiometric considerations indicate that in some cases Mn^{2+} must also substitute for Ca on the A sites. In these cases, it most probably substitutes in A1 (Smith and Albee 1967; Chopin 1978; Reinecke 1986; Bonazzi et al. 1992) in good accordance with zoisite that also indicate substitution of Mn^{2+} for Ca in A1 (Ghose and Tsang 1971; see below). Due to their large cation size, the other divalent cations like Sr, Pb, and Ba will substitute for Ca in the larger A2 site. Like these the REE are expected to substitute in A2 although Cressey and Steel (1988) found

evidence that the MREE and HREE also substitute in A1. For the smallest HREE these authors even speculated about incorporation in an octahedral site (Cressey and Steel 1988).

Order-disorder phenomena. Studies on order-disorder phenomena in monoclinic epidote minerals are restricted to the Al-Fe^{3+} solid solution series in which two different order-disorder processes must be distinguished, the non-convergent ordering of Al and Fe^{3+} between the different crystallographic sites, which is not associated by a symmetry change, and their convergent ordering on M3 (Fehr and Heuss-Aßbichler 1997; Heuss-Aßbichler 2000) that leads to a splitting of M3 into two slightly different sites (labeled M3 and M3´ by the above authors) and a concomitant symmetry reduction.

As shown by the site occupancy data (see above) the non-convergent ordering of Al and Fe^{3+} between the different octahedral sites only becomes important at total Fe^{3+} contents higher than about $X_{Ep} = 0.6$ and is restricted to the M1 and M3 sites except for high temperature and high Fe content at which conditions small amounts of Fe^{3+} may also enter the M2 site (Giuli et al. 1999). Based on the data available at that time, Bird and Helgeson (1980) derived a mixing model for the partitioning of Al and Fe^{3+} between M1 and M3 and showed that the Fe^{3+} content in M1 increases with both temperature and total Fe content (see Gottschalk 2004). Bird et al. (1988) and Patrier et al. (1991) found metastable disorder higher than that predicted from the theoretical model (Bird and Helgeson 1980) in natural hydrothermal Al-Fe^{3+} solid solutions (see Bird and Spieler 2004). Contrary, Fehr and Heuss-Aßbichler (1997) by means of Mössbauer spectroscopy on natural heat-treated Al-Fe^{3+} solid solutions (see Liebscher 2004) and Bonazzi and Menchetti (1995) by means of X-ray diffraction on natural Al-Fe^{3+} solid solutions determined a significant lower disorder than theoretically predicted. In synthetic Al-Fe^{3+} solid solutions Giuli et al. (1999) found good agreement between their data and the theoretical model for runs at 700°C but a considerable higher disorder than predicted in the runs at 600°C.

Gottschalk (2004) calculated the partition coefficient

$$K_D = \frac{^{M3}X_{Fe^{3+}} \times {}^{M1}X_{Al}}{^{M1}X_{Fe^{3+}} \times {}^{M3}X_{Al}}$$

for the reaction

$$^{M1}Fe^{3+} + {}^{M3}Al = {}^{M3}Fe^{3+} + {}^{M1}Al$$

based on the data of Dollase (1973), Bird and Helgeson (1980), Patrier et al. (1991), Fehr and Heuss-Aßbichler (1997), and Giuli et al. (1999). In a $\ln K_D$ vs. $1/T$ plot, the data are inconsistent (see Fig. 20 in Gottschalk 2004) leaving much room for speculation. Taking only the data from Dollase (1973), Fehr and Heuss-Aßbichler (1997), and the 700°C data of Giuli et al. (1999) the temperature dependence of $\ln K_D$ calculates to $\ln K_D = -8800/T + 5.4$ (T in K), which slightly differs from the data of Bird and Helgeson (1980). Assuming ideal behavior for Fe^{3+} and Al on M3 and M1, respectively, and $\Delta V = 0$ and $\Delta c_p = 0$ for the above reaction, the temperature dependence of ln K_D results in $\Delta S = 45$ J/(mol K) and $\Delta H = 73$ kJ/mol for the intracrystalline Fe^{3+}–Al exchange. The curves for the calculated Fe^{3+} content on M1 as a function of the total Fe^{3+} content at different temperatures following the procedure described in Bird and Helgeson (1980) show (Fig. 14) that only for T > 600°C and/or $Fe^{3+} > 0.8$ to 0.9 pfu M1 incorporates significant amounts of Fe^{3+}.

In addition to this non-convergent intracrystalline Al-Fe^{3+} distribution, the data by Fehr and Heuss-Aßbichler (1997), Heuss-Aßbichler and Fehr (1997), and Heuss-Aßbichler (2000) indicate a convergent ordering process of Al and Fe^{3+} exclusively on the M3 site. In a study on the intercrystalline Al-Fe^{3+} distribution between epidote and grossularite-andradite Heuss-

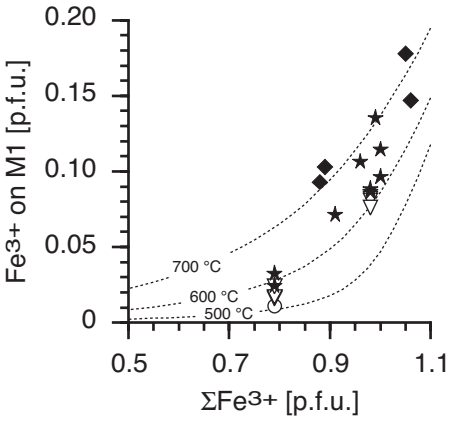

Figure 14. Theoretical partitioning curves of Fe^{3+} on M1 in epidote in relation to total Fe^{3+} content for different temperatures calculated with the temperature dependence of KD of the order-disorder reaction $Fe^{3+}(M1) + Al(M3) = Fe^{3+}(M3) + Al(M1)$ (see text); data points are from Dollase (1972); Fehr and Heuss-Aßbichler (1997); Giuli et al. (1999) for 500°C (open circles), 600°C (triangles), 650°C (asterisks), 700°C (diamonds).

Aßbichler and Fehr (1997) found two solvi along the clinozoisite–epidote solid solution series that are separated by an intermediate composition of about $X_{Ep} = 0.5$. In addition, the authors were only able to fit their measured Mössbauer spectra of Al-Fe^{3+} solid solutions with X_{Ep} = 0.39, 0.43, 0.48, 0.60, and 0.72 by two doublets that both show the principal characteristics of Fe^{3+} on M3 but display small differences in their quadrupol splitting (see Liebscher 2004). The authors interpreted this as due to two slightly different M3 sites, labeled M3 and M3´. These belong to two different monoclinic epidote phases, one with Al-Fe^{3+} disorder on M3 (M3 doublet) and one with an ordered distribution of Al and Fe^{3+} on M3 (M3´ doublet), the latter representing the intermediate composition of about $X_{Ep} = 0.5$ (Fehr and Heuss-Aßbichler 1997; Heuss-Aßbichler 2000). Depending on the geometric nature of the Al-Fe^{3+} ordering in M3 the space group of the intermediate composition should reduce from $P2_1/m$ to either Pm or $P\bar{1}$. In case of space group $P\bar{1}$ the lattice parameters a, b, and c of the ordered phase will be twice that of the disordered phase (Heuss-Aßbichler 2000). However, up to now no structural refinement of epidote minerals showed space group Pm or $P\bar{1}$.

Zoisite (the orthorhombic epidote minerals)

Compositional range. Zoisite displays a much more restricted deviation from the endmember composition $Ca_2Al_3Si_3O_{12}(OH)$ than the monoclinic epidote minerals (Franz and Selverstone 1992). Important octahedral substitutions include the incorporation of Fe^{3+}, Mn^{3+}, Cr^{3+}, and V^{3+} for Al. The Fe^{3+} content in zoisite normally does not exceed about $X_{Fe} = 0.15$. Higher Fe^{3+} contents are reported, e.g., by Raith (1976) in zoisite from amphibolite to eclogite facies metabasites with $X_{Fe} = 0.17$, by Brunsmann et al. (2000) in zoisite from high-pressure segregations with $X_{Fe} = 0.18$, and by Cooper (1980) in chromian zoisite with $X_{Fe} = 0.20$. The highest Fe^{3+} contents in zoisite so far reported are $X_{Fe} = 0.21$ (Brunsmann et al. 2000) and $X_{Fe} = 0.23$ (Vogel and Bahezre 1965) from high-pressure vein zoisites. However, it is not clear if these data are from pure zoisite, as the analysis from Brunsmann et al. (2000) was taken from a zoisite crystal which interference color displayed very fine lamellae suggesting fine, lamellar intergrowths of zoisite and clinozoisite, and the analysis from Vogel and Bahezre (1965) represents a wet chemical bulk analysis of a zoned zoisite crystal and might contain small undetected inclusions of other phases.

The Mn^{3+} content of zoisite is normally very low and rarely exceeds 1 wt% Mn_2O_3 which corresponds to about 0.02 Mn^{3+} pfu. The highest Mn^{3+} contents in natural zoisite are reported from highly oxidized low-grade metamorphic rocks with 1.6 to 3.7 wt% Mn_2O_3 (0.09–0.22 Mn^{3+} pfu; Reinecke 1986). Higher Mn^{3+} contents are only known from synthetic zoisite

samples. Anastasiou and Langer (1977) report 0.25 Mn^{3+} pfu and Langer et al. (2002) found 0.50–0.53 Mn^{3+} pfu in zoisite synthesized at 800°C/1.5 GPa and f_{O_2} of the Mn_2O_3/MnO_2 oxygen buffer. As the latter coexists with piemontite it should represent the maximum Mn^{3+} content in zoisite at these experimental conditions.

Like in the monoclinic epidote minerals the Cr^{3+} content in zoisite rarely exceeds the trace element level. Game (1954) reports 0.33 wt% Cr_2O_3 in zoisite from Tanzania and Grapes (1981) 0.23 to 0.40 wt% Cr_2O_3 (0.014 to 0.024 Cr^{3+} pfu) in zoisite from New Zealand. Own, unpublished data show up to 1.66 wt% Cr_2O_3 (0.10 Cr^{3+} pfu) in zoisite from Tanganyika. The highest Cr^{3+} content found in zoisite so far is 2.46 wt% Cr_2O_3 (0.15 Cr^{3+} pfu) in a chromian zoisite in a fuchsite-margarite pseudomorph after kyanite from New Zealand (Cooper 1980).

Geochemical important homovalent substitutions for Ca in the A sites of zoisite include Sr^{2+} and Pb^{2+}. As both A sites in zoisite have a size comparable to the monoclinic A1 site in which no Sr^{2+} or Pb^{2+} substitution occurs, zoisite normally contains Sr^{2+} and Pb^{2+} only at the trace or minor element level. In case of Sr^{2+} this holds especially for normal rock compositions metamorphosed under *P–T* conditions where other potential Sr^{2+} carriers such as calcic plagioclase are stable. However, in very Sr^{2+} rich rock compositions and/or outside the stability fields of other potential Sr^{2+} carriers, the Sr^{2+} content in zoisite may reach several wt%. Brastad (1985) reports up to 7.4 wt% SrO (0.33 Sr^{2+} pfu) in zoisite from metasomatized eclogite from Norway, which is the highest so far reported. Zoisite in eclogite from Su-Lu, China has up to 3.2 wt% SrO (Nagasaki and Enami 1998), zoisite in albitites from Guatemala and in zoisite-pegmatites from Spain has 1.2 to 1.4 wt% SrO (Maaskant 1985; Harlow 1994). Contrary to the monoclinic epidote minerals in which it can reach several weight percent the PbO content of zoisite, at least so far reported, is generally in the range of only a few hundred ppm (Frei et al. 2004).

Site occupancy. Structural, electron paramagnetic resonance, and spectroscopic data show that Fe^{3+}, Cr^{3+}, and Mn^{3+} substitute for Al exclusively in the M3 site (e.g., Hutton 1951; Ghose and Tsang 1971; Tsang and Ghose 1971; Schmetzer and Berdesinski 1978; Grapes 1981; Langer et al. 2002). Optical spectroscopy suggests that V^{3+} may enter the M1,2 as well as the M3 site although it shows a preference for M3 (Tsang and Ghose 1971). As the A2 site has a slightly larger mean A–O distance and is more distorted than the A1 site (see above), any substitution of cations larger than Ca such as Sr^{2+} and Pb^{2+} will occur at the A2 site. In contrast, as indicated by electron paramagnetic resonance data, Mn^{2+} is most likely located in A1 whereas V^{2+} occupies both A sites with a preference for A1 (Ghose and Tsang 1971).

Microanalysis

Minerals are commonly analyzed with the electron microprobe, and this is also recommended for epidote minerals. It is the only routine method, which allows resolving chemical zoning, but one should be aware that, for example, oscillatory zoning might be on a scale below the resolution of the electron microprobe. In addition to the microprobe, optical examination may give qualitative information about composition, because interference colors are very sensitive to small changes in Al-Fe substitution, especially well visible at low birefringence. It is not recommended, however, to use optical data to derive quantitative information about composition, because of the many possibilities of simple and coupled substitutions. Epidote minerals are stable under the electron beam at normal conditions of 10 to 20 kV, 15 to 20 nA, even with a fine focused beam.

We recommend to analyze epidote minerals with the following strategy: Distinguish optically between orthorhombic and monoclinic by a combination of observation of extinction angle and low birefringence; be aware that with small crystals this might be very difficult, and in many cases actually impossible, if the crystals are not oriented in the correct position. Oblique extinction is only visible in (010), whereas {010] always shows straight extinction.

Check your determination with the electron microprobe: If the Fe_2O_3 content is below X_{Fe} 0.15 - 20, the mineral is probably zoisite. If your optical determination was "monoclinic" with Fe_2O_3 content significantly below X_{Fe} 0.15, then you have one of the rare cases of very Fe-poor clinozoisite. Check with X-ray methods or transmission electron microscopy! If you have no exact optical and/or chemical characterization and in the absence of X-ray determination, characterize the minerals as "epidote minerals".

Analyze first for the common components SiO_2, Al_2O_3, Fe_2O_3, Mn_2O_3, Cr_2O_3, TiO_2, CaO, and MgO and calculate the formula on a basis of 12.5 or 25 oxygen pfu for common epidote minerals. Alternatively you can calculate on a basis of 8 cations pfu or on 3 Si pfu. All three methods yield very similar results. In a first step calculate all Fe and Mn as trivalent. Check the formula for internal consistency:

- The total should be 98 ± 1 wt% except for metamict allanite. If the sum is lower, there are possibly other less common elements present. It is best to use EDS parallel to WDS;
- If Ca is < 2 pfu check for Sr, REE, Pb; there might also be Mn^{2+} instead of Mn^{3+};
- If alkalis are present, the mineral might be strongly altered (except in some very rare cases of allanite);
- If there are REE present, check for Mg and recalculate the formula with charge balance for Fe^{2+} by simultaneous normalization to 25 oxygen and 8 cations pfu; if in addition Mn is present, first assume all Mn as Mn^{3+}, then Mn^{2+};
- If $\sum$A1,2 is still < 2.0, check calculations, if Mn^{2+} is possible;
- If $\sum$M1,2,3 (including Ti) is < 3.0, check for V;
- If Si is below or above 3.0, the analysis is probably not reliable, except for metamict allanite;
- Anions: it is normally not necessary to analyze for Cl and F (for common epidote minerals below detection limit), only in the case of REE bearing minerals they must be checked;
- Selection of points to analyze: Optical zoning gives an important hint to chemical zoning. Also, the difference in Al-Fe as well as Al-Mn atomic weight is large enough to be seen quite well in back scattered electron images. However, Fe-Mn zoning is less visible. Be aware of the grain shape of the epidote minerals, with the highest growth rate in *b* (elongation of prismatic crystals), and be aware of possible sector and oscillatory zoning;
- Coexisting minerals: Grossularite-andradite, prehnite, pumpellyite and sodic amphibole also show Al-Fe^{3+} substitution and the distribution of these elements can be used to check for equilibrium. In the case of Sr- rich epidote minerals check for distribution in coexisting pyroxene, plagioclase, carbonate, and apatite; for Cr-rich epidotes, check chlorite, mica, amphibole, and spinel.

CHEMICAL ZONING

Like other neso- and soro-silicates with low diffusion rates chemical zoning is a common feature in minerals of the epidote group (see e.g., Grapes and Hoskins 2004; Enami et al. 2004). In thin section the zoning is sometimes obvious from the color intensity, but very typically shows up in the interference colors, because birefringence is a strong function of the chemical composition, especially the Fe-Al content. Small changes in Fe-Al, which are at the

limit of the resolution of the electron microprobe, can be seen very well in crossed polarized light. Zoning is mostly growth zoning, less modified by diffusion, because the typical epidote occurrences are from rocks, which have not experienced temperatures above 700°C. Zoning is often modified by retrograde dissolution-precipitation. It reflects the changing *P-T* parameters (Grapes and Hoskins 2004), and is strongly influenced by the miscibility gaps in the solid solution series and by the zoisite-clinozoisite phase transition (Franz and Selverstone 1992). Very importantly it depends also on f_{O_2}, which can be controlled internally by the solid mineral phases with or without a fluid, or externally via the fluid phase. Zoning can also be controlled by the local presence of immobile cations such as Cr^{3+}. Sánchez-Viscaíno et al. (1995) described such a case, where the presence of relic chromite grains strongly influenced the local composition of epidote, which results in a very complex irregular zoning pattern. Cr content varies from below 4 wt% to > 10 wt% over a distance of 50 μm and the whole zoning pattern mimics the locally inherited composition. Similar irregular zoning patterns are frequently observed in low-temperature metamorphic rocks, where small individual grains of epidote minerals assembled into one single crystal. Gieré and Sorensen (2004) show an example of allanite-epidote core-rim zoning, where the outlines of the inner core zone shows such an irregular pattern.

Core-rim zoning is, however, the general case, and Grapes and Hoskins (2004) give some rules. In many cases, Fe rich epidote grows first at subgreenschist facies conditions and the Al content increases up to amphibolite facies conditions, but note that there are also many exceptions. In zoisite, cores are often rich in Fe, and the individual zones mimic the euhedral shape (e.g., Franz and Smelik 1995) such that in sections perpendicular to (010) it is of optically diagnostic value (Pichler and Schmitt-Riegraf 1993). Replacement of the Fe rich zones by Al rich zones parallel to (100) results in a lamellar appearance in sections parallel to the crystallographic *b* axis. Also the fan shaped growth of zoisite in segregations (Brunsmann et al. 2000) with several growth stages produces a lamellar appearance in sections parallel to (100) with alternating Fe rich and Fe poor lamellae.

Sector zoning was described in zoisite (Enami 1977, see also Enami et al. 2004 and back cover) in three sectors {100}, {010} and {001}, in which X_{Fe} is highest in {100} (≈ 0.09) and lower in {010} and {001} (both ≈ 0.06). Because [100] is the slowest growth direction is seems that Al is preferentially incorporated compared to Fe. In epidote, (Yoshizawa 1984; Banno and Yoshizawa 1993) the sectors are {100}, {110}, {001} and {101}, and the order of X_{Ep} is {100} ≥ {110} ≥ {001} > {101}. Sector zoning was also observed in Cr-rich epidote from quartzitic schist (Treloar 1987a,b), in epidote from high-pressure segregations (own unpublished results), and in hydrothermal epidote from geothermal fields (Bird and Spieler 2004), and might in fact be a rather common phenomenon (Banno and Yoshizawa 1993).

Oscillatory zoning is rarely observed in common metamorphic epidote; an exception is oscillatory zoning of Cr-epidote superimposed on sector zoning (Treloar 1987a). In hydrothermal epidote it is not rare. Bird and Spieler (2004) mention several references, and we analyzed for this review a Mn-bearing clinozoisite from a hydrothermal quartz vein (Baja California; sample # 81/370, Fig. 15a-d; see also back cover). The overview (Fig. 15a) shows the outer part of radially grown clinozoisite (X_{Ep} = 0.44 to ≈ 0.50 from core to rim) with an inner overgrowth of epidote (X_{Ep} ≈ 1.0). This is separated by a discontinuity, which was created by dissolution, from an outer overgrowth of epidote with X_{Ep} ≈ 0.55 to 0.85. The oscillatory zoning is present in the Fe-rich outer part (Fig. 15b), where it is dominantly Al-Fe-zoning, but also in the clinozoisite, where it shows up already in plain polarized light as a herring-bone structure (Fig. 15c). A profile of 15 zones over a distance of 25 μm shows also Mn-Fe zoning (Fig. 15d), which is, however, not completely complimentary to each other. The size of the small zones of ≈ 1–2 μm is below the resolution of the electron microprobe, but the profile shows that in general the Mn_2O_3 content varies between 0.2 and 0.3 wt%, whereas the

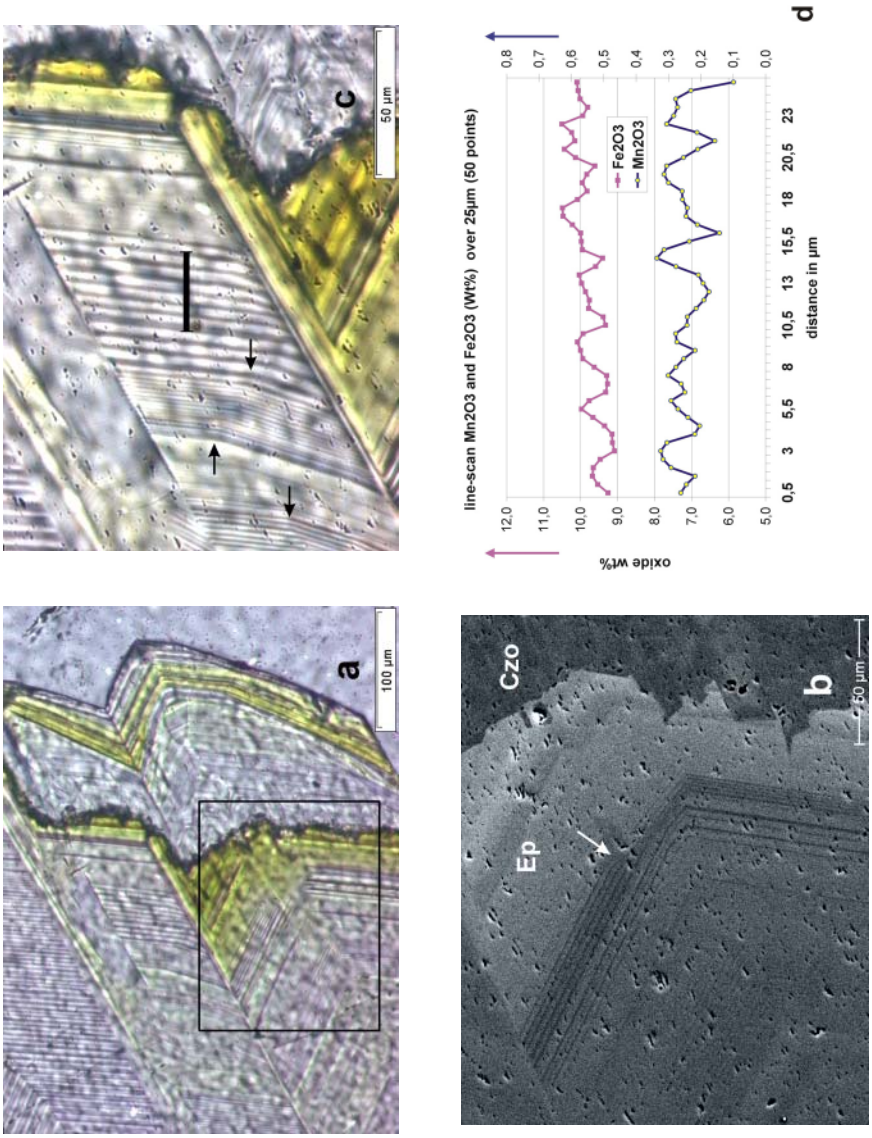

Figure 15. Oscillatory zoning in a Mn-bearing clinozoisite-epidote, from a hydrothermal quartz vein (sample 81-270, Baja California). (a) Outer part of a radially grown aggregate in quartz (qz) with a dissolution discontinuity (dark rim), outlined area is Figure (b); photomicrograph, plain polarized light. (b) Secondary electron image, showing the discontinuity, which separates epidote with $X_{Ep} \approx 1.0$ (from center to the left) from epidote with $X_{Ep} = 0.55$ to 0.85 (right part) and the oscillatory zoning in Fe-Al. Arrow points to an area where the width of five dark zones decreases from ≈ 12 µm to ≈ 6 µm. (c) Detail of an area in the crystal with $X_{Ep} \approx 0.50$ with oscillatory zoning. Line indicates line scan in Figure (d); arrows point to locations where the oscillatory zones show kinks. (d) Line scans for Fe_2O_3 and Mn_2O_3 (wt%).

differences in Fe_2O_3 content from zone to zone are ≈ 0.5 wt% between 9 and 10.5 wt%. This sample also shows interesting growth features, such as a decrease in width of five zones (arrow in Fig. 15b) from 12 μm to 6 μm, and slight kinks in the zones (arrows in Fig. 15c). There are also parts of the crystal, which are free of oscillatory zones (upper left of Fig. 15c). These features indicate that the local environment significantly influences the growth mechanisms. It is beyond the purpose of the introduction to this volume to derive a conclusion about the growth conditions from this example, but we want to emphasize that there is a potential wealth of information hidden in such phenomena.

OPTICAL PROPERTIES

Monoclinic epidote minerals

Earliest studies on the optical properties of monoclinic epidote minerals are from Brewster (1819), Klein (1874), Forbes (1896), Weinschenk (1896), Zambonini (1903, 1920, quoted from Strens 1966), Andersen (1911), Becke (1914), Goldschlag (1917), and Orlov (1926). Compilations of the optical data are from Johnston (1948), Winchell and Winchell (1962), Tröger (1982), Deer et al. (1986), Strens (1966), and Kepezhinskas (1969). Thorough and systematic studies on the relationships between optical properties and composition of the Al-Fe^{3+} solid solution series came from Myer (1966) and Hörmann and Raith (1971). The latter also compiled and re-evaluated the previously published optical data. Systematic studies on optical properties of Al-Mn^{3+} solid solutions are restricted to a study on synthetic piemontite from Langer et al. (2002). Optical data for Al-Fe^{3+}-Mn^{3+} solid solutions were published by Malmqvist (1929), Short (1933), Guild (1935), Otto (1935), Tsuboi (1936), Hutton (1938, 1940), Hirowatari (1956), Marmo et al. (1959), Nayak and Neuvonen (1963) and Ernst (1964), which were compiled, extended and systematically evaluated by Strens (1966). Below we give a brief review of the optical properties of the different monoclinic solid solutions. Based on the published data we extended and modified the well-known figures from Tröger (1982) in Figure 15.

Al-Fe^{3+} solid solutions. All members of the Al-Fe^{3+} solid solution series have *Y* parallel to [010], *X* approximately parallel to [001] and *Z* slightly inclined to [100] (Fig. 16). With increasing Fe^{3+} the indicatrix rotates around [010] and the extinction angle between *X* and [001] decreases from ~ +12° to –5° and the angle between *Z* and [100] increases from ~ +13° to +30° (Fig. 16). Fe^{3+} poor solid solutions are almost colorless in thin section whereas with increasing Fe^{3+} they become colored with the typical pistacite like yellowish to greenish colors. The pleochroism is weak to distinct and its scheme is *X* = pale yellow, *Y* = greenish yellow, and *Z* = yellowish green (Burns and Strens 1967; Fig. 16). All three refractive indices increase with increasing Fe^{3+}. This increase is strongest in $n\gamma$ and $n\beta$ and smallest in $n\alpha$. Because of this difference, birefringence ($n\gamma$–$n\alpha$) significantly increases by one order of magnitude from about 0.005 in Fe^{3+} poorest clinozoisite to about 0.05 in the most Fe^{3+} rich samples (Fig. 17). $2V_z$ increases from about 40 to 60° in Fe^{3+} poor clinozoisite to about 120° in Fe^{3+} rich clinozoisite leading to a change in the optic sign at X_{Ep} ~0.35 (Figs. 16, 17). All three refractive indices as well as the birefringence display changes in their correlation trends with Fe^{3+} content at about X_{Ep} = 0.6 thus precluding linear correlation trends as proposed by Strens (1966) and Kepezhinskas (1969). These changes are in good accordance with the results from structural refinements (see above) and reflect the change in the Fe-Al substitution from exclusively in M3 to a combined one in M1 and M3. The dispersion of refractive indices and birefringence ($n\gamma$–$n\alpha$), ($n\gamma$–$n\beta$), and ($n\beta$–$n\alpha$) increases linearly with Fe^{3+} content and is generally $v > r$. This leads to positive Ehringhaus numbers of ≤ +5 and anomalous interference colors (Hörmann and Raith 1971). Contrary, Goldschlag (1917) determined the dispersion of ($n\gamma$–$n\alpha$) for two Fe^{3+} rich epidotes with $X_{Ep} \geq 0.9$ as $v < r$. The dispersion of $2V_z$ is $v < r$ for $X_{Ep} < \sim 0.35$ and $v > r$ for $X_{Ep} > \sim 0.35$ (Hörmann and Raith 1971;

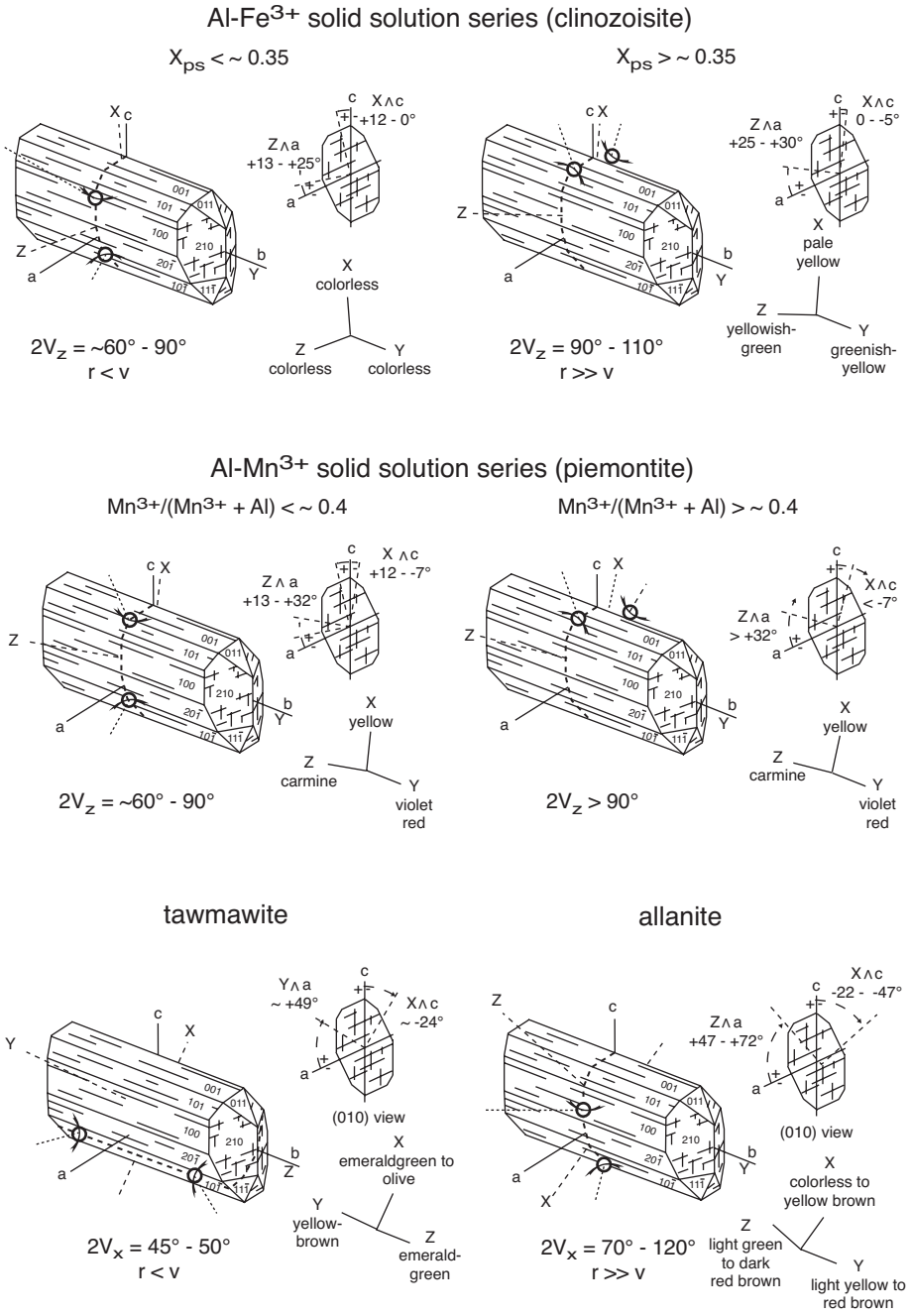

Figure 16. Optical orientation of monoclinic clinozoisite-epidote (upper part), epidote-piemontite (center), tawmawite and allanite (bottom); modified after Tröger 1982.

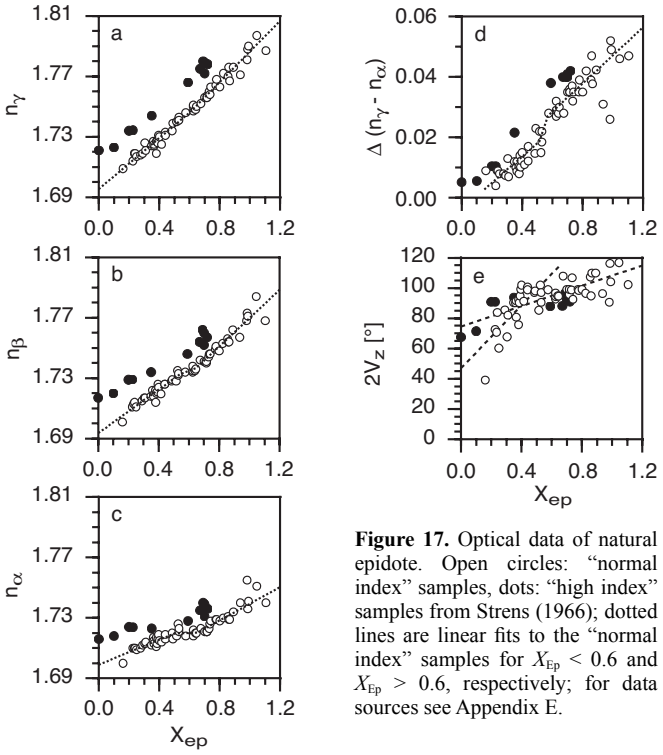

Figure 17. Optical data of natural epidote. Open circles: "normal index" samples, dots: "high index" samples from Strens (1966); dotted lines are linear fits to the "normal index" samples for $X_{Ep} < 0.6$ and $X_{Ep} > 0.6$, respectively; for data sources see Appendix E.

Fig. 16) and that of the extinction angle between *nx* and [001] is generally *r* > *v* (Klein 1874; Goldschlag 1917; Johnston 1948; Hörmann and Raith 1971).

Al-Mn*$^{3+}$ *solid solutions. Data on the optical properties of binary Al-Mn^{3+} solid solutions are restricted to the studies on synthetic samples (Anastasiou and Langer 1977; Langer et al. 2002). Langer et al. (2002) stated that the optical data from Anastasiou and Langer (1977) are questionable and especially those for *n*β are incorrect. We will therefore refer only to the data of Langer et al. (2002) who also provide electron microprobe analyses. As in the Al-Fe^{3+} solid solution series *n*β is generally parallel [010], *n*α approximately parallel to [001], and *n*γ is slightly inclined to [100] (Fig. 16). With increasing Mn^{3+} content the indicatrix rotates around [010] and the extinction angle between *X* and [001] decreases from ~ +12° to < –7°and the angle between *Z* and [100] increases from ~ +13° to > +32° (Fig. 16). Piemontites are generally strongly colored and show an impressive pleochroism in thin section with *X* = yellow, *Y* = violet red, and *Z* = carmine (Fig. 16). All three refractive indices increase with increasing Mn^{3+} content and show values comparable to those of Al-Fe^{3+} solid solutions with comparable degrees of Al substitution (Fig. 18). As in Al-Fe^{3+} solid solutions this increase is strongest in *n*γ and *n*β and smallest in *n*α, and the birefringence significantly increases up to about 0.10 for Mn^{3+} contents of 1.5 Mn^{3+} pfu. $2V_z$ is < 90° for $Mn^{3+}/(Mn^{3+}+Al)$ < ~0.4 and > 90° for $Mn^{3+}/(Mn^{3+}+Al)$ > ~0.4 leading to optical positive and negative signs, respectively (Figs. 16, 18). The change in substitution mechanism, which is evident from the X-ray data (see above), is not apparent in the optical properties, because of the small number of data; for more details about piemontite see Bonazzi and Menchetti (2004).

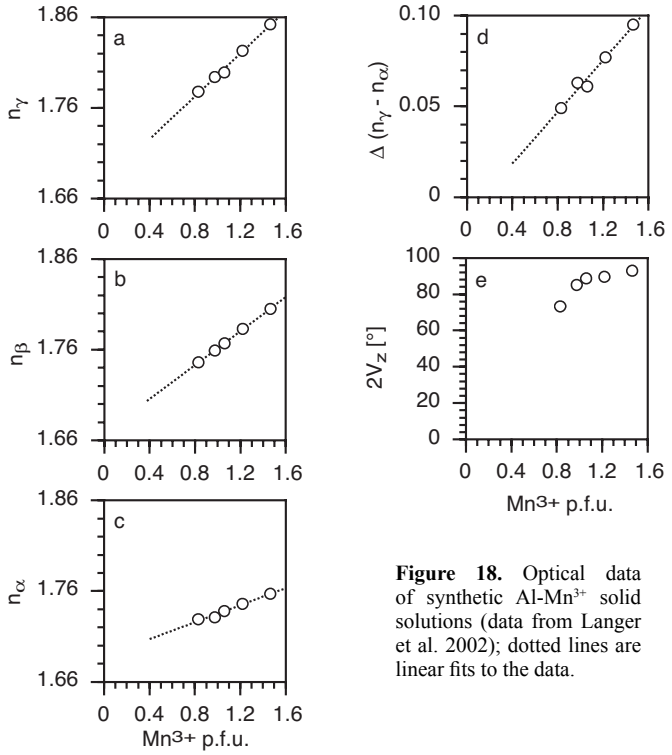

Figure 18. Optical data of synthetic Al-Mn^{3+} solid solutions (data from Langer et al. 2002); dotted lines are linear fits to the data.

Al-Fe^{3+}-Mn^{3+} solid solutions. Members of the ternary Al-Fe^{3+}-Mn^{3+} solid solution series display optical properties that are mixtures of those of the respective binary solid solutions (Strens 1966) and are thus not suitable to derive optical properties of the binary solid solutions. Tröger (1982) for example published optical properties of piemontite based on the data from Marmo et al. (1959) for Al-Fe^{3+}-Mn^{3+} solid solutions. These data indicate an optical negative sign for Mn^{3+}-poor piemontite, which is obviously wrong (see Figs. 18, 19). Likewise, his extrapolation of the refractive indices to Mn^{3+}-free composition yielded values, which are significantly higher than those derived for pure Al clinozoisite by extrapolation of the data for Al-Fe^{3+} solid solutions (Tröger 1982; see above). Published optical signs for Al-Fe^{3+}-Mn^{3+} solid solutions (Fig. 19) as function of composition in a ternary plot define a field of optical positive sign on the Al-rich side of the ternary system, and this field extends to much higher degree of substitution for Mn^{3+}-bearing solid solutions than for Fe^{3+}-bearing solid solutions. Due to the lack of data for high Fe^{3+} + Mn^{3+} solid solutions it is not clear if the stippled lines in Figure 18 meet or if the field of optical positive sign extends to the Fe^{3+}–Mn^{3+} binary. Like the other optical parameters both color and pleochroism of Al-Fe^{3+}-Mn^{3+} solid solutions are mixtures of those of the two binaries. Their general pleochroic scheme in thin section can be described as *X* = lemon or orange yellow, *Y* = amethyst, violet, or pink, and *Z* = bright red (Burns and Strens 1967; see also Bonazzi and Menchetti 2004).

Cr^{3+}-bearing solid solutions. Data on optical properties of Cr^{3+}-bearing solid solutions (tawmawite) are sparse due to the rare occurrence of this mineral. According to Tröger (1982) refractive indices and birefringence increase with increasing Cr^{3+}. They vary between $n\alpha$ = 1.695 and $n\gamma$ = 1.715 and birefringence is generally below 0.008, considerable smaller than in

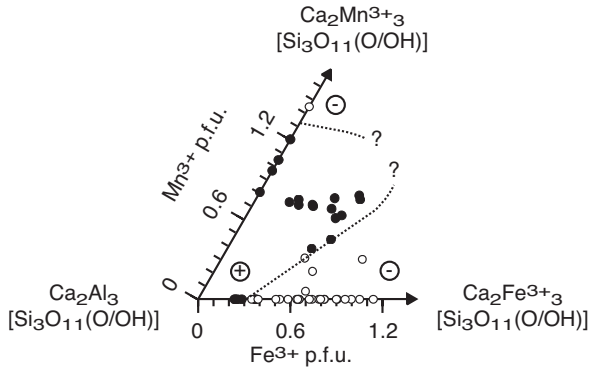

Figure 19. Optical character of monoclinic clinozoisite-epidote-piemontite solid solutions. Dots: optic positive, open circles: optic negative; dotted lines are only drawn somewhat arbitrarily for visualization; for data sources see Appendix E.

Al-Fe^{3+}-Mn^{3+} solid solutions. The most significant difference is the position of the optic axial plane, which is not orientated perpendicular but parallel to [010] with *Z* in [010] (Fig. 16). Assuming complete solid solution and thus continuous change of the optical properties along the Al–Cr^{3+} binary, the position of the optic axial plane parallel to [010] with *Z* in [010] implies that the [010] direction exhibits the strongest increase of its refractive indices with increasing Cr^{3+}. The orientation of the indicatrix, the optic axial angle, and the optic character will thus change in following manner along the Al–Cr^{3+} binary (Fig. 16, upper left and lower left): At low Cr^{3+} contents Al–Cr^{3+} solid solutions have $2V_z < 90°$ and are optically positive with *Y* in [010] comparable to Fe^{3+} poor clinozoisite. With increasing Cr^{3+} $n\beta$ in [010] significantly increases leading to $2V_z > 90°$ and an optical negative sign comparable to Fe^{3+}-rich clinozoisite (Fig. 20). Further increase of Cr^{3+} increases $2V_z$ up to 180° at which composition $n\beta = n\gamma$ and

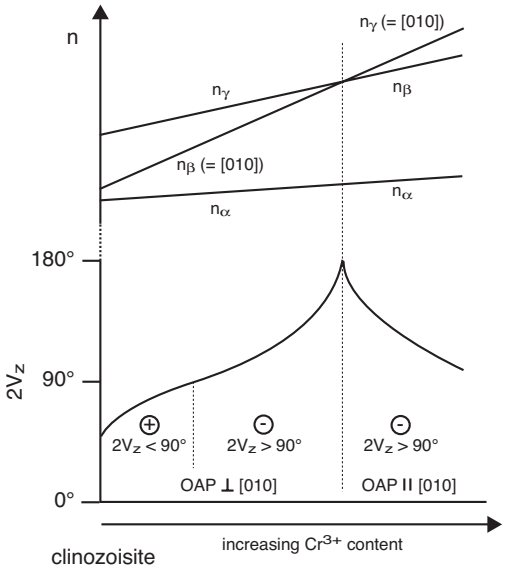

Figure 20. Change of n (upper part) and $2V_Z$ (lower part) in clinozoisite-tawmawite solid solutions and the change in orientation of the optical axial plane; the diagram is not to scale due to the small number of data.

the Al–Cr^{3+} solid solution is uniaxial negative. At still higher Cr^{3+} contents $2V_z$ will decrease and the Al–Cr^{3+} solid solution will be again biaxial negative with the optic axial plane parallel to [010] and Z in [010]. Al–Cr^{3+} solid solutions are generally pleochroic in thin section although the pleochroic schemes given in the literature significantly differ. Tröger (1982) describes two pleochroic schemes with $X = Z$ = emerald green and Y = yellow and X = olive, Y = brown, and Z = emerald green whereas Burns and Strens (1967) described $X = Y$ = emerald green and Z = yellow. The reason for this discrepancy is probably a different composition of the samples and the corresponding change of $n\beta$ and $n\gamma$. Because Burns and Strens (1967) also give the exact crystallographic directions for the refractive indices, their data are adopted in Figure 15.

Allanite and other REE-bearing epidote minerals. There are many elements, which accompany REE in a coupled substitution for Ca and Al-Fe^{3+} in epidote leading to a large chemical variety, different end members (Table 2) and very variable optical parameters. Among these elements are the radioactive elements Th and U, which lead to metamictization, and in addition to the variability caused by substitutions, different degrees of metamictization change the optical parameters. In completely amorphous metamict crystals refractive indices are minimal and double refraction is zero (see Gieré and Sorensen 2004).

Zoisite (the orthorhombic epidote minerals)

Tschermak and Sipöcz (1882) were the first who systematically studied the optical properties of zoisite. Their work was extended by Weinschenk (1896) who studied two zoisite samples with different Fe content. He already concluded that the refractive indices as well as the birefringence of zoisite increase with increasing Fe content and noticed two different optical orientations in zoisite, one with the optic axial plane parallel (010) and dispersion $r > v$ and the other with the optic axial plane parallel (100) and dispersion $r < v$ (see below). These two different orientations were later studied by Termier (1898, 1900) who named β-zoisite the orientation with optic axial plane parallel (010), Y (= $n\beta$) parallel [010] (this orientation was later termed "pseudozoisite" by Tröger 1982) according to the refractive index that lies parallel to the crystallographic b-axis (Fig. 20). The orientation with optic axial plane parallel (100), X (= $n\alpha$) parallel [010] was named α-zoisite, and later termed zoisite by Tröger 1982. Orlov (1926) compiled the early optical data for zoisite and compared them with those of the monoclinic epidote minerals. Myer (1966), who studied the variation of the optical properties with composition on five natural zoisite samples spanning the compositional range $X_{Fe} = 0.015$ to 0.14, found that the optical properties change continuously from the β-orientation to the α-orientation with increasing Fe^{3+}-content and concluded that the two optical orientations of zoisite do not represent two polymorphs. To avoid confusion with the α–β-terminology normally used for polymorphs, he emphasized to use the terms zoisite for the β-orientation and ferrian zoisite for the α-orientation (Myer 1966; Fig. 21). A detailed study on the relationship between the optic axial angle and Fe^{3+}-content was performed by Maaskant (1985) on natural zoisite samples spanning the compositional range X_{Fe} = 0.015 to 0.14, however without publishing the refractive indices.

The published data indicate that all three refractive indices increase with increasing Fe^{3+} whereas the birefringence slightly decreases (Fig. 22). The optic axial angle clearly shows the change in the optical orientation. With increasing Fe^{3+} the optic axial angle decreases from about $2V_z = 55°$ for Fe-free zoisite to $2V_z = 0°$ for about $X_{Fe} = 0.09$. Further Fe^{3+} substitution again increases the optic axial angle. At about $X_{Fe} = 0.165$ zoisite is optically neutral with an optic axial angle of 90°. At still higher Fe^{3+}-content zoisite becomes optically negative. Zoisite is normally colorless in thin section, has a strong dispersion, and displays pronounced anomalous interference colors.

Due to the low degrees of substitution by other elements the optical differences of the other orthorhombic varieties are only minor. Most noticeable is a change in color and pleochroism that accompanies the incorporation of small amounts of Mn^{3+}, Cr^{3+}, and V. Mn^{3+} bearing zoisite

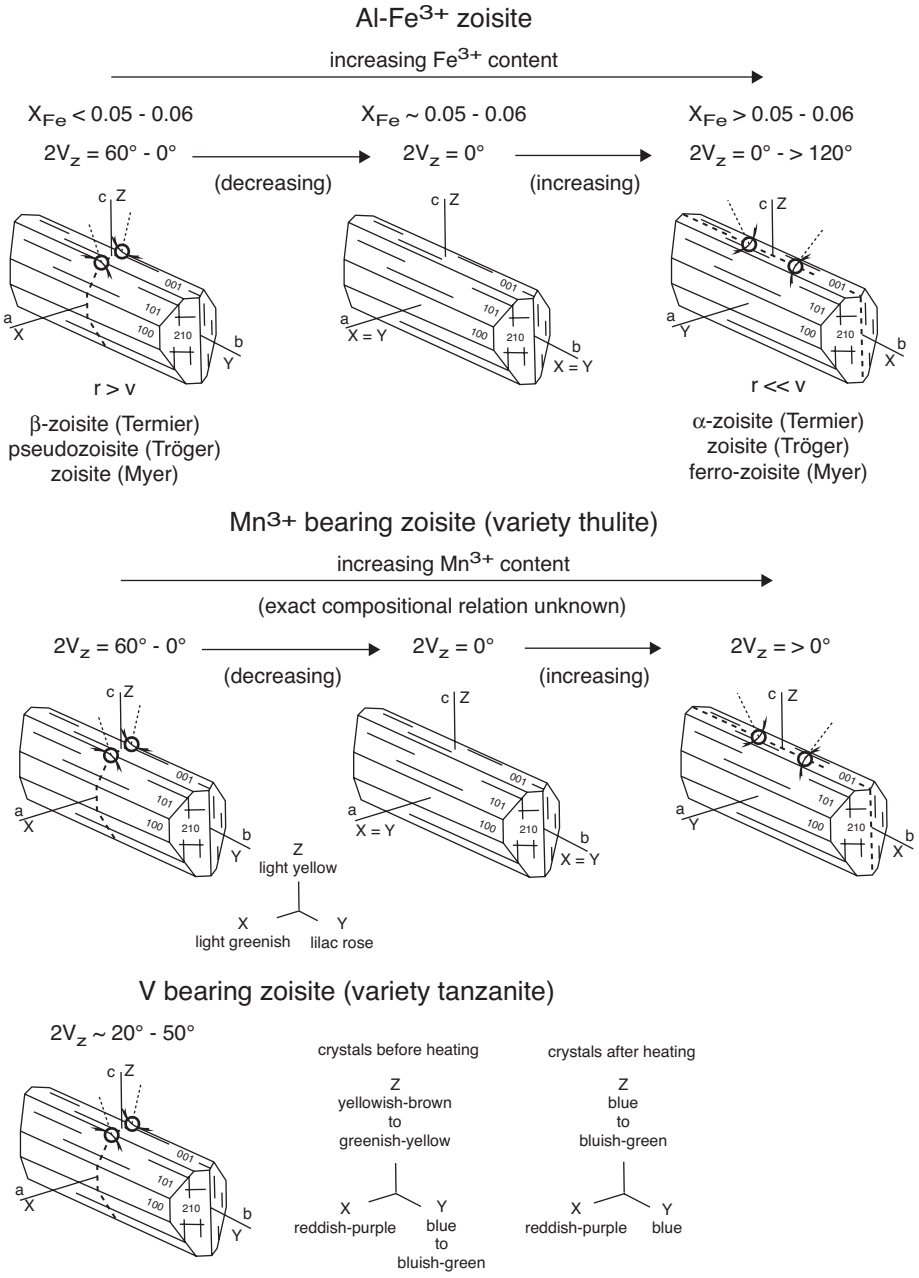

Figure 21. Optical orientation of zoisite and its Mn^{3+} and V bearing varieties thulite and tanzanite. The terminology for Al-Fe^{3+} solid solutions with the optic axial plane parallel (010) and (100), respectively, is from Termier (1898, 1900), Tröger (1982), and Myer (1966). The irreversible color change in V bearing zoisite occurs during heating above about 450°C (see text). The greenish colors in V bearing zoisite are probably due to small amounts of Cr^{3+}; modified after Tröger 1982.

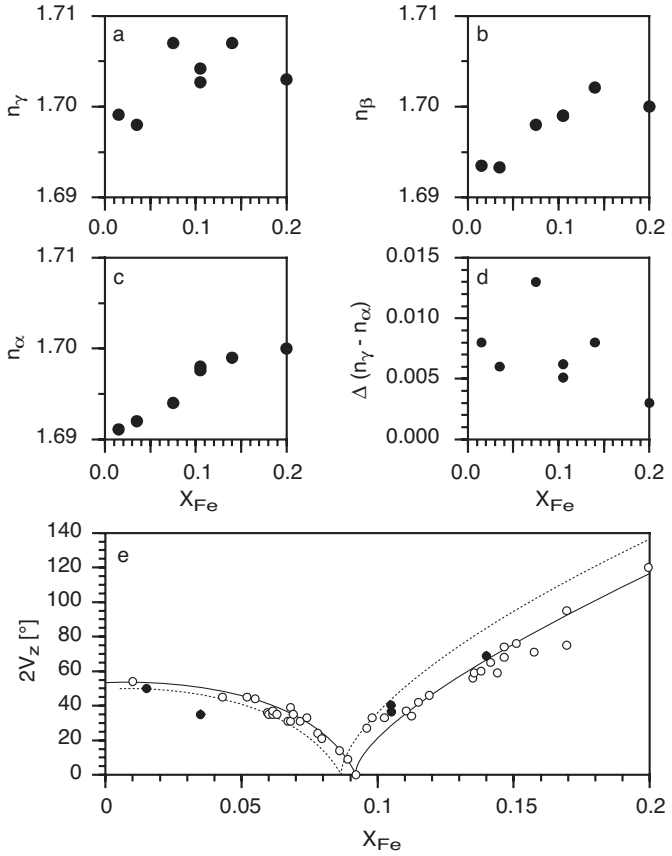

Figure 22. Optical data for zoisite; dots: data from Myer (1966), Seki (1959), and Kiseleva et al. (1974), open circles: data from Maaskant (1985) for 589 nm; solid and dotted lines in (e) are fits to the data from Maaskant (1985) for 589 nm and 470 nm (data not shown by symbols) respectively; see Appendix F.

("thulite") is violet to pink. It displays the two identical optic orientations as normal zoisite although the compositional dependence of these orientations is unknown. Its pleochroic scheme is *X* = pale yellowish green, *Y* = violet rose, and *Z* = yellowish. Cr^{3+}-bearing zoisite has the typical emerald green colors (Weinschenk 1896; Game 1954). Its refractive indices do not differ from those of Cr^{3+}-free zoisite of comparable Fe^{3+}-content (Fig. 22). Small amounts of vanadium ("tanzanite") lead to blue colors (Bank et al. 1967; Fay and Nickel 1971; Tsang and Ghose 1971; Schmetzer and Bank 1979; see below under Gem Materials). Substitution of Sr for Ca in the A sites results in a lower optic axial angle (Maaskant 1985).

Gem materials

Though epidote frequently occurs in gem quality crystals, cut stones are generally unimportant on the market. This is due to the relatively low Moh's hardness of 6.5 and the fact that beautiful color varieties with the exceptions listed below are rare (Bauer 1968). The strong pleochroism of Fe rich crystals produces a rather unattractive olive-brownish to yellowish color (Fischer 1977). Crystals from the locality Knappenwand in Tyrol, Austria have been used for faceted stones, and (Fischer 1977) gives the angles of the appropriate orientation of

the facets to obtain the best color. In the process of gem testing it was found that epidote is practically opaque to X-rays (Webster 1962).

The only variety, which is commercially important, is "tanzanite" (Anderson 1968, Hurlbut 1969), found in the Merelani area in NE Tanzania (Malisa 1987). Sapphire blue zoisite occurs in hydrothermally formed calc-silicate rocks, associated with graphitic gneiss with kyanite/sillimanite-quartz-anorthite, which were intruded by Pan-African granite pegmatites and quartz veins at ≈600 Ma. Conditions of metamorphism were in the upper amphibolite facies of ≈650°C and 0.8 GPa. The gneisses are rich in graphite and the trace elements V, U, Mo and W, and most silicates are enriched in V_2O_3 (Malisa 1987). Two color varieties exist, a brown and a blue one. Brown crystals can be converted into blue ones by heat treatment at 400 to 650°C, and most stones available on the market are heat-treated. The color change is caused by the disappearance of an absorption band in the blue part of the visible spectrum (Schmetzer and Bank 1979). Webster and Anderson (1983) note that heat treatment above 380°C must be carried out with care because the stones tend to disintegrate. Brown stones may also convert into colorless stones after heat treatment (Bank 1969). Tanzanite crystals also show bluish-green, yellow, pink and khaki colors. The pleochroism of two varieties is given in Table 4 (Schmetzer and Bank 1979). The interpretation of the cause of color was controversial; Ghose and Tsang (1971) interpreted it as V^{2+}, Schmetzer and Bank (1979) as V^{3+} and in the bluish-green variety as a combination of $V^{3+} + Cr^{3+}$, and Faye and Nickel (1971) also as V^{3+} in combination with Ti^{4+}. Zoisite crystals from this locality have been used frequently as starting material for experiments (e.g., Matthews 1985; Matthews and Goldsmith 1984; Perkins et al. 1980; Smelik et al. 2001) because they are free of inclusions and essentially pure zoisite.

Pink zoisite varieties from several localities worldwide ("thulite") are used as cabochons. Only rarely such crystals can be used as cut stones. Bank (1980a,b) described clear transparent zoisite and also clinozoisite from Norway, but this seems to be the exception.

Green zoisite from Longido Mts. (Kenya) is also important on the mineral market. The Cr-bearing zoisite forms the matrix for red corundum (ruby) crystals, and together with black amphibole, these rocks exhibit an impressive color contrast. Zoisite has X_{Fe} = 0.04 to 0.12 and up to 0.10 Cr pfu. Clinozoisite is very rarely present, has X_{Ep} = 0.48 to 0.55, and contains only up to 0.03 Cr pfu. The black amphibole is pargasite with 0.58 to 2.24 wt% Cr_2O_3. Spinel is a Mg-Fe^{2+}-Cr^{3+}-Al solid solution with generally 0.08 to 0.44 Cr pfu, rarely up to 0.9 Cr pfu. Corundum (ruby) has also up to 0.035 Cr pfu. Anorthite, which occurs in thin layers as well as in reaction textures with amphibole, is almost pure (An 98-100), except in some cores (An 85-90) and in a late generation (~An 62). The textures indicate a (? retrograde) decomposition of corundum together with amphibole and the formation of zoisite and spinel (own unpublished results). For more information concerning the trace element content and distribution see Frei et al. (2004).

Table 4. Pleochroism of untreated and heat treated "tanzanite" (Schmetzer and Bank 1979)

color variety	X//*a*	Y//*b*	Z//*c*
brown (untreated)	reddish purple	blue	yellowish brown
blue (heat treated)			blue
bluish green (untreated)		bluish green	greenish yellow
bluish green (heat treated)		blue	bluish yellow

The mottled green-pink massive variety "unakite" of epidosite (from Unaka/North Carolina) is used as cabochon (Webster and Anderson 1983), and similar material is reported from Zimbabwe and Ireland.

OCCURRENCE AND PHASE RELATIONS

Epidote minerals are stable over an extremely wide range of pressure and temperature. They are considered as typical metamorphic minerals, but are also known from igneous rocks, are very important as hydrothermal minerals and occur as detrital heavy minerals in sediments. It is not only the large range of pressure and temperature, but also the large range in composition of epidotes, which makes them important constituents in many rocks. The chemical variation concerns both the major components of crustal rocks Al_2O_3 and Fe_2O_3 and the minor and trace components Mn_2O_3, Cr_2O_3, SrO, PbO and REE. Therefore epidotes occur in rocks with a common composition as well as in rare rocks, which are enriched in the trace components such as ore deposits. However, a certain rock must not necessarily be enriched in the trace elements to stabilize epidote, it is often the preference of the epidote structure for these minor and trace elements which makes them their carrier in the accessory minerals.

Besides being major rock forming minerals epidotes are also very abundant in veins, segregations and cavities, which developed during various stages and in various shapes and dimension in metamorphic, igneous and hydrothermal rocks. This points to the fact that metasomatism and fluid-rock interaction can play an important role in the formation of epidote. Epidosite (Johannson 1937) is a rock, which consists mainly of epidote and quartz and its genesis is commonly explained as due to mass transport via a fluid phase. Epidotization—the formation of epidote from mainly feldspar—is observed in many igneous rocks during a low-temperature stage of hydrothermal overprint. They are very common in geothermal fields and in altered oceanic crust (Bird and Spieler 2004). The term "helsinkite" has also been applied to such rocks, and "saussuritization" for the process. Rosenbusch already noted in 1887 (Johannson 1937) that saussuritization is a metamorphic process, not a weathering phenomenon, and Johannson (1937) pointed to the important reaction albite + anorthite + water = zoisite + paragonite + quartz. However, this assemblage only forms at high pressure above approximately 0.8 GPa (Franz and Althaus 1977). In the presence of K, either as K-feldspar, as a K-feldspar component in ternary feldspars, or as K^+ in the fluid, muscovite-phengite instead or together with paragonite can form, CO_2 in the fluid can be fixed as carbonate, and also scapolite can be found, if Cl^- is available. Often the retrograde overprint is accompanied by brittle deformation and results in the formation of epidote in cataclastic zones (forming a rock called "unakite").

In the sedimentary environment epidote minerals have not yet been reported as an authigenic low-temperature mineral, but may already form at the high-temperature part of diagenesis. In sediments they are also important as detrital minerals and were used for provenance studies (see the common textbooks on sedimentary petrology). They can make up to 90 vol% of the heavy mineral spectrum (v. Eynatten 2003). Epidote minerals are frequently attributed to source rocks of low to medium grade metamorphism, which must be considered carefully because of the extremely large stability field for the whole mineral group. Most recent studies show that a combination of chemical composition of the epidotes and their isotope ratios (e.g., Spiegel et al. 2002) will yield a better result, because they allow to distinguish between mantle derived rocks (roughly equivalent to a source with metabasites) and crustal derived rocks (roughly equivalent to metagranitoids). The most promising approach will be to use single grain analysis in heavy mineral concentrates by laser ablation coupled with ICP MS analysis.

The minimum pressure to stabilize epidote is not known. Epidote minerals were found in shallow geothermal fields at a few hundred meters depth, suggesting a pressure of much

less than 100 MPa, and at a temperature below 200°C (Bird and Spieler 2004). On the other extreme, the maximum pressure at which zoisite is stable, is in the range of 7 GPa, far outside of what is possible even in extremely overthickened crust (Poli and Schmidt 2004). Common epidote–clinozoisite solid solutions break down in the range of 600 to 700°C, but they can be stabilized by incorporation of REE and thus allanite occurs in a variety of igneous rocks with high crystallization temperature, and has been reported from experimental studies at 1050°C at 3 to 4.5 GPa (Green and Pearson 1983; Hermann 2002). Thus from the petrogenetic point of view the epidote minerals are rather unspecific. On the other hand, they have a large potential for petrogenetic applications once their crystal chemical and thermodynamic properties are better understood. The major problem encountered by the petrologist is to distinguish between different stages of formation of epidote, especially on the retrograde path, but also on the prograde path through the peak stage of metamorphism, where complex zoning can be preserved (see also Grapes and Hoskins 2004, Enami et al. 2004). Here we give a general overview about the occurrences of epidote. For a detailed review of special members of the epidote minerals and for special localities, the reader is referred to the individual chapters of the volume, and also to Deer et al. (1986).

Al-rich clinozosite and zoisite

In igneous rocks, Al-rich clinozosite and zoisite are very rare (for Fe-rich epidote see below). The only exception is zoisite in pegmatites from high-pressure areas, which are explained as melting products of eclogites and which crystallized at high pressure. In such an environment, the concentration of Fe in the melt is very low, and when the pressure is too high for plagioclase to crystallize, zoisite (with minor amounts of clinozoisite) is the liquidus phase.

In common regionally metamorphic rocks, Al-rich clinozosite and zoisite are found mainly in two types of environments, where Ca and Al are enriched (Fig. 23). The one is in meta-igneous rocks, where the enrichment occurs in the anorthite component of plagioclase. The other one is in metasediments, where Ca and Al are enriched in the sedimentary protolith (marl and impure limestone) in carbonate and clay minerals. A third type, much less abundant but of large petrogenetic importance, is the enrichment in metamorphic blasts of lawsonite. Characteristic assemblages of clinozoisite and zoisite are therefore for type a) as inclusions in mostly Na rich plagioclase, replacing the anorthite component, b) in calcsilicate rocks of all metamorphic grades, and c) in lawsonite pseudomorphs.

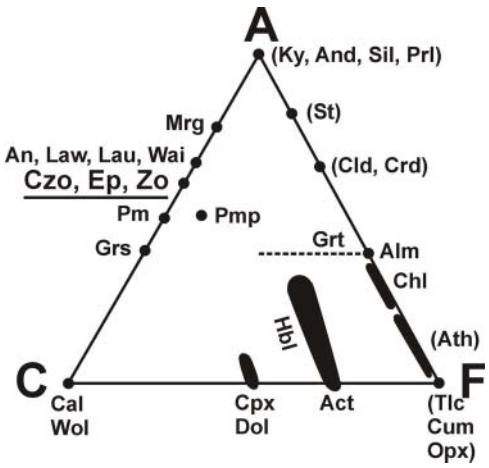

Figure 23. Simplified ACF diagram, showing the close chemical relationship of clinozoisite-epidote and zoisite with anorthite (component in plagioclase), lawsonite and Ca-zeolites. In metabasites at greenschist facies conditions, tie lines czo-chl-act-dol are stable, which are substituted at amphibolite facies conditions by plagioclase-amphibole. At eclogite facies conditions, where garnet can be rich in grossularite component, the common assemblage clinopyroxene-garnet limits the occurrence of epidote minerals. Only in compositions poor in mafic components epidote minerals are stable.

A typical occurrence for type a) is in metagabbro, especially in cumulate layers of such protoliths, and in fact clinozoisite and zoisite rich parts of metagabbro have often been interpreted as former cumulates. They are also found as part of

an inclusion assemblage in igneous porphyritic plagioclase crystals in metagranitoids. Often the distribution of the inclusion minerals mimics a former zoning of the plagioclase crystal. Because the anorthite component is not stable at high pressure due to the reaction anorthite + water = zoisite + kyanite + quartz, or albite + anorthite + water = zoisite + paragonite + quartz in many localities such occurrences of clinozoisite and zoisite are a good indication of a minimum pressure of approximately 0.7 to 1.0 GPa. Associated minerals are white mica or kyanite and quartz. Because anorthite is also not stable at a temperature below approximately 400°C due to the transformation of anorthite + water into epidote, and/or Ca-Al zeolites, margarite and sericitic white mica, the formation of inclusions in a plagioclase crystal can also be due to a retrograde metamorphism or to a hydrothermal overprint. Both processes, the decomposition of primary igneous plagioclase due to a higher pressure than in the protolith, as well as the decomposition due to a low temperature have been called saussuritization, and one should try to distinguish between them. Note however that it will be extremely difficult to distinguish between a retrograde low temperature metamorphism and a hydrothermal event, which can also be transitional to a weathering stage.

Occurrences of type b) in metasediments are found at all metamorphic grades, from low pressure subgreenschist facies rocks together with prehnite, pumpellyite up to the granulite facies where zoisite and clinozoisite occur together with spinel and corundum, in low pressure contact aureoles and also in the high and ultrahigh pressure rocks.

Occurrences of type c) are found mainly in metabasite. Lawsonite typically occurs in large blasts in former fine-grained basaltic rocks, thus creating a local chemical environment dominated by Ca and Al. If such a rock is heated and crosses the upper temperature stability limit of lawsonite it should decompose into an aggregate of zoisite, kyanite and quartz, but the association clinozoisite, white mica and quartz is much more common. Very often this heating of a rocks takes place without a penetrative deformation such that the shape relics of the lawsonite is preserved in clearly visible pseudomorphs, which have been described from many blueschist and eclogite terranes. Fe, Na and K are transported into the Ca-Al rich micro-domain of the rock, and therefore kyanite is less frequently observed in the pseudomorphs, white mica is typically paragonite or a mixture of paragonite and phengite, and clinozoisite (also depending on the local position in the center or in the rim of the pseudomorph) is rich in Fe. Spear and Franz (1986) noted such pseudomorphs inside garnet, where they are completely protected from deformation, and argued that garnet must have been stable before lawsonite broke down, and the intersection of the garnet-in reaction with the lawsonite-out reaction gives a lower pressure limit for the prograde path, a very useful interpretation for the *P-T* path of a high pressure rock.

Fe rich epidote

The formation of Fe rich epidotes requires in addition to the enrichment in Ca and Al enrichment of Fe and a relatively high f_{O_2}. They can therefore not be found in common igneous rocks of basaltic-andesitic composition, where f_{O_2} is generally low, and where also plagioclase is stable instead of the clinozoisite component in epidote. Enrichment of Fe (relative to Mg) in an igneous rock with high Ca and Al contents is typical for granodiorite-granite, and epidote minerals are considered as primary igneous phases in such rocks (see Schmidt and Poli 2004). If, however, the epidote minerals are relatively rich in REE, this stabilizes the epidotes towards high temperature and also towards other compositions, where epidote minerals are normally absent, such as andesite (Gieré and Sorensen 2004). Epidote minerals are also not typical in metapelite with low Ca content, but may occur in metapsammite, especially in metagraywacke. Fe rich epidotes are also not typical for metamorphosed impure limestone and marl, because Mg generally dominates in these rocks.

In rocks with the appropriate composition and f_{O_2} epidote may form at pressure-temperature conditions, where the anorthite component in plagioclase is not stable. The most

common rock type is metabasite, i.e. a rock of basaltic-andesitic composition, either as a volcanic, subvolcanic, plutonic or pyroclastic igneous rock or volcanoclastic sediment, which is dominated by plagioclase and mafic minerals. Starting the discussion at surface conditions and going to high-grade metamorphism, in such rocks epidote can form even below very-low grade (<200°C, Bird and Spieler 2004) metamorphism. Associated Ca minerals are zeolites, grossularite and carbonate together with chlorite and quartz (see ACF diagram Fig. 23). Disequilibrium or only local equilibrium in small domains is the rule rather than the exception. In the lowermost greenschist facies the typical assemblage is epidote + chlorite + albite + quartz + carbonate. Epidote together with chlorite is a common constituent of pseudomorphs after mafic igneous minerals pyroxene and amphibole. The Al component for epidote is derived from breakdown of nearby plagioclase, and mass transfer on the grain scale is mainly from plagioclase to the mafic crystallization site. Note that in a coarse grained protolith it is of course possible to have both processes, the formation of Fe-rich epidote in mafic micro-domains as well as the formation of Al-rich clinozoisite or zoisite in Ca-Al rich micro-domains (plagioclase) present in the same thin section, as the product of the same mineral forming process. Only at sufficiently high temperature or strong deformation of the rock, equilibrium on a larger scale can be achieved.

The two dominant reactions, which produce more epidote in such a rock with heating, are chlorite + calcite = epidote + dolomite, and chlorite + dolomite = epidote + actinolite (Fig. 23). In the upper greenschist facies, transitional to the amphibolite facies the modal amount of epidote starts to decrease by continuous reactions of the type epidote + chlorite + quartz = Al-rich amphibole + anorthite (component in plagioclase) + H_2O (Fig. 23). However this transition is very sensitive to total pressure (note that Fe rich epidote is a dense mineral with a density of up to 3.5 g/cm^3) and also to f_{O_2}. At high P_{tot}- f_{O_2} epidote is favored, giving rise to the epidote-amphibolite facies (Spear 1993) between approximately 0.4 GPa/500°C and 1.1 GPa/650°C. For more details see Grapes and Hoskin (2004). Epidote minerals are common major rock-forming minerals in blueschist facies and in eclogite facies rocks (see Enami et al. 2004). The transition from greenschist to blueschist facies is given by the reaction actinolite + chlorite + albite = epidote + glaucophane + quartz, which can be written as a water-conserving reaction when the Tschermaks exchange vector $Al_2M_{-1}Si_{-1}$ is considered for amphibole and chlorite (Spear 1993). The transition from blueschist to eclogite facies is dominated by the lawsonite breakdown (with or without jadeite) to epidote minerals. At the *P-T* conditions of the eclogite facies, epidote minerals are stable, but their occurrence is chemically restricted because the common assemblage clinopyroxene + garnet (which can be rich in grossularite component, Fig. 23) covers a wide range of composition. Only in rocks that are relatively rich in Ca and Al epidote will be part of the assemblage (Spear 1993). At granulite facies, epidote is absent in common metabasite.

Metasomatism

Alternatively, the appropriate composition in the Ca-Al rich system as well as in the system rich in Fe^{3+} can be achieved by mass transport. Starting from plagioclase as a common precursor mineral it can be transformed by the model reactions

3 anorthite + 1 Ca^{2+} + 1 CO_3^{2-} + H_2O = 2 zoisite + 1 CO_2

3 anorthite + 1 Ca^{2+} + 2 Cl^- + 2 H_2O = 2 zoisite + 2 HCl

3 anorthite + 1 Ca^{2+} + 2 F^- + 2 H_2O = 2 zoisite + 2 HF

(see Klemd 2004). In these reactions, the Ca component can easily be transported as a $CaCO_3$ or as a $CaCl_2$ bearing solution. Fluorine is also a likely metasomatic agent, but will most probably result in the formation of fluorite. The equilibria indicate that in general the formation of epidosite requires Ca-metasomatism, with a low CO_2 and low HCl content in

the fluid, i.e. with a low acidity (see Bird and Spieler 2004). Note that the reactions can also be used to describe the formation of zoisite and epidote inclusions inside plagioclase by mass transport on the thin section scale. The decarbonation reactions can be so important that CO_2 from this source was actually mined in the Salton Sea geothermal field from 1934 to 1954 (see Bird and Spieler 2004).

During contact metamorphism-metasomatism, especially in a situation where at the contact of an igneous body to limestone the typical skarn assemblages formed, model reactions for the Al-free hypothetical endmember are

$$2 \text{ calcite} + 1.5 \text{ hematite} + 3 \text{ quartz} + 0.5\ H_2O = 1\ Ca_2Fe_3Si_3O_{12}(OH) + 2\ CO_2$$

and

$$2 \text{ calcite} + 1 \text{ magnetite} + 3 \text{ quartz} + 0.5\ H_2O + 0.5\ O_2 = 1\ Ca_2Fe_3Si_3O_{12}(OH) + 2\ CO_2$$

In such a case the assemblage carbonate-oxide can be transformed into epidote component with a SiO_2 rich aqueous solution. Klemd (2004) gives examples for such reactions involving anorthite or grossularite, which represent the Al component in marl-limestone mixtures. Fe^{2+} can also be present in the starting assemblage in carbonate or silicate, and many important metasomatic reactions are redox equilibria.

Alternatively, Fe may be the metasomatic agent as a late stage chloridic solution from an acid igneous rock

$$2 \text{ calcite} + 3\ FeCl_3 + 3 \text{ quartz} + 5\ H_2O = 1\ Ca_2Fe_3Si_3O_{12}(OH) + 9\ HCl$$

In summary, metasomatism of Ca, Si and/or Fe may be responsible for epidote formation.

The occurrence of epidote minerals in open cavities and druses, in veins and quartz-carbonate segregations of very variable shape and mineral association is different from metasomatism. In this case the fluid did not only transport specific components for a metasomatic solid-fluid reaction, but all components to precipitate the minerals. The very common occurrence of all types of epidote minerals, Fe-poor zoisite to Fe-rich epidote, in veins and segregations points to the fact that Al as a major component must be transported via a fluid phase and can not be considered as immobile. In summary, metasomatic reactions that form epidote minerals can be explained as mass transport of all major elements essential for epidote, Ca, Al, Fe and Si.

Miscibility vs. miscibility gaps

One of the interesting and controversial discussed questions in research about the epidote minerals is that of immiscibility along the (monoclinic and orthorhombic) $Al\text{-}Fe^{3+}$ solid solution join. This subject is discussed in detail in Grapes and Hoskins (2004) for natural occurrences and in Poli and Schmidt (2004) from the experimental point of view. Gottschalk (2004) presents a calculated phase diagram based on newly derived thermodynamic data. The conclusions drawn from experimental studies and investigations on natural epidote minerals are not unequivocal. Experimental studies by Fehr and Heuss-Aßbichler (1997), Heuss-Aßbichler and Fehr (1997), Brunsmann (2000), and Brunsmann et al. (2002) point to two solvi along the $Al\text{-}Fe^{3+}$ solid solution join. Strens (1963, 1964), Hietanen (1974), and Raith (1976) provide good evidences for miscibility gaps of variable extend along the $Al\text{-}Fe^{3+}$ solid solution join from natural epidote parageneses (see also Grapes and Hoskin 2004). Contrary, Enami et al. (2004) and Bird and Spieler (2004) describe clinozoisite-epidote compositions from blueschist facies and geothermal clinozoisite-epidote occurrences, respectively, that lie within the proposed miscibility gaps and interpreted these as pointing to complete miscibility. However, it is generally accepted that a two-phase area ("two-phase loop") between clinozoisite and zoisite exists for the transition from the monoclinic to the orthorhombic

polymorphs (Gottschalk 2004, his Fig. 21). At 0.5 GPa, the equilibrium temperature for the clinozoisite-zoisite transition in the Fe-free system is about 125°C. Above 730°C, there is continuous solid solution between disordered clinozoisite and disordered epidote; intermediate clinozoisite (X_{Ep} = 0.5) starts to order, and at ≈630°C two solvi start to open towards lower temperature. The situation can be compared with the jadeite-omphacite-diopside system or with the calcite-dolomite-magnesite system. The diagram, however, does not include possible complications like the potential intersection of the low Fe solvus with the two-phase area (see Poli and Schmidt 2004, their Fig. 5). The position of the solvi is quite sensitive to the chosen values of the Margules parameters, and it is possible that at 200 to 400°C the low Fe solvus intersects the two phase loop and changes the phase relations as shown schematically by Franz and Selverstone (1992).

The position of the proposed solvi is a strong function of the ordering in epidote. This may explain why in many low temperature environments, such as geothermal fields, a large range of compositions inside the theoretical solvi are found (see Bird and Spieler 2004). Metastable formation of disordered clinozoisite-epidote seems very likely to occur in a hydrothermal environment. Also small amounts of other components such as Sr, Mn, REE, Cr etc. will change the position of the solvi significantly, first by a change in the thermodynamic parameters, and also by their possible influence on the order-disorder behavior. This may explain the contradictory results from the natural occurrences. Not much information is available on the question of miscibility gaps in other systems, such as the Mn-bearing epidote minerals (Bonazzi and Menchetti 2004) and REE-bearing epidote minerals (Gieré and Sorensen 2004).

MORPHOLOGY, TWINNING AND DEFORMATION

Morphology, growth and dissolution

Freely grown epidote and zoisite crystals generally form elongated prisms, where the long axis is the *b*-axis, or platy crystals with the plates in the *b*-*c* plane (note that in old literature one might find for zoisite the orientation with the long axis = *c,* such that $a_{morph} = c_{X\text{-}ray}$; $b_{morph} = a_{X\text{-}ray}$; $c_{morph} = b_{X\text{-}ray}$; Game 1954). Therefore the relative growth velocities are *b*>>*c*>*a*. The fastest growth direction *b* is the direction of the octahedral chains, *a* is the direction in which the building units of octahedral chains are connected by the large A sites. An overview of the common euhedral crystal shapes of epidote, piemontite, allanite ("orthite") and zoisite is given by Goldschmidt (1916) who lists 372 crystal drawings of different forms of epidote and 18 of zoisite (Goldschmidt, 1923; Fig. 24). Common forms of the terminal faces of epidote are {210}, {011} and {111} (Fig. 25a). For the prism faces the common forms are {001}, {101}, {201}. Striation parallel to the long (= crystallographic *b*) axis due to subordinately developed {301} up to {801} is frequent. Striation of the prism faces is a rather regular alternation of two different {*h*0*l*} faces with mostly sharp edges (Fig. 25c). However, this is not always the case, and the edges may show systematic etch phenomena, which indicate that one of the faces is less stable (Figs. 25d,e,f). Scanning electron microscopy of single crystals of epidote (Fig. 25b) show that also terminal faces can be striated. Etching on the terminal faces is frequently observed (Figs. 25g,h) both in a regular (g) and an irregular (h) shape. Etching also occurs on the prism faces (Fig. 25i), where it can be confused with striation due to alternating faces.

Allan and Fawcett (1982) observed that faces in the [010] zone of synthetic zoisite (synthesized at 0.5 GPa, 500 to 700°C) are striated due to rapid growth, when the rate of spreading of surface layers by addition of material in steps is a slow process relative to the rate at which new layers nucleate. They also demonstrated in their study that zoisite is preferentially dissolved parallel to the *b* crystallographic direction, as expected from the Law of Bravais (i.e. the rate of dissolution in a particular direction is inversely proportional to

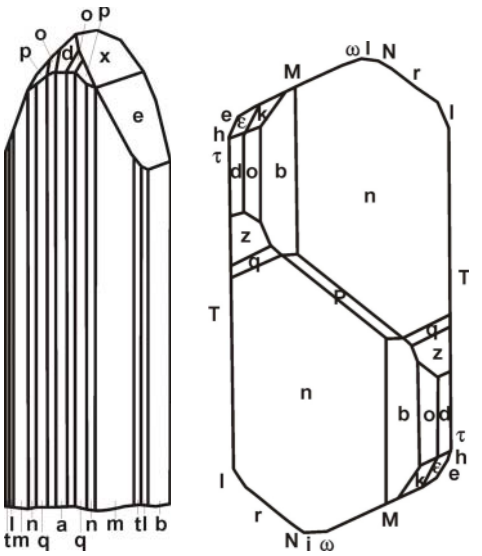

Figure 24. Crystal drawings for zoisite (*left*) and epidote (*right*); redrawn from Goldschmidt (1916, 1923).

the lattice dimension in that direction). This observation agrees with that shown above (Fig. 25i) that etching in natural crystals occurs parallel to *b*. In an experimental study using a natural zoisite (var. "tanzanite") at 650°C to 800°C/ 0.1 to 0.2 GPa, Matthews (1985) observed preferred dissolution on the terminal faces which produced saw-tooth shaped structures and in an advanced stage rod-like structures (his Fig. 6b,c,e). Etching (resorption) and subsequent growth of clinozoisite parallel to (100) was observed in pegmatitic zoisite from eclogites of the Münchberg area (Franz and Smelik 1995), which led to lamellar zoisite-clinozoisite intergrowths. Heuss-Aßbichler and Fehr (1997) interpreted a saw-tooth shape of synthetic epidote-clinozoisite prisms as a result of etching of the terminal faces and subsequent growth on these etch pits. Brandon et al. (1996) determined the epidote dissolution kinetics to constrain the rates of granitic magma transport.

Epidote grains as rock forming minerals often have a less distinct elongated form. Euhedral crystals are less common, but clinozoisite and zoisite, especially as small inclusions in plagioclase, often show well-developed platy crystals. Porphyroblast and poikiloblasts are common. Zoisite, epidote and piemontite may show radially grown prismatic crystals (Tröger 1982), especially when formed hydrothermally, zoisite from segregations often has a fan shape (Brunsmann et al. 2000), interpreted as a result of rapid growth. Synthetic zoisite (Allan and Fawcett 1982; Matthews and Goldsmith 1984; Liebscher et al. 2002) and epidote (Heuss-Aßbichler and Fehr 1997) varies from needle-shaped to prismatic and tabular.

Perfect cleavage in zoisite is parallel to (100), imperfect cleavage parallel to (001) (Tröger 1982; Deer et al. 1986) consistent with relative weak bonding at the A sites. In epidote cleavage parallel (100) is only weak, whereas cleavage parallel to (001) is perfect, due to the fact that the M3 at the octahedral chains alternate in two directions and therefore hinder a perfect cleavage in (100).

Figure 25 (*on facing page).* (a) SEM micrograph of the terminal faces of a single crystal of clinozoisite (X_{Ep} = 0.28; analyses see Smelik et al. 2001) from Untersulzbachtal, Tyrol/Austria. (b) Enlarged part of a (lower arrow), showing rare striations on a terminal face. (c) SEM micrograph of a striated prism face of an epidote crystal (X_{Ep} = 0.88; analyses see Smelik et al. 2001) from Knappenwand, Tyrol/Austria, with generally sharp edges between the two differently developed {*h*0*l*} faces; note however the irregular feature on the edge in the upper left. (d) SEM micrograph of a striated prism face of a clinozoisite-epidote crystal (X_{Ep} = 0.48; analyses see Smelik et al. 2001) from Gilgat/Pakistan with etch phenomena. (e) Enlarged part of Figure d (lower center), showing the transition from an unstable (left part) to a stable {*h*0*l*} face. Note the transition from elongated etch pits in the right to arrow-like shapes and to crystallographically bound large steps. (f) Enlarged part of Figure d (upper right), showing the transition from an unstable (right) to a stable {*h*0*l*} face. Note the difference to (e) – preferred etching of the unstable face leaves step-like forms and elongated rods. *(continued on following page)*

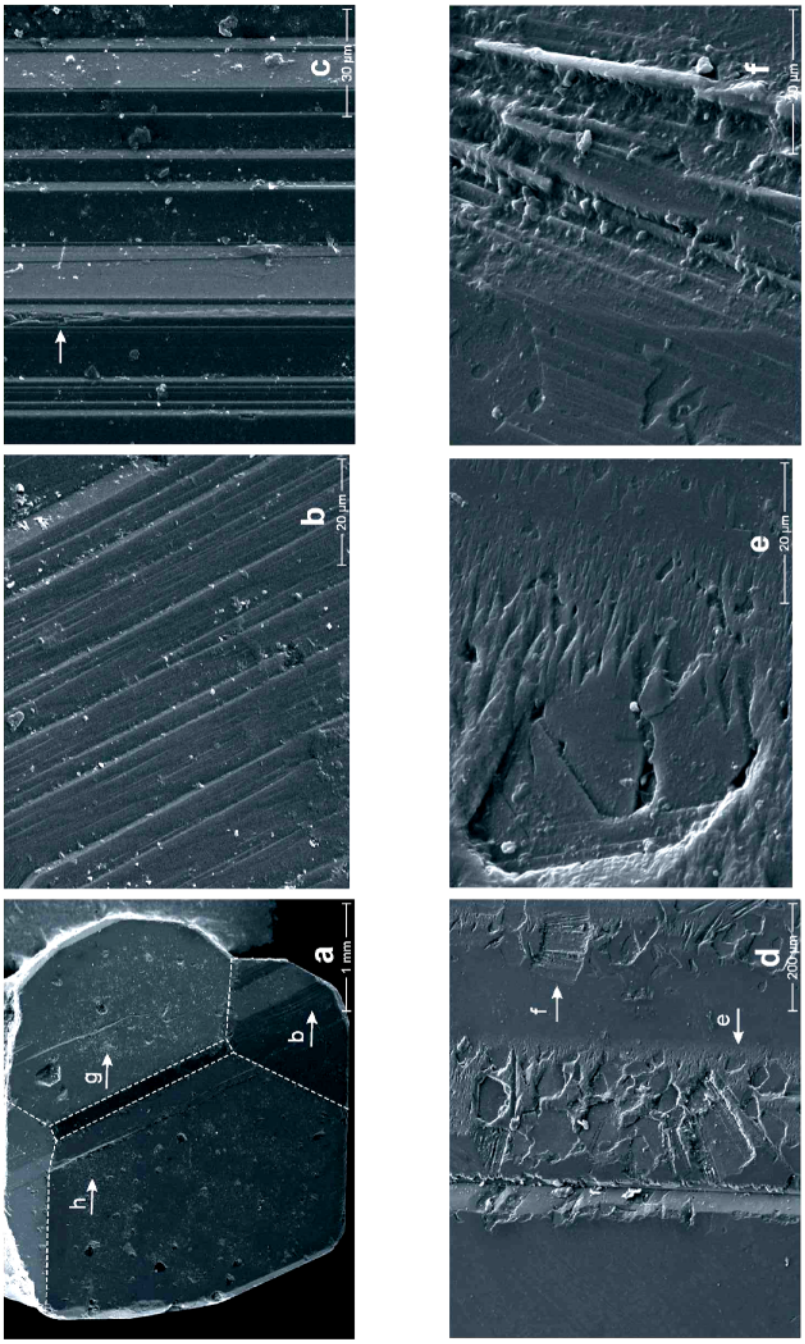

Figure 25. *caption on facing page*

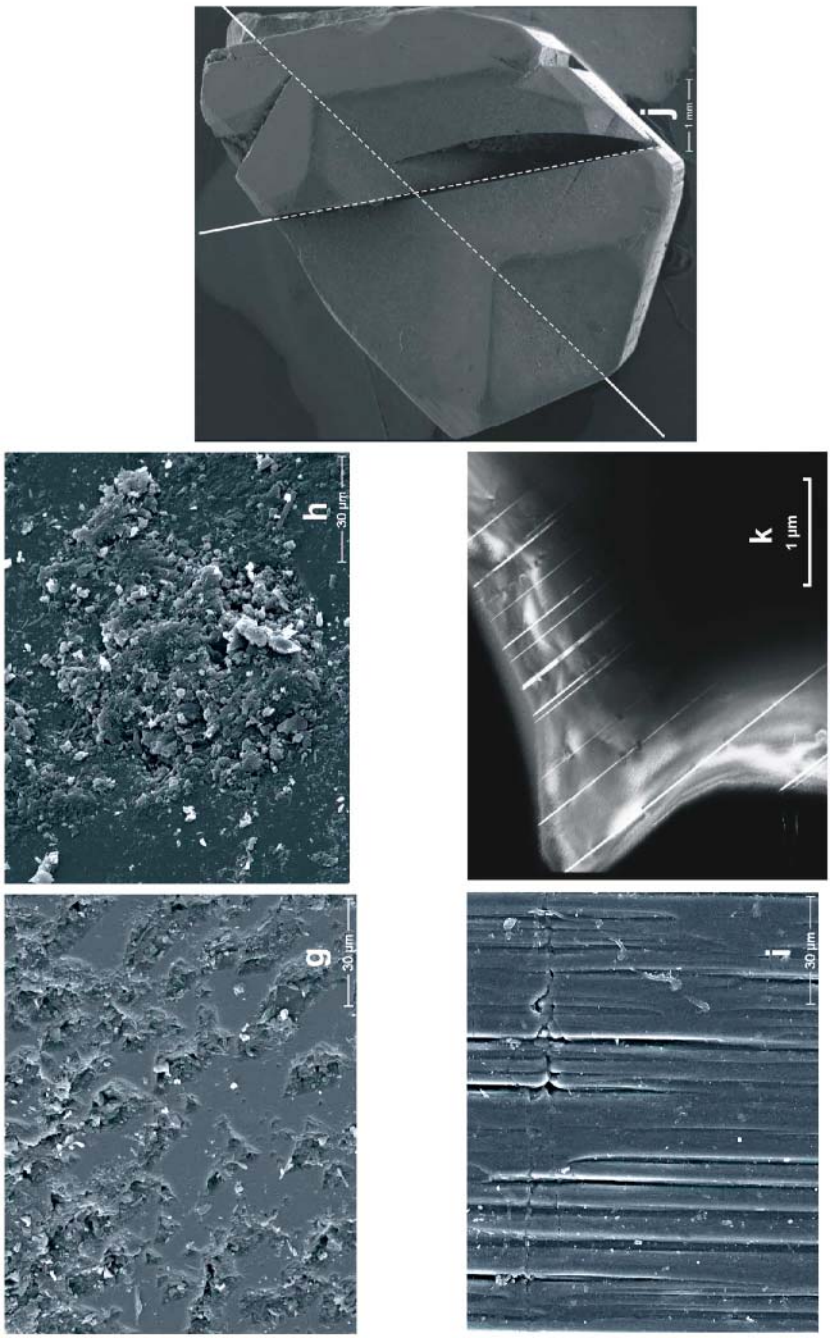

Figure 25 continued. *caption on facing page*

Twinning

Both Tröger (1982) and Deer et al. (1986) list lamellar twinning in epidote as "not common", with the twin plane in (100), in allanite also rarely in (001), no twinning in zoisite. Own observations show that freely grown hydrothermal epidote crystals from certain localities such as the Knappenwand (Austria) are very often macroscopically twinned. Figure 25j shows the terminal faces of such a twin. The crystal also shows the phenomenon of parallel intergrowth, which is visible similarly as the twinning as incised terminal faces. In thin section parallel to the crystallographic *b* axis of such crystals the lamellar character of this twinning can be seen. Ray et al. (1986) observed in TEM investigations from a variety of epidote crystals with different Fe content also that growth twins are very common in freely grown euhedral crystals. As a rock-forming mineral, epidote may show simple and more rarely lamellar twinning in thin section, but it is not a good diagnostic feature. Twins are probably growth twins, because they occur in freely grown undeformed crystals.

TEM investigations (Müller, Darmstadt, pers. comm. 2003) on minerals from a strongly deformed eclogite body of the Frosnitztal/Tauern Window (Austria) indicate mechanical twinning with the twin lamellae parallel (100) and the twin law *m* parallel (100). Width of the twin lamellae varies from 40 nm down to 0.8 nm, which corresponds to a single elementary period. Distances are irregular between 30 nm and 0.5 μm (Fig. 25k).

Deformation behavior

Little is known about the behavior of epidote minerals during deformation. Field observations show that it is relatively rigid. Epidote rich layers in a matrix of chlorite-amphibole-plagioclase show a strong competence contrast at deformation conditions of upper greenschist to lower amphibolite facies, and are boudinaged (Fig. 26a). In contrast, layers of epidote in an eclogite are harmonically folded together with pyroxene-garnet rich layers and quartz-rich layers at approximately 600°C/2 GPa (Fig. 26b). The fold shapes do not show great differences indicating a similar rheological behavior similar for epidote and pyroxene-garnet aggregates. Masuda et al. (1990, 1995) investigated the rheological behavior of piemontite, which is probably very similar to epidote, compared to quartz and albite. Piemontite prisms define the lineation and stretching direction of quartz-rich schist. The crystals are micro-boudinaged, i.e., cracked perpendicular to the elongation of the prisms [010] and torn apart, and the interstices are filled with quartz and albite. The deformation was of nearly pure shear type, no rotation of the piemontite crystals into the stretching direction was found, and the deformation temperature was above that of the brittle-plastic transition of albite. No ductile deformation was apparent at the edges of the sharp fracture planes of piemontite, consistent with the conclusion that epidote minerals are significantly more rigid than feldspar.

In thin section, apart from cracking mentioned above, potential development of subgrain boundaries, kinking and bending have been observed (Fig. 27). Monomineralic layers of epidote frequently show grains with low misorientation angles, possibly representing subgrain boundaries (Fig. 27a), oriented approximately parallel to the cleavage {100} and {001}.

Figure 25 continued (*on facing page).* (g) Enlarged part of Figure a (right large face) with regular etch pits. (h) Enlarged part of Figure a (left large face) with irregular etch pits. (i) Etch pits on prism face of an epidote crystal from Sustenpass/Switzerland; note the oblique bending at the end of the pits and their connection with crack-like features (center, upper part). (j) SEM micrograph of terminal faces of a twinned epidote from Knappenwand, Austria (88 mol% Ep) viewed almost perpendicular down the crystallographic *b* axis. Twin plane (100) runs from lower left to upper right (dashed line); the almost vertically running line separates parallel intergrowths of epidote crystals, marked by an open space. A similar parallel intergrowth is seen in the upper right (not marked by dashed line); composite of four individual pictures. (k) TEM micrograph of mechanical twinning of clinozoisite (sample F 146; see Müller et al, in press, for more information about the sample) from an eclogite body; the width of the twin lamellae are from 40 nm down to 0.8 nm, the width of one elementary period in (100); photo by courtesy W. Müller, Darmstadt.

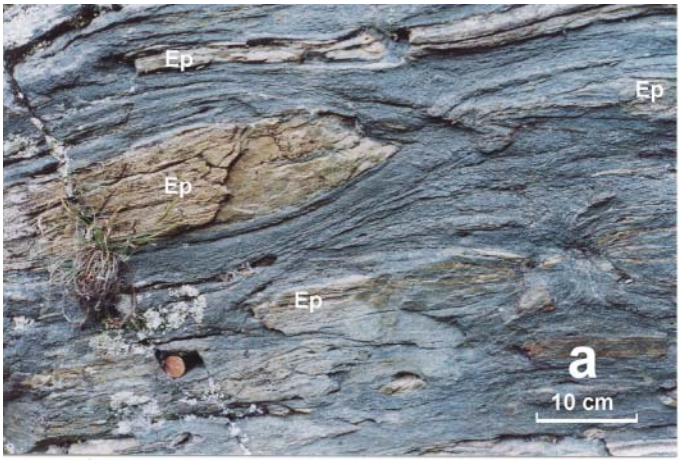

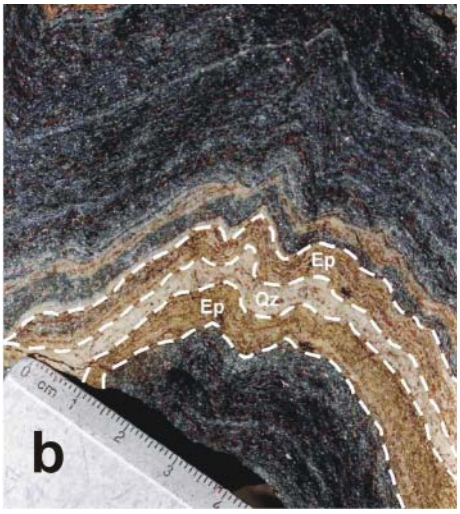

Figure 26. Deformation of epidote-rich rocks. (a) Boudinaged epidote rich layers in a greenschist; Upper Schieferhülle, Frosnitztal, Tauern Window/Austria. (b) Harmonic folding an in a layered eclogite; outlined are two layers of clinozoisite-epidote (Ep) separated by a quartz layer (Qz); upper and lower part is garnet-omphacite dominated rock. Eclogite Zone, Frosnitztal, Tauern Window/Austria).

However, the misorientation may also be due to microfracturing. Recrystallization has not been observed as a typical feature, but along cracks and subgrain boundaries, a few differently oriented small grains develop. Ray et al. (1986) also found polygonal subgrains with subhedral outlines dominated by the cleavage planes, as determined by TEM investigations. Dislocations can be observed, some of which are partials trailing stacking faults. These are inclined but their orientation is consistent with (100) planes. Partial dislocations form the subgrain walls. No fine scale multiple twins were found, but Müller (pers. comm. 2003; see Fig. 25k) observed mechanical twinning as a response to very strong deformation in epidote from a small eclogite body near to a shear zone in the Tauern Window.

Zoisite from sheared segregations in metabasite rocks (Lower Schieferhülle Tauern Window, Brunsmann et al. 2000) are rotated with their long axis into the foliation and, depending on the orientation, stretched in [010] or show bookshelf gliding on the (100) cleavage planes. These large crystals also show kinking with the kink axis [010] and the kink plane (001), and shearing parallel to (010). The same type of kinking was observed by

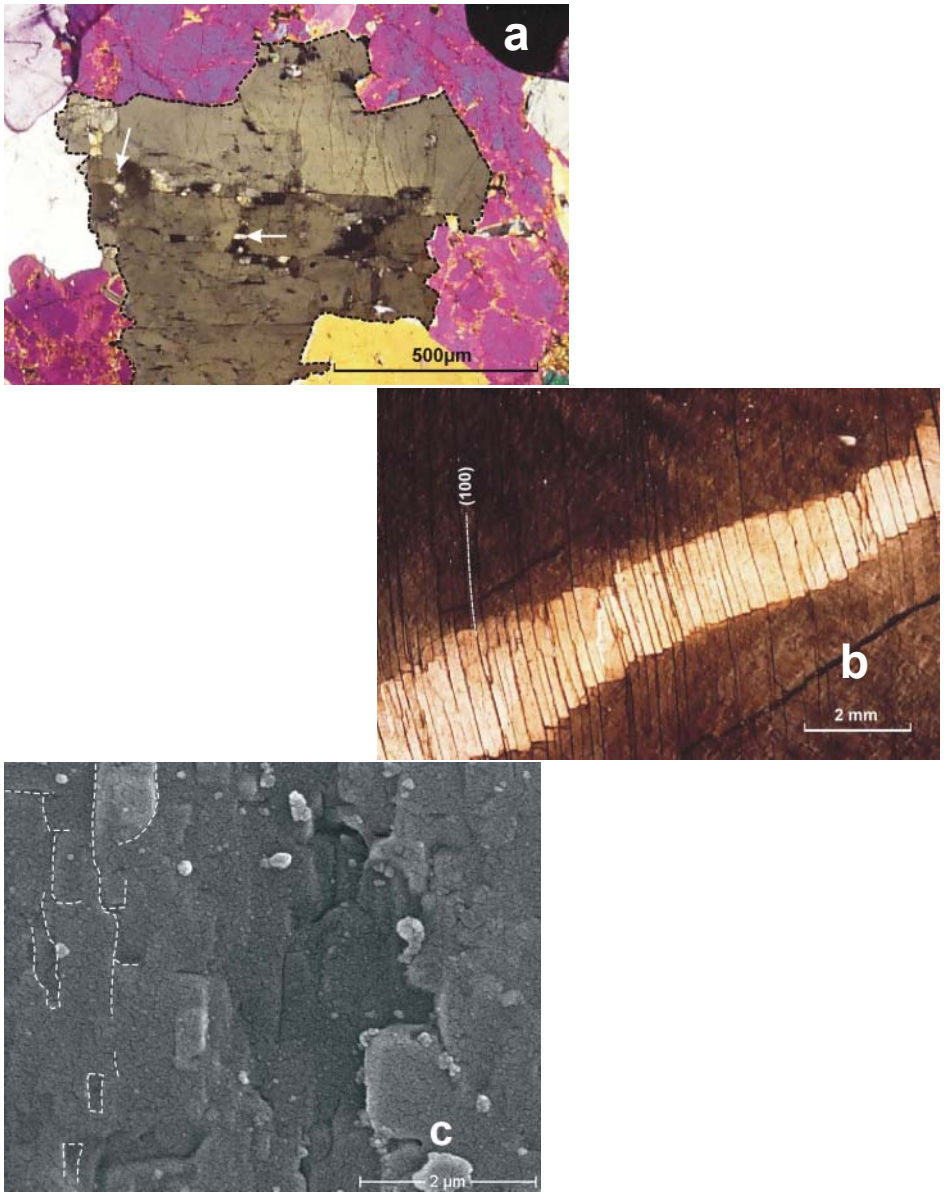

Figure 27. Deformation of epidote minerals on a microscopic scale. (a) Subgrain boundaries in epidote oriented approximately parallel to the cleavage; sample # 1427 Schriesheim, Odenwald/Germany, photomicrograph with crossed polarized light. (b) Kinkbands and book shelf gliding parallel to (100) with the kink axis [010] in zoisite; sample HU93-8 from Sterzing, Tauern/Italy; photomicrograph with crossed polarized light (c) SEM photograph of the concave upward bent cleavage plane (100) of zoisite (sample HU93-8), oriented perpendicular to the electron beam, with the axis of bending east-west, and the elongation (*b*) axis north-south. The plane shows a rough surface, structured by approximately rectangular domains in the size of 1 µm × 0.2 µm (outlined in the left part of the figure), which are slightly tilted against each other. *(continued on following page)*

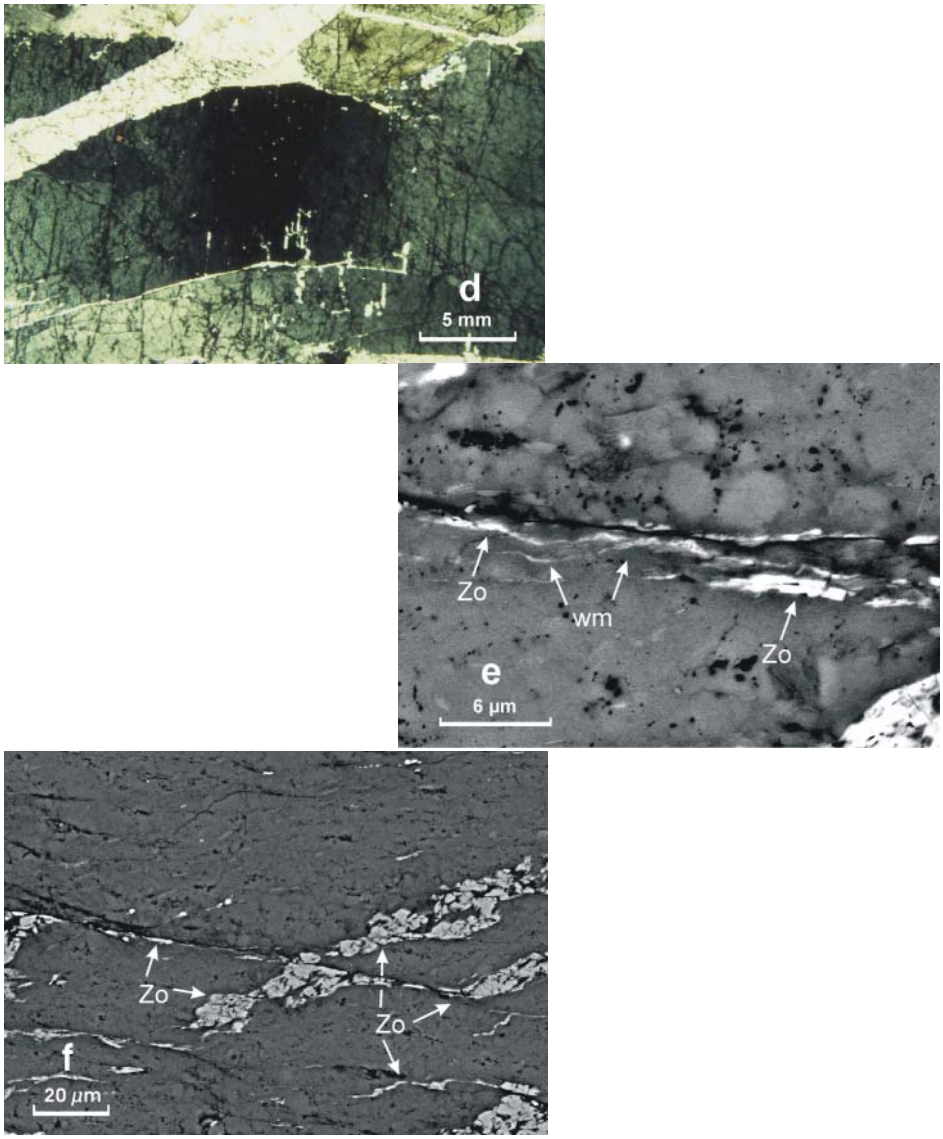

Figure 27 continued. (d) Bent zoisite crystal (grey to dark grey) with undulose extinction (white = plagioclase) from a deformed pegmatite (sample # 84-3, Weißenstein, Münchberg Massif, Bavaria/Germany). Deformation conditions were in the order of 1.0 GPa/500 to 600°C. Cracks were formed in a subsequent event of brittle deformation at lower greenschist to subgreenschist facies conditions. (e) BSE image of synthetic zoisite (white, Zo) with small amounts of white mica (thin white streaks, wm) in a matrix of reacted plagioclase (light grey An 54 = relict starting composition, dark grey An 35 = newly formed, experimentally produced at 1.5 GPa, 750°C; see Stünitz and Tullis 2001). The extremely small zoisite platelets are aligned in an east-west running shear band. (f) BSE image of synthetic zoisite (white, Zo) with small amounts of white mica (thin white streaks) in a matrix of reacted plagioclase (grey An 60 = starting composition, transformed into An 35), experimentally produced at 1.5 GPa, 750°C; see Stünitz and Tullis 2001). A WNW-ESE running shear band shears the larger zoisite crystals. Small grains of albitic plagioclase, white mica, and zoisite nucleate during deformation in the shear band (Figs. e and f courtesy of H. Stünitz).

Ray et al. (1986) in zoisite from the Eclogite Zone (Tauern Window). Large crystals of zoisite from another locality in the Tauern (Sterzing, sample HU 93-8) also show such kink bands (Fig. 27b) in thin section. The kinking produces glide on the cleavage plane (100) as a bookshelf gliding.

Large crystals of zoisite are also bent. Figure 27d shows such a crystal from a deformed pegmatite with continuous undulose extinction. The deformation conditions are estimated as epidote-amphibolite facies near 500 to 600°C/1.0 GPa. The zoisite crystal shown above, which shows kinking (Fig. 27b), also shows bending. When viewed with the scanning electron microscope onto the concave bent part of a cleavage plane (100) of these crystals (Fig. 27c), they show a surface, which is structured into small domains in the size of 1 μm × 0.2 μm. The domains are slightly tilted against each other. When viewed onto the convex face, they show a similar structure. In summary, the optical and electron microscopic investigations of bent and kinked crystals show that {100}, {010}, {001} planes play a major role in the deformation of epidote group minerals, either as slip planes or as cleavage planes for fracturing.

Stünitz and Tullis (2001) verified experimentally the observation from natural rocks that epidote minerals are relatively rigid. They performed deformation experiments of plagioclase, which reacts to zoisite (+ albitic plagioclase, kyanite, quartz and white mica) during deformation at 1.5 GPa and 750°C. The microstructures indicate that zoisite underwent preferred growth and some fracturing at low strain, whereas at high strain it develops shear bands, which separate long crystals (or crystal aggregates) of > 100 μm length in domains of < ≈ 30 μm. The shear bands themselves are only 1-3 μm wide and form an angle of ≈ 15 to 25° to the shear zone boundary. The deformation mechanism in the fine-grained aggregates of the shear bands is granular flow, a diffusion-assisted grain boundary sliding process, by which the rock deforms at low stress. This type of deformation mechanism operates in very fine-grained materials. The most effective way to produce such fine-grained aggregates is to recrystallize or neocrystallize the material. Plagioclase breakdown reactions producing epidote group minerals are classic examples for neocrystallization leading to very fine-grained material in shear zones (Stünitz 1993; Stünitz and Fitzgerald 1993). The main reason for the fine grain size is the rapid nucleation rate of these phases. Thus, epidote group minerals are important for affecting the deformation properties of plagioclase rocks, especially in the middle to upper crust. The plagioclase breakdown reactions involving epidote group minerals commonly cause a change in deformation mechanism to grain size sensitive mechanisms and in this way weaken the crust mechanically.

ACKNOWLEDGMENTS

We thank J. Nissen, F. Galbert, I. Preuss at ZELMI at TU Berlin for SEM photographs, analyses and figures (Figs. 15, 25a-j, 27c); they were of invaluable help for our exploratory studies of surface and growth phenomena of epidotes. S. Herting-Agthe (Berlin) and G. Smelik (North Carolina) kindly provided specimens. V. Schenk (Kiel) and S. Herting-Agthe helped with literature research; J. Kruhl (München) and H. Stünitz (Basel) are thanked for comments on deformation, and M. Raith (Bonn) for comments on optical data. S. Bernau (Berlin) patiently helped in preparation of this manuscript (and others of this volume) and we thank R. Geffe (Berlin) for help in drawing and preparation of figures.

REFERENCES

Akasaka M, Sakakibara M, Togari K (1988) Piemontite from the manganiferous hematite ore deposits in the Togoro belt, Hokkaido, Japan. Min Pet 38:105-116

Allen JM, Fawcett JJ (1982) Zoisite-anorthite-calcite stability relations in H_2O-CO_2 fluids at 500 bars - An experimental and SEM study. J Petrol 23:215-239

Anastasiou P, Langer K (1977) Synthesis and physical properties of piemontite $Ca_2Al_{3p}Mn_p^{3+}(Si_2O_7/SiO_4/O/OH)$. Contrib Mineral Petrol 60:225-245

Andersen O (1911) On epidote and other minerals from pegmatite veins in granulite at Notodden, Telemarken, Norway. Archiv Mathem Naturvidenskab B 31/15:313-362

Anderson BW (1968) Three items of interest to gemmologists. J Gemmol 11:1-6

Armbruster Z, Gnos E, Dixon R, Gutzmer J, Hejny C, Döbelin N, Medenbach O (2002) Manganvesuvianite and tweddilite, two new Mn^{3+}-silicate minerals from the Kalahari manganese fields, South Africa. Mineral Mag 66:137-150

Ashley PM, Martin JE (1987) Chromium-bearing minerals from a metamorphosed hydrothermal alteration zone in the Archean of Western Australia. N Jahrb Mineral Abh 157:81-111

Bank H (1969) Hellbraune bis farblos durchsichtige Zoisite aus Tansania. Z Dtsch Gemmol Ges 18:61-65

Bank H (1980a) Geschliffener durchsichtiger roter Klinozoisit aus Arendale/Norwegen. Z Dtsch Gemmol Ges 29:186-188

Bank H (1980b) Schleifwürdiger manganhaltiger durchscheinender roter Zoisit (Thulit) aus Norwegen. Z Dtsch Gemmol Ges 29:188-189.

Bank H, Beredesinski W, Nuber B (1967) Strontiumhältiger trichroitischer Zoisit von Edelsteinqualität. Z Dtsch Gemmol Ges 61:27-29

Banno S, Yoshizawa H (1993) Sector zoning of epidote in the Sanbagawa schists and the question of an epidote miscibility gap. Minal Mag 57:739-743

Bauer M (1968) Precious stones. Dover Publications, New York

Becke F (1914) Über den Zusammenhang der physikalischen, besonders der optischen Eigenschaften mit der chemischen Zusammensetzung der Silikate. *In*: Handbuch der Mineralchemie, 2, I Doelters (ed), Dresden

Belov NV, Rumanova JM (1953) The crystal structure of epidote $Ca_2Al_2FeSi_3O_{12}(OH)$. Dokl Akad Nauk SSSR 89:853-856 (Abstract in Struct Rep 17:567-568)

Belov NV, Rumanova JM (1954) The crystal structure of epidote. Trudy Inst Krist Akad Nauk SSSR 9:103-164 (Abstract in Struct Rep 18:544-545)

Bermanec V, Armbruster Th, Oberhänsli R, Zebec V (1994) Crystal chemistry of Pb- and REE-rich piemontite from Nezilovo, Macedonia. Schweiz Mineral Petrogr Mitt 74:321-328

Berzelius (1818) Afhandel i. Fys 5:32 (quoted in Hintze 1897)

Bird D, Spieler AR (2004) Epidote in geothermal systems. Rev Mineral Geochem 56:235-300

Bird DK, Cho M, Janik CJ, Liou JG, Caruso LJ (1988) Compositional, order/disorder, and stable isotope characteristics of Al-Fe epidote, State 2-14 Drill Hole, Salton Sea Geothermal System. J Geophys Res 93:13,135-13,144

Bird DK, Helgeson HC (1980) Chemical interaction of aqueous solutions with epidote-feldspar mineral assemblages in geologic systems. 1. Thermodynamic analysis of phase relations in the system CaO-FeO-Fe_2O_3-Al_2O_3-SiO_2-H_2O-CO_2. Am J Sci 280:907-941

Blackburn WH, Dennen WH (1997) Encyclopedia of mineral names. The Canadian Mineralogsit Spec Publ 1, Mineral Assoc Canada, Ontario, p 360

Bleek AWG (1907) Die Jadeitlagerstätten in Upper Burma. Z prak Geol:341-365

Bonazzi P, Bindi L, Parodi G (2003) Gatelite-(Ce), a new REE-bearing mineral from Trimouns, French Pyrenees; crystal structure and polysomatic relationships with epidote and törnebohmite-(Ce). Am Mineral 88:223-228

Bonazzi P, Garbarino C, Menchetti S (1992) Crystal chemistry of piemontites: REE-bearing piemontite from Monte Brugiana, Alpi Apuane, Italy. Eur J Mineral 4:23–34

Bonazzi P, Menchetti S (1995) Monoclinic members of the epidote group: effects of the $Al \Leftrightarrow Fe^{3+} \Leftrightarrow Fe^{2+}$ substitution and of the entry of REE^{3+}. Mineral Petrol 53:133-153

Bonazzi P, Menchetti S (2004) Manganese in monoclinic members of the epidote group: piemontite and related minerals. Rev Mineral Geochem 56:495-552

Bonazzi P, Menchetti S, Palenzona A (1990) Strontiopiemontite, a new member of the epidote group, from Val Graveglia, Liguria, Italy. Eur J Mineral 2:519-523

Bonazzi P, Menchetti S, Reinecke T (1996) Solid solution between piedmontite and androsite-(La), a new mineral of the epidote group from Andros Island, Greece. Am Mineral 81:735-744

Brandon AD, Creaser RA, Chacko T (1996) Constraints on rates of granitic magma transport from epidote dissolution kinetics. Science 271:1845-1848

Brastad K (1985) Sr metasomatism and partition of Sr between the mineral phases of a meta-eclogite from Björkedalen, West Norway. Tschermaks Mineral Petrogr Mitt 34:87–103

Brese NE, O'Keeffe M (1991) Bond-valence parameters for solids. Acta Crystall B 47:192-197

Brewster (1819) On the absorption of polarized light by doubly refracting crystals. Phil Transact London 19
Brunsmann A (2000) Strukturelle, kristallchemische und phasenpetrologische Untersuchungen an synthetischen und natürlichen Zoisit und Klinozoisit Mischkristallen. Dissertation, Technical University of Berlin, Germany (http://edocs.tu-berlin.de/diss/2000/brunsmann_axel.htm)
Brunsmann A, Franz G, Erzinger J, Landwehr D (2000) Zoisite- and clinozoisite-segregations in metabasites (Tauern Window, Austria) as evidence for high-pressure fluid-rock interaction. J metam Geol 18:1–21
Brunsmann A, Franz G, Heinrich W (2002) Experimental determination of zoisite-clinozoisite phase equilibria in the system CaO-Al_2O_3-Fe_2O_3-SiO_2-H_2O. Contrib Mineral Petrol 143:115-130
Burns RG, Strens RGJ (1967) Structural interpretation of polarized absorption spectra of the Al-Fe-Mn-Cr epidotes. Min Mag 36:204-226
Carbonin S, Molin G (1980) Crystal-chemical considerations on eight metamorphic epidotes. N Jahrb Mineral Abh 139:205-215
Catti M, Ferraris G, Ivaldi G (1988) Thermal behavior of the crystal structure of strontian piemontite. Am Mineral 73:1370-1376
Catti M, Ferraris G, Ivaldi G (1989) On the crystal chemistry of strontian piemontite with some remarks on the Nomenclature of the epidote group. N Jahrb Mineral Monatsh 1989:357-366
Cech F, Vrána S, Povondra P (1972) A non-metamict allanite from Zambia. N Jahrb Mineral Abh 116:208-223
Challis A, Grapes R, Palmer K (1995) Chromian muscovite, uvarovite and zincian chromite: products of regional metasomatism in northwest Nelson, New Zealand. Can Mineral 33:1263-1284
Chatterjee ND, Johannes W, Leistner H (1984) The system CaO-Al_2O_3-SiO_2-H_2O: new phase equilibria data, some calculated phase relations, and their petrological applications. Contrib Mineral Petrol 88:1-13
Chopin C (1978) Les paragenèses réduites ou oxydées de concentrations manganésifères de "schistes lustrés" de Hate-Maurienne (Alps francaises). Bulletin Minéral 101:514-531
Comodi P, Zanazzi PF (1997) The pressure behavior of clinozoisite and zoisite: An X-ray diffraction study. Am Mineral 82:61-68
Cooper AF (1980) Retrograde alteration of chromian kyanite in metachert and amphibolite whiteschist from the Southern Alps, New Zealand, with implication for uplift on the Alpine fault. Contrib Mineral Petrol 75:153-164
Cordier L (1803) Analyse du Minéralconnu sus le nom de Mine de Manganese violet du Piédmont, faite au Labratoire de l'Ecole de Mines. J Mineral 13:135
Cressey G, Steel AT (1988) An EXAFS study on Gd, Er and Lu site location in the epidote structure. Phys Chem Mineral 15:304-312
Deer WA, Howie RA, Zussman J (1986) Epidote group. *In*: Deer WA, Howie RA, Zussman J Disilicates and ring silicates. Second edition. London, Longman Scientific and Technical, pp 2-179
DeRudder RD, Beck CW (1964) Clinozoisite from the Willsboro wollastonite deposit, New York. Special Paper, Geol Soc Am 76:42-43
Devaraju TC, Raith MM, Spiering B (1999) Mineralogy of the archean barite deposit of Ghattihosahalli, Karnataka, India. Can Mineral 37:603-617
Dollase WA (1968) Refinement and comparison of the structures of zoisite and clinozoisite. Am Mineral 53: 1882-1898
Dollase WA (1969) Crystal structure and cation ordering of piemontite. Am Mineral 54:710-717
Dollase WA (1971) Refinement of the crystal structures of epidote, allanite and hancockite. Am Mineral 56: 447-464
Dollase WA (1973) Mössbauer spectra and iron distribution in the epidote group minerals. Z Krist 138:41-63
Dunn PJ (1985) The lead silicates from Franklin, New Jersey: occurrence and composition. Mineral Mag 49: 721-727
Enami M (1977) Sector zoning of zoisite from a metagabbro at Fujiwara, Sanbagawa metamorphic terrane in central Shikoku. J Geol Soc Japan 83:693-697
Enami M, Banno Y (2001) Partitioning of Sr between coexisting minerals of the hollandite- and piemontite-groups in a quartz-rich schist from the Sanbagawa metamorphic belt, Japan. Am Mineral 86:205-214
Enami M, Liou JG, Mattinson CG (2004) Epidote minerals in high P/T metamorphic terranes: Subduction zone and high- to ultrahigh-pressure metamorphism. Rev Mineral Geochem 56:347-398
Ernst WG (1964) Petrochemical study of coexisting minerals from low-grade schists, Eastern Shikoku, Japan. Geochim Cosmochim Acta 28:1631-1668
Ernst WG (1977) Mineralogic study of eclogitic rocks from Alpe Arami, Lepontine Alps, southern Switzerland. J Petrol 18:371-398
Eskola P (1933) On the chrome minerals of Outokumpu. Bulletin de la Commission Geologique de Finlande p 26-44

Faye GH, Nickel EH (1971) On the pleochroism of vanadium-bearing zoisite from Tanzania. Can Mineral 10: 812-821

Fehr KT, Heuss-Aßbichler S (1997) Intracrystalline equilibria and immiscibility gap along the join clinozoisite - epidote: An experimental and ^{57}Fe Mössbauer study. N Jb Mineral Abh 172:43-67

Ferraris G, Ivaldi G, Fuess H, Gregson D (1989) Manganese/iron distribution in a strontian piemontite by neutron diffraction. Z Krist 187:145-151

Fesenko EG, Rumanova IM, Belov NV (1955) The crystal structure of zoisite. Dokl Akad Nauk SSSR 102: 275-278 (Abstract in Structural Report 19:464-465)

Fesenko EG, Rumanova IM, Belov NV (1956) Crystal structure of zoisite. Kristallografiya SSSR 1:132-151 (Abstract in Structural Report 20:396-398)

Fischer K (1977) Edelstein Epidot. Lapis 2:10-13

Fleischer M (1970) New Mineral Names. Am Mineral 55:317-323

Forbes EH (1896) Über den Epidot von Huttington, Mass., und über die optischen Eigenschaften des Epidots. Z Kryst 26:138-142

Franz G, Althaus E (1977) The stability relations of the paragenesis paragonite-zoisite-quartz. N Jb Mineral Abh 130:159-167

Franz G, Selverstone J (1992) An empirical phase diagram for the clinozoisite – zoisite transformation in the system $Ca_2Al_3Si_3O_{12}(OH) – Ca_2Al_2Fe^{3+}Si_3O_{12}(OH)$. Am Mineral 77:631–642

Franz G, Smelik, EA (1995) Zoisite-clinozoisite bearing pegmatites and their importance for decompressional melting in eclogites. Eur J Mineral 7:1421-1436

Frei D, Liebscher A, Franz G, Dulski P (2004) Trace element geochemistry of epidote minerals. Rev Mineral Geochem 56:553-605

Gabe EJ, Portheine FC, Whitlow SH (1973) A reinvestigation of the epidote structure: confirmation of the iron location. Am Mineral 58:218-223

Game PM (1954) Zoisite-amphibolite with corundum from Tanganyika. Mineral Mag 30:458-466

Ghose S, Tsang T (1971) Ordering of V^{2+}, Mn^{2+}, and Fe^{3+} ions in zoisite, $Ca_2Al_3Si_3O_{12}(OH)$. Science 171: 374-376

Gieré R, Sorensen SS (2004) Allanite and other REE-rich epidote-group minerals. Rev Mineral Geochem 56: 431-494

Giuli G, Bonazzi P, Menchetti S (1999) Al-Fe disorder in synthetic epidotes: a single-crystal X-ray diffraction study. Am Mineral 84:933-936

Goldschlag M (1917) Über die optischen Eigenschaften der Epidote. Tscherm Mineral Petr Mitt NF 23-60

Goldschmidt V (1916) Atlas der Kristallformen, Tafeln. Vol. 3, Carl Winters Universitätsbuchhandlung, Heidelberg p 247

Goldschmidt V (1923) Atlas der Kristallformen, Tafeln. Vol. 9, Carl Winters Universitätsbuchhandlung, Heidelberg p 128

Gottardi G (1954) Dati ed osservazioni sulla struttura dell'epidoto. Period Mineral 23:245-250

Gottschalk M (2004) Thermodynamic properties of zoisite, clinozoisite and epidote. Rev Mineral Geochem. 56:83-124

Grapes R, Watanabe T (1984) Al – Fe^{3+} and Ca – Sr^{2+} epidotes in metagreywacke – quartzofeldspathic schist, Southern Alps, New Zealand. Am Mineral 69:490–498

Grapes RH (1981) Chromian epidote and zoisite in kyanite amphibolite, Southern Alps, New Zealand. Am Mineral 66:974-975

Grapes RH, Hoskin PWO (2004) Epidote group minerals in low–medium pressure metamorphic terranes. Rev Mineral Geochem 56:301-345

Green TH, Pearson NJ (1983) REE partitioning betweenb sphene, allanite and chevkinite and coexisting intermediate - felsic liquids at high P, T. Lithosphere dynamics and evolution of the continental crust, Abstract Vol, p. 157. Geological Soc Australia, Canberra

Grevel KD, Nowlan EU, Faßhauer DW, Burchard M (2000) *In situ* X-ray difraction investigation of lawsonite and zoisite at high pressures and temperatures. Am Mineral 85:206-216

Grew ES, Essene EJ, Peacor DR, Su S-C, Asami M (1991) Dissakisite-(Ce), a new member of the epidote group and the Mg analogue of allanite-(Ce), from Antartica. Am Mineral 76:1990-1997

Guild (1935) Piedmontite in Arizona. Am Mineral 20:679-692

Hanisch K, Zemann J (1966) Messung des Ultrarot-Pleochroismus von Mineralen. IV. Der Pleochroismus der OH-Streckfrequenz in Epidot. N Jb Mineral Monatshefte 1966:19-23

Harlow GE (1994) Jadeitites, albitites and related rocks from the Motagua Fault Zone, Guatemala. J Metam Geol 12:49-68

Haüy RJ (1822) Traité de Mineralogie. 2:575

Hermann J (2002) Allanite: thorium and light rare earth element carrier in subducted crust. Chem Geol 192: 289-306

Heuss-Aßbichler S (2000) Ein neues Ordnungsmodell für die Mischkristallreihe Klinozoisit-Epidot und das Granat-Epidot-Geothermometer. Habilitationthesis, Munich p105

Heuss-Aßbichler S, Fehr KT (1997) Intercrystalline exchange of Al and Fe^{3+} between grossular – andradite and clinozoisite – epidote solid solutions. N Jahrb Mineral Abh 172:69–100

Hietanen (1974) Amphibole pairs, epidote minerals, chlorite and plagioclase in metamorphic rocks. Am Mineral 59:22-40

Hintze CH (1897) Handbuch der Mineralogie, Vol 2 Silicate und Titanate Verlag Veit & Comp. Leipzig

Hirowatari F (1956) Manganiferous epidote from the Kakinomoto Mine, Kochi Prefecture. J Min Soc Japan 2: 331-346 (quoted in Strens 1966)

Holdaway MJ (1972) Thermal stability of Al-Fe epidote as a function of f_{O2} and Fe content. Contrib Mineral Petrol 37:307-340

Holland TJB, Redfern SAT, Pawley AR (1996) Volume behavior of hydrous minerals at high pressure and temperature: II. Compressibilities of lawsonite, zoisite, clinozoisite, and epidote. Am Mineral 81:341-348

Holtstam D, Langhof J (1994) Hancockite from Jacobsberg, Filipstad, Sweden: the second world occurrence. Mineral Mag 58:172-174

Hörmann PK, Raith M (1971) Optische Daten, Gitterkonstanten, Dichte und magnetische Susceptibilität von Al-Fe(III)-Epidoten. N Jahrb Mineral Abh 116:41-60

Hurlbut CS (1969) Gem zoisite from Tanzania. Am Mineral 54:702-709

Hutton CO (1938) On the nature of withamite from GlenCoe, Scotland. Mineral Mag 25:119-124

Hutton CO (1940) Metamorphism in the Lake Wakatipu region, western Otago, New Zealand. Dept Sci Ind Res, New Zealand, Geol Mem 5

Hutton CO (1951) Allanite from Yosemity National Park, Tuolumne Co, California. Am Mineral 36:233-248

Ito T (1950) X-ray studies on polymorphism. Tokyo, Maruzen Co., chapter 5

Ito T, Morimoto N, Sadanga R (1954) On the structure of Epidote. Acta Cryst 7:53-59

Jambor JL, Puziewicz J, Roberts AC (1995) New Mineral Names. Am Mineral 80:404-409.

Jancev S, Bermanec V (1998) Solid solution between epidote and hancockite from Nezilovo, Macedonia. Geol Croat 51/1:23-26

Janeczek J, Eby RK (1993) Annealing of radiation damage in allanite and gadolinite. Phys Chem Mineral 19: 343-356

Johannes W, Ziegenbein D (1980) Stabilität von Zoisit in H_2O-CO_2-Gasphasen. Fortschr Mineral 50:46-47

Johannson A (1937) A Descriptive Petrography of the Igneous Rocks. The University of Chicago Press, Chicago

Johnston RW (1948) Clinozoisite from Camaderry Mountain, Co. Wicklow. Min Mag 28:505-515

Kartashov PM, Ferraris G, Ivaldi G, Sokolova E, McCammon CA (2002) Ferriallanite-(Ce), $CaCeFe^{3+}AlFe^{2+}(SiO_4)(Si_2O_7)O(OH)$, a new member of the epidote group: Description, X-ray and Mössbauer study. Can Mineral 40:1641-1648

Kepezhinskas KB (1969) Determination of the composition of minerals of the epidote group from their physical properties. Dokl Acad Sci, USSR, Earth Sci Sect 185:104-106

Kepezhinskas KB, Khlestov VV (1971) Statistical analysis of the epidote group minerals. Trudy Inst Geol Geifiz Akad Nauk, USSR. Nowosibirsk, p 310

Kiseleva JA, Topor ND, Andreyenko EO (1974) Thermodynamic parameters of minerals of the epidote group. Geochem Internat 11:389-398

Klein C (1874) Die optischen Eigenschaften des Sulzbacher Epidot. N Jahrb Mineral 1-21

Klemd R (2004) Fluid inclusions in epidote minerals and fluid development in epidote-bearing rocks. Rev Mineral Geochem. 56:197-234

Kvick Å, Pluth JJ, Richardson Jr. JW, Smith JV (1988) The ferric iron distribution and hydrogen bonding in epidote: a neutron diffraction study at 15 K. Acta Cryst B 44:351-355

Langer K, Lattard L (1980) Identification of a low-energy OH-valence vibration in zoisite. Am Mineral 65: 779-783

Langer K, Raith M (1974) Infrared spectra of Al-Fe(III)-epidotes and zoisites, $Ca_2(Al_{1-p}Fe^{3+}_p)Al_2O(OH)[Si_2O_7][SiO_4]$. Am Mineral 59:1249–1258

Langer K, Tillmanns E, Kersten M, Almen H, Arni RK (2002) The crystal chemistry of Mn^{3+} in the clino- and orthozoisite structure types, $Ca_2M_3^{3+}[OH/O/SiO_4/Si_2O_7]$: A structural and spectroscopic study of some natural piemontites and "thulites" and their synthetic equivalents. Z Krist 217:563-580

Liebscher A (2004) Spectroscopy of epidote minerals. Rev Mineral Geochem. 56:125-170

Liebscher A, Gottschalk M, Franz G (2002) The substitution Fe^{3+} - Al and the isosymmetric displacive phase transition in synthetic zoisite: A powder X-ray and infrared spectroscopy study. Am Mineral 87:909-921

Linke W (1970) Messung des Ultrarot-Pleochroismus von Mineralen. X. Der Pleochroismus der OH-Streckfrequenz in Zoisit. Tschermaks Mineral Petrogr Mitteil 14:61-63

Liou JG (1973) Synthesis and stability relations of epidote, $Ca_2Al_2FeSi_3O_{12}(OH)$. J Petrol 14:381-314
Lüschen H (1979) Die Namen der Steine. Ott Verlag, Thun (Switzerland), p 380
Maaskant P (1985) The iron content and the optic axial angle in zoisites from Galicia, NW Spain. Mineral Mag 49:97-100
Malisa E (1987) Geology of the tanzanite gemstone deposits in the Lelanterna area, NE Tanzania. Ann Acad Sci Fennicae A 111:146
Malmqvist D (1929) Studien innerhalb der Epidotgruppe mit besonderer Rücksicht auf die manganhältigen Glieder. Bull Geol Inst Uppsala 22:223-280
Marmo V, Neuvonen KJ, Ojanpera P (1959) The piemontite of Piedmont (Italy) Kajlidongri (India) and Marampa (Sierra Leone). Bull Comm géol Finlande 184:11-20 (quoted in Strens 1966)
Masuda T, Shibutani T, Kuriyama M, Igarashi T (1990) Development of microboudinage: an estimate of changing differential stress with increasing strain. Tectonophysics 178:379-387
Masuda T, Shibutani T, Yamaguchi H (1995) Comparative rheological behaviour of albite and quartz in siliceous schists revealed by the microboudinage of piedmontite. J Struc Geol 11:1523-1533
Matthews A (1985) Kinetics and mechanisms of the reaction of zoisite to anorthite under hydrothermal conditions: reaction phenomenology away from the equilibrium region. Contrib Mineral Petrol 89:110-121
Matthews A, Goldsmith JR (1984) The influence of metastability on reaction kinetics involving zoisite formation from anorthite at elevated pressures and temperatures. Am Mineral 69:848-857
Mingsheng P, Dien L (1987) Spectroscopy, genesis and process properties of partly metamict allanite. J Central-south Inst Mining Metallurgy 18:362-368
Miyajima H, Matsubara S, Miyawaki R, Hirokawa K (2003) Niigataite, $CaSrAl_3(Si_2O_7)(SiO_4)O(OH)$: Sr-analogue of clinozoisite, a new member of the epidote group from the Itoigawa-Ohmi district, Niigata Prefecture, central Japan. J Mineral Petrol Sci 98:118-129
Morrison J (2004) Stable and radiogenic isotope systematics in epidote group minerals. Rev Mineral Geochem 56:607-628
Mottana A (1986) Blueschist-facies metamorphism of manganiferous cherts: A review of the alpine occurrence. *In:* Blueschists and Eclogites. Evans BW, Brown EH (eds) Memoir Geol Soc Amer 164:267-300
Myer GH (1965)X-Ray determinative curve for epidote. Am J Sci 263:78-86
Myer GH (1966) New data on zoisite and epidote. Am J Sci 264:364-385
Nagasaki A, Enami M (1998) Sr-bearing zoisite and epidote in ultra-high pressure (UHP) metamorphic rocks from the Su-Lu province, eastern China: an important Sr reservoir under UHP conditions. Am Mineral 83:240–247
Nayak VK, Neuvonen KJ (1963). Some manganese minerals from India. Bull Comm géol Finlande 212:27-36 (quoted in Strens 1966)
Neumann H (1985) The norwegian minerals. Nor Geol Unders Skr 68, p 278
Newton RC (1965) The thermal stability of zoisite. J Geol 73:431-441
Nozik YK, Kanepit VN, Fykin LY, Makarov YS (1978) A neutron diffraction study of the structure of epidote. Geochem Int 15:66-69
Orlov A (1926) On the iron poor members of the zoisite-epidote group.Mem Soc Roy Bohème 19:1-42 (in Czech)
Otto H (1935) Tschermaks Min Petr Mitt 47:89 (quoted in Strens 1966)
Paesano A (1983) A ^{57}Fe Mössbauer study of epidote. Hyperfine Interactions 15/16:841-844
Patrier P, Beaufort D, Meunier A, Eymery J-P, Petit S (1991) Determination of the nonequilibrium ordering state in epidote from the ancient geothermal field of Saint Martin: Application of Mössbauer spectroscopy. Am Mineral 76:602-610
Pautov LA, Khorov PV, Ignatenko KI, Sokolova EV, Nadezhina TN (1993) Khristovite (Ce) - (Ca,REE)-RE E(Mg,Fe)$AlMnSi_3O_{11}$(OH)(F,O): A new mineral in the epidote group. Zapsiki Vseross Mineral Obshch 122(3): 103-111 (in Russian)
Pawley AR, Chinnery NJ, Clark SM (1998) Volume measurements of zoisite at simultaneously elevated pressure and temperature. Am Mineral 83:1030-1036
Pawley AR, Redfern SAT, Holland TJB (1996) Volume behavior of hydrous minerals at high pressure and temperature: I. Thermal expansion of lawsonite, zoisite, clinozoisite, and diaspore. Am Mineral 81:335-340
Peacor DR, Dunn PJ (1988) Dollaseite-(Ce) (magnesium orthite redefined): Structure refinement and implications for F+M2+ substituitions in epidote group minerals. Am Mineral 73:838-842
Penfield SL, Warren CH (1899) Some new minerals from thezinc mines at Franklin, N. J. and note concerning the chemical composition of ganomalite. Amer Jour Sci 4th Ser 8:339-353
Perkins III D, Westrum EFJ, Essene EJ (1980) The thermodynamic properties and phase relations of some minerals in the system CaO-Al_2O_3-SiO_2-H_2O. Geoch Cosmochim Acta 44:61-84

Perseil EA (1990) Sur la présence du strontium dans les minérallisations manganésifères de Falotta et de Parsettens (Grisonsuisse) – Evolution des paragenèes. Schweiz Min Petrogr Mitt 70:315-320
Pichler S-R (1993) Gesteinsbildende Minerale im Dünnschliff. Enke Verlag, Stuttgart, p 233
Pistorius CWFT (1961) Synthesis and lattice constants of pure zoisite and clinozoisite. J Geol 69:604-609
Poli S, Schmidt MW (2004) Experimental subsolidus studies on epidote minerals. Rev Mineral Geochem 56: 171-195
Raith M (1976) The Al – Fe(III) epidote miscibility gap in a metamorphic profile through the Penninic Series of the Tauern Window. Contrib Mineral Petrol 57:99–117
Rammelsberg KF (1856) Über den Zoisit und seine Beziehung zum Epidot, so wie über die Zusammensetzung des letzteren. Monatsberichte der Königlich Preußischen Akademie der Wissenschaften zu Berlin 1856: 605-617
Ray NJ, Putnis A, Gillet P (1986) Polytypic relationship between clinozoisite and zoisite. Bull Mineral 109: 667-685
Reinecke T (1986) Crystal chemistry and reaction relations of piemontites and thulites from highly oxidized low grade metamorphic rocks at Vitali, Andros Island, Greece. Contrib Mineral Petrol 93:56-76
Robinson K, Gibbs GV, Ribbe PH (1971) Quadratic elongation: a quantitative measure of distortion in coordination polyhedra. Science 172:567-570
Rouse RC, Peacor DR (1993) The crystal structure of dissakisite-(Ce), the Mg analogue of allanite-(Ce). Can Mineral 31:153-157
Rumanova IM, Nikolaeva TV (1960) Crystal structure of orthite. Soviet Phys – Crystallography 4:789-795
Sánchez-Viscaíno VL, Franz G, Gomez-Pugnaire MT (1995) The behaviour of Cr during metamorphism of carbonate rocks from the Nevado-Filabride complex, Betic Cordilleras, Spain. Can Mineral 33:85-104
Schiffmann P, Liou JG (1983) Synthesis of Fe-pumpellyite and its stability relations with epidote. J Metamor Geol 1:91-101
Schmetzer K, Bank H (1979) Bluish-green zoisite from Merelani, Tanzania. J Gemmol 16:512-513.
Schmetzer K, Berdesinski W (1978) Das Absorptionsspektrum von Cr^{3+} in Zoisit. Neu Jahrb Mineral Monatsh 1978:197-202
Schmidt MW, Poli S (1994) The stability of lawsonite and zoisite at high pressures: Experiments in CASH to 92 kbar and implications for the presence of hydrous phases in subducted lithosphere. Earth Planet Sci Lett 124:105-118
Schmidt MW, Poli S (2004) Magmatic epidote. Rev Mineral Geochem 56:399-430
Seki Y (1959) Relation between chemical composition and lattice constants of epidote. Am Mineral 44:720-730
Shepel AB, Karpenko MV (1969) Mukhinite, a new variety of epidote. Dokl Akad Nauk SSR 185:1342-1345 (in Russian)
Short AM (1933) A chemical study of piedmontite from Shadow Lake, madera County, California. Am Mineral 18:493-500
Smelik EA, Franz G, Navrotsky A (2001) A calorimetric study of zoisite and clinozoisite solid solutions. Am Mineral 86:80-91
Smith D, Albee AL (1967) Petrology of a piemontite-bearing gneiss, San Ggiorgonio Pass, California. Contrib Mineral Petrol 16:189-203
Smith G, Halenius U, Langer K (1982) Low temperature spectral studies of Mn^{3+}-bearing andalusite and epidote type minerals in the range 30,000-5,000 cm^{-1}. Phys Chem Mineral 8:136-142
Smith JV, Pluth JJ, Richardson Jr. JW, Kvick Å (1987) Neutron diffraction study of zoisite at 15 K and X-ray study at room temperature. Z Krist 179:305-321
Smyth JR, Bish DL (1988) Crystal structures and cation sites of the rock-forming minerals. Allen and Unwin, Boston, p 332
Spear FS (1993) Metamorphic Phase Equilibria and Pressure-Temperature-Time Paths. Min Soc Am, Washington DC
Spear FS, Franz G (1986) P-T-evolution of metasediments from the Eclogite Zone, south-central Tauern Window, Austria. Lithos 19:219-234
Spiegel C, Siebel W, Frisch W, Berner Z (2002) Nd and Sr isotopic ratios and trace element geochemistry of epidote from the Swiss Molasse Basin as provenance indicators: implications for the reconstruction of the exhumation history of the Central Alps. Chem Geol 189:231-250
Stergiou AC, Rentzeperis PJ, Sklavounos S (1987) Refinement of the crystal structure of a medium iron epidote. Z Krist 178:297-305
Storre B, Johannes W, Nitsch KH (1982) The stability of zoisite in H_2O-CO_2 mixtures. N Jahrb Mineral Monatsh 1982:395-406
Strens RGJ (1963) Some relationship between members of the epidote group. Nature 198:80-81

Strens RGJ (1964) Epidotes of the Borrowdale volcanic rocks of central Borrowdale. Mineral Mag 33:868-886
Strens RGJ (1966) Properties of the Al-Fe-Mn epidotes. Mineral Mag 25:928-944
Strunz H, Nickel EH (2001) Strunz mineralogical tables. E Schweizerbart'sche Verlagsbuchhandlung Stuttgart. p 870
Stünitz F (1993) Deformation of granitoids at low metamorphic grade. I: Reactions and grain size reduction. Tectonophysics 221:269-297
Stünitz F(1993) Transition from fracturing to viscous flow in a naturally deformed metagabbro. *In*: Defects and Processes in the Solid State: Geoscience Applications. JN Boland, JD Fitz Gerald (eds) Elsevier, Amsterdam, p 121-150
Stünitz T (2001) Weakening and strain localization produced by syn-deformational reaction of plagioclase. Int J Earth Sciences (Geol Rundsch) 90:136-148
Termier P (1898) Sur une variete de zoisite des schistes metamorphiques des Alpes et sur les properties optiques de la zoisite classique. Soc franc mineral Bull 21:148-170
Termier P (1900) Sur une association d´epidote et de zoisite et sur les rapports cristallographiques de ces especes minerales. Soc franc mineral Bull 21:148–170
Thomson T (1810) Experiments on allanite, a new mineral from Greenland. R Soc Edinburgh Trans 8:371-386
Treloar PJ (1987a) Chromian muscovites and epidotes from Outukumpu, Finland. Minal Mag 51:593-599
Treloar PJ (1987b) The Cr-minerals of Outukumpu - their chemistry and significance. J Petrol 28:867-886
Tröger WE (1982) Optische Bestimmung der gesteinsbildenden Minerale, Teil 1 Bestimmungstabellen. E Schweizerbarth'sche Verlagsbuchhandlung Stuttgart. p 188
Tsang T, Ghose S (1971) Ordering of transition metal ions in zoisite. EOS Transactions Am Geophys Union 52,4:380-381
Tschermak G, Sipöcz L (1882) Beitrag zur Kenntnis des Zoisits. Z Kryst Mineral 6:200-202
Tsuboi S (1936) Japan J Geol Geog 13:333 (quoted in Strens 1966)
Tullock AJ (1979) Secondary Ca-Al silicates as low-grade alteration products of granitoid biotite. Contrib Mineral Petrol 69:105-117
Ueda T (1955) The crystal structure of allanite, $OH(Ca,Ce)_2(Fe^{3+}Fe^{2+})Al_2OSi_2O_7SiO_4$. Mem Coll Sci Univ Kyotot B12:145-163
v Eynatten H (2003) Petrography and chemistry of sandstones from the Swiss Molasse Basin: an archive of the Oligocene to Miocene evolution of the Central Alps. Sedimentol 50:703-724
Vogel DE, Bahezre C (1965) The composition of partially zoned garnet and zoisite from Cabo Ortegal, N.W, Spain. N Jahrb Mineral Monatsh 1965:140-149
Webster R (1962) Gems: Their Sources, Descriptions and Identification. Butterworths, London
Webster R, Anderson BW (1983) Gems: Their Sources, Descriptions and Identification. Butterworths, London
Weinschenk E (1896) Über Epidot und Zoisit. Z Kryst Mineral 26:154-177
Weiss ChS (1820) Über die Theorie des Epidotsystemes. Abhandlungen der Königlich Preußischen Akademie der Wissenschaften zu Berlin 1818/1819 Phys:242-269
Weiss ChS (1828) Über die Verhältnisse in den Dimensionen der Krystallsysteme, und insbesondere des Quarzes, des Feldspathes, der Hornblende, des Augites und des Epidotes. Abh König Preuß Akad Wissensch Berlin 1825 Phys:163-200
Winchell AN, Winchell H (1962) Elements of optical mineralogy.- Part III: Determinative Tables. 2nd ed, Wiley and Sons, New York p 231
Winkler B, Langer K, Johannsen PG (1989) The influence of pressure on the OH valence vibration of zoisite. Physics and Chemistry of Minerals 16:668-671
Yoshizawa H (1984) Notes on petrography and rock-forming mineralogy; (16), Sector-zoned epidote from Sanbagawa Schist in central Shikoku, Japan. J Japan Assoc Mineral Petrol Econ Geol 79:101-110
Zambonini F (1903) Krystallographisches über den Epidot. Z Krist 37:70 (quoted in Strens 1966)
Zambonini F (1920) Sulla clinozoisite di Chiampernotto in Val d´Ala. Boll Com Geol Ital 47:65-99 (quoted in Strens 1966)

Appendices found on the following pages.

APPENDIX A

Lattice constants of natural and synthetic monoclinic epidote minerals

Composition	Sample
Al-Fe Epidotes	
$Ca_2Al_3[Si_3O_{11}(O/OH)]$	Synth.
$Ca_2(Al_{2.996}Fe^{3+}_{0.019})[Si_{2.989}O_{11}(O/OH)]$	Nat.
$Ca_2(Al_{2.97}Fe^{3+}_{0.03})[Si_3O_{11}(O/OH)]$	Nat.
$(Ca_{1.975}Fe^{2+}_{0.01}Mn^{2+}_{0.01})(Al_{2.79}Fe^{3+}_{0.16})[Si_{3.04}O_{11}(O/OH)]$	Nat.
$Ca_2(Al_{2.78}Fe^{3+}_{0.22})[Si_3O_{11}(O/OH)]$	Nat.
$Ca_{2.003}(Al_{2.809}Fe_{0.224}Mn_{0.009})[Si_{2.956}O_{11}(O/OH)]$	Nat.
$(Ca_{1.975}Fe^{2+}_{0.04}Na_{0.005}K_{0.005}Mn^{2+}_{0.015}Mg_{0.005})(Al_{2.705}Fe^{3+}_{0.225}Ti_{0.003})[Si_{3.00}O_{11}(O/OH)]$	Nat.
$Ca_{1.985}(Al_{2.73}Fe^{3+}_{0.235}Fe^{2+}_{0.02}Mn^{2+}_{0.04})[Si_{3.005}O_{11}(O/OH)]$	Nat.
$(Ca_{2.015}Na_{0.015})(Al_{2.725}Fe^{3+}_{0.24}Fe^{2+}_{0.04}Mn^{2+}_{0.01})[Si_{2.95}Al_{0.05}O_{11}(O/OH)]$	Nat.
$(Ca_{1.99}Fe^{2+}_{0.01}Na_{0.015}K_{0.02})(Al_{2.68}Fe^{3+}_{0.25}Mg_{0.015}Mn^{2+}_{0.02}Ti_{0.005})[Si_{3.00}P_{0.005}O_{11}(O/OH)]$	Nat.
$(Ca_{1.925}Fe^{2+}_{0.04}Na_{0.005}K_{0.005}Mn^{2+}_{0.005}Mg_{0.035})(Al_{2.665}Fe^{3+}_{0.29}Ti_{0.025})[Si_{2.995}Al_{0.005}O_{11}(O/OH)]$	Nat.
$Ca_2(Al_{2.7}Fe^{3+}_{0.3})[Si_3O_{11}(O/OH)]$	Nat.
$(Ca_{1.985}Fe^{2+}_{0.02}Mn^{2+}_{0.005})(Al_{2.465}Fe^{3+}_{0.305}Ti_{0.015})[Si_{2.915}O_{11}(O/OH)]$	Nat.
$(Ca_{1.965}Fe^{2+}_{0.045}Na_{0.015}K_{0.015}Mn^{2+}_{0.01}Mg_{0.035})(Al_{2.585}Fe^{3+}_{0.31}Ti_{0.055})[Si_{2.975}Al_{0.025}O_{11}(O/OH)]$	Nat.
$Ca_2(Al_{2.66}Fe^{3+}_{0.34})[Si_3O_{11}(O/OH)]$	Nat.
$(Ca_{1.982}Fe^{2+}_{0.005}Mn^{2+}_{0.007}Mg_{0.03})(Al_{2.644}Fe^{3+}_{0.348}Ti_{0.008})[Si_{3.002}O_{11}(O/OH)]$	Nat.
$(Ca_{1.975}Fe^{2+}_{0.04}Na_{0.005}K_{0.005}Mn^{2+}_{0.005}Mg_{0.005})(Al_{2.56}Fe^{3+}_{0.36}Ti_{0.05})[Si_{2.96}Al_{0.04}O_{11}(O/OH)]$	Nat.
$(Ca_2Fe^{2+}_{0.03}Na_{0.01}K_{0.02})(Al_{2.59}Fe^{3+}_{0.365}Mg_{0.01}Mn^{2+}_{0.005}Ti_{0.01})[Si_{2.995}O_{11}(O/OH)]$	Nat.
$(Ca_{1.955}Fe^{2+}_{0.04}Na_{0.005}K_{0.005}Mn^{2+}_{0.005}Mg_{0.005})(Al_{2.595}Fe^{3+}_{0.365}Ti_{0.03})[Si_{2.98}Al_{0.02}O_{11}(O/OH)]$	Nat.
$(Ca_{1.90}Fe^{2+}_{0.035}Na_{0.01}K_{0.005}Mn^{2+}_{0.01})(Al_{2.595}Fe^{3+}_{0.37}Mg_{0.045}Ti_{0.03})[Si_{2.97}Al_{0.025}P_{0.005}O_{11}(O/OH)]$	Nat.
$(Ca_{1.955}Fe^{2+}_{0.035}Na_{0.005}K_{0.005}Mn^{2+}_{0.005})(Al_{2.595}Fe^{3+}_{0.38}Ti_{0.02})[Si_{2.995}Al_{0.005}O_{11}(O/OH)]$	Nat.
$(Ca_{1.999}Fe^{2+}_{0.027}Mg_{0.018})(Al_{2.57}Fe^{3+}_{0.385})[Si_{2.955}Al_{0.045}O_{11}(O/OH)]$	Nat.
$(Ca_{1.985}Fe^{2+}_{0.04}Na_{0.005}K_{0.005}Mn^{2+}_{0.005})(Al_{2.53}Fe^{3+}_{0.39}Ti_{0.05})[Si_{2.985}Al_{0.015}O_{11}(O/OH)]$	Nat.
$(Ca_{1.95}Fe^{2+}_{0.04}Na_{0.015}Mn^{2+}_{0.005})(Al_{2.93}Fe^{3+}_{0.395}Ti_{0.03})[Si_{3.04}O_{11}(O/OH)]$	Nat.
$Ca_{1.99}(Al_{2.649}Fe_{0.396})[Si_{2.965}O_{11}(O/OH)]$	Nat.
$Ca_2(Al_{2.60}Fe^{3+}_{0.40})[Si_3O_{11}(O/OH)]$	Nat.
$Ca_2(Al_{2.6}Fe^{3+}_{0.4})[Si_3O_{11}(O/OH)]$	Nat.
$(Ca_{2.00}Fe^{2+}_{0.015}Mn^{2+}_{0.005})(Al_{2.475}Fe^{3+}_{0.40}Ti_{0.01})[Si_{3.075}O_{11}(O/OH)]$	Nat.
$Ca_{1.992}(Al_{2.624}Fe_{0.429}Mn_{0.007})[Si_{2.947}O_{11}(O/OH)]$	Nat.
$(Ca_{1.955}Fe^{2+}_{0.01}Mn^{2+}_{0.005})(Al_{2.5}Fe^{3+}_{0.44}Ti_{0.01})[Si_{3.05}O_{11}(O/OH)]$	Nat.
$(Ca_{1.925}Fe^{2+}_{0.045}Na_{0.005}K_{0.005}Mn^{2+}_{0.005})(Al_{2.48}Fe^{3+}_{0.44}Ti_{0.025})[Si_{3.05}O_{11}(O/OH)]$	Nat.
$(Ca_{1.90}Fe^{2+}_{0.04}Na_{0.01}K_{0.005}Mn^{2+}_{0.005})(Al_{2.55}Fe^{3+}_{0.455}Mg_{0.055}Ti_{0.015})[Si_{2.91}Al_{0.08}P_{0.01}O_{11}(O/OH)]$	Nat.
$(Ca_{1.978}Th_{0.004})(Al_{2.584}Fe_{0.458})[Si_{2.977}O_{11}(O/OH)]$	Nat.
$Ca_2(Al_{2.53}Fe^{3+}_{0.47})[Si_3O_{11}(O/OH)]$	Nat.
$(Ca_{1.93}Fe^{2+}_{0.04}Na_{0.01}K_{0.005}Mn^{2+}_{0.005})(Al_{2.475}Fe^{3+}_{0.485}Mg_{0.04}Ti_{0.02})[Si_{2.96}Al_{0.035}P_{0.005}O_{11}(O/OH)]$	Nat.
$(Ca_{1.92}Fe^{2+}_{0.05}Na_{0.02}K_{0.01}Mn^{2+}_{0.005}Mg_{0.01})(Al_{2.465}Fe^{3+}_{0.485}Ti_{0.025})[Si_{3.015}O_{11}(O/OH)]$	Nat.
$(Ca_{1.975}Fe^{2+}_{0.02}Na_{0.01}K_{0.025})(Al_{2.41}Fe^{3+}_{0.49}Mg_{0.01}Mn^{2+}_{0.01}Ti_{0.005})[Si_{3.045}P_{0.005}O_{11}(O/OH)]$	Nat.
$Ca_2(Al_{2.5}Fe^{3+}_{0.5})[Si_3O_{11}(O/OH)]$	Nat.
$(Ca_{1.95}Fe^{2+}_{0.02}Mn^{2+}_{0.01})(Al_{2.425}Fe^{3+}_{0.515})[Si_{3.05}O_{11}(O/OH)]$	Nat.
$Ca_{1.855}(Al_{2.51}Fe^{3+}_{0.525}Fe^{2+}_{0.065}Mn^{2+}_{0.01}Mg_{0.04})[Si_{2.98}Al_{0.02}O_{11}(O/OH)]$	Nat.
$(Ca_{1.981}Mn^{2+}_{0.018}Mg_{0.003})(Al_{2.461}Fe^{3+}_{0.53}Ti_{0.006})[Si_{2.997}Al_{0.003}O_{11}(O/OH)]$	Nat.
$(Ca_{1.93}Fe^{2+}_{0.05}Na_{0.025}K_{0.02}Mn^{2+}_{0.015})(Al_{2.425}Fe^{3+}_{0.53}Ti_{0.025})[Si_{3.005}O_{11}(O/OH)]$	Nat.
$(Ca_{1.905}Fe^{2+}_{0.045}Na_{0.01}K_{0.005}Mn^{2+}_{0.01})(Al_{2.40}Fe^{3+}_{0.535}Mg_{0.085}Ti_{0.02})[Si_{2.96}Al_{0.04}P_{0.01}O_{11}(O/OH)]$	Nat.
$(Ca_{1.95}Fe^{2+}_{0.04}Sr_{0.015})(Al_{2.37}Fe^{3+}_{0.575}Mg_{0.015}Mn^{2+}_{0.005}Ti_{0.03}V_{0.005}Cr_{0.005})[Si_{3.005}O_{11}(O/OH)]$	Nat.
$Ca_2(Al_{2.40}Fe^{3+}_{0.60})[Si_3O_{11}(O/OH)]$	Nat.
$(Ca_{1.965}Fe^{2+}_{0.015}K_{0.02})(Al_{2.295}Fe^{3+}_{0.625}Mg_{0.015}Mn^{2+}_{0.005}Ti_{0.005})[Si_{3.045}P_{0.005}O_{11}(O/OH)]$	Nat.
$(Ca_{1.99}Fe^{2+}_{0.02}Na_{0.015}K_{0.02})(Al_{2.225}Fe^{3+}_{0.625}Mg_{0.04}Mn^{2+}_{0.005}Ti_{0.005})[Si_{3.07}O_{11}(O/OH)]$	Nat.
$(Ca_{1.98}Fe^{2+}_{0.025}Na_{0.01}K_{0.02})(Al_{2.265}Fe^{3+}_{0.625}Mg_{0.02}Ti_{0.005})[Si_{3.08}O_{11}(O/OH)]$	Nat.
$Ca_2(Al_{2.37}Fe^{3+}_{0.63})[Si_3O_{11}(O/OH)]$	Nat.
$(Ca_{1.96}Fe^{2+}_{0.03}Na_{0.01}K_{0.015})(Al_{2.30}Fe^{3+}_{0.64}Mg_{0.005}Mn^{2+}_{0.01}Ti_{0.01})[Si_{3.025}O_{11}(O/OH)]$	Nat.
$(Ca_2Fe^{2+}_{0.02}Na_{0.01}K_{0.02})(Al_{2.295}Fe^{3+}_{0.645}Mg_{0.015}Mn^{2+}_{0.005}Ti_{0.005})[Si_{3.08}O_{11}(O/OH)]$	Nat.
$(Ca_{1.992}Sr_{0.017})(Al_{2.413}Fe_{0.67})[Si_{2.908}O_{11}(O/OH)]$	Nat.
$(Ca_{1.93}Fe^{2+}_{0.05}Na_{0.03}K_{0.005}Mn^{2+}_{0.015})(Al_{2.24}Fe^{3+}_{0.675}Mg_{0.065}Ti_{0.035})[Si_{2.93}Al_{0.07}O_{11}(O/OH)]$	Nat.
$(Ca_{1.895}Fe^{2+}_{0.04}Na_{0.0025}K_{0.0025}Mn^{2+}_{0.015}Mg_{0.005})(Al_{2.17}Fe^{3+}_{0.675}Ti_{0.02})[Si_{2.96}Al_{0.04}O_{11}(O/OH)]$	Nat.
$Ca_{1.967}(Al_{2.389}Fe_{0.678}Ti_{0.007})[Si_{2.960}O_{11}(O/OH)]$	Nat.
$(Ca_{1.96}Fe^{2+}_{0.025}Mn^{2+}_{0.01})(Al_{2.185}Fe^{3+}_{0.70}Ti_{0.015})[Si_{3.07}O_{11}(O/OH)]$	Nat.
$(Ca_{1.845}Fe^{2+}_{0.035}Na_{0.015}Mn^{2+}_{0.025})(Al_{2.245}Fe^{3+}_{0.715}Mg_{0.045}Ti_{0.01})[Si_{3.055}O_{11}(O/OH)]$	Nat.
$(Ca_{1.945}Fe^{2+}_{0.02}Mn^{2+}_{0.005})(Al_{2.205}Fe^{3+}_{0.715}Ti_{0.01})[Si_{3.065}O_{11}(O/OH)]$	Nat.
$(Ca_{1.945}Fe^{2+}_{0.02}Mn^{2+}_{0.005})(Al_{2.185}Fe^{3+}_{0.715}Ti_{0.03})[Si_{3.06}O_{11}(O/OH)]$	Nat.

a [Å]	*b* [Å]	*c* [Å]	β [°]	*V* [Å^3]	Source
8.887 (1)	5.5810 (1)	10.14 (2)	115.93 (13)	452.3 (25)	Pistorius 1961
8.861 (3)	5.5830 (1)	10.141 (6)	115.46 (2)	453.0 (1)	Pawley et al. 1996
8.879 (5)	5.5830 (5)	10.155 (6)	115.50 (5)	454.4	Dollase 1969
8.872 (3)	5.590 (2)	10.14 (4)	115.500 (35)	454.25 (21)	Myer 1965
8.870 (1)	5.5920 (1)	10.144 (2)	115.4 (2)	454.5 (2)	Comodi and Zanazzi 1997
8.872 (1)	5.5930 (1)	10.144 (1)	115.46 (1)	454.5 (1)	Bonazzi and Menchetti 1995
8.881 (4)	5.605 (2)	10.156 (4)	115.45 (3)	456.49 (46)	Hörmann and Raith 1971
8.87 (1)	5.59 (1)	10.15 (1)	115.45 (3)	454.4 (1)	Seki 1959
8.87 (1)	5.59 (1)	10.15 (1)	115.45 (3)	454.4 (1)	Seki 1959
8.874 (2)	5.596 (1)	10.153 (3)	115.52 (3)	455.0 (12)	Myer 1966
8.887 (3)	5.611 (1)	10.170 (4)	115.44 (3)	457.98 (39)	Hörmann and Raith 1971
8.869 (1)	5.598 (1)	10.146 (1)	115.450 (1)	454.9	Carbonin and Molin 1980
8.879 (4)	5.603 (1)	10.151 (5)	115.477 (45)	455.93 (23)	Myer 1965
8.886 (4)	5.609 (2)	10.160 (5)	115.43 (3)	457.27 (47)	Hörmann and Raith 1971
8.879 (1)	5.608 (1)	10.154 (1)	115.46 (1)	456.5	Carbonin and Molin 1980
8.874 (4)	5.602 (2)	10.147 (5)	115.45 (4)	455.50 (51)	Holdaway 1972
8.881 (7)	5.611 (3)	10.157 (8)	115.39 (5)	457.25 (74)	Hörmann and Raith 1971
8.879 (2)	5.609 (1)	10.154 (2)	115.44 (2)	456.70 (11)	Myer 1966
8.892 (6)	5.615 (2)	10.168 (6)	115.46 (5)	457.34 (6)	Hörmann and Raith 1971
8.880 (1)	5.607 (1)	10.154 (2)	115.46 (1)	456.50 (8)	Myer 1966
8.882 (7)	5.613 (3)	10.156 (8)	115.37 (5)	457.44 (79)	Hörmann and Raith 1971
8.878 (4)	5.600 (2)	10.145 (5)	115.44 (4)	455.50 (51)	Holdaway 1972
8.881 (8)	5.617 (3)	10.157 (9)	115.39 (6)	457.70 (92)	Hörmann and Raith 1971
8.880 (8)	5.617 (3)	10.153 (9)	115.35 (6)	457.71 (87)	Hörmann and Raith 1971
8.880 (2)	5.603 (1)	10.148 (1)	115.44 (1)	456.0 (1)	Bonazzi and Menchetti 1995
8.8802 (10)	5.6043 (8)	10.1511 (13)	115.455 (12)	456.2	Gabe et al. 1973
8.8756 (10)	5.608 (1)	10.151 (1)	115.41 (1)	456.4	Carbonin and Molin 1980
8.886 (4)	5.606 (2)	10.155 (5)	115.490 (47)	456.61 (31)	Myer 1965
8.884 (1)	5.603 (3)	10.157 (1)	115.45 (1)	456.5 (2)	Bonazzi and Menchetti 1995
8.883 (4)	5.608 (2)	10.151 (4)	115.438 (37)	456.70 (34)	Myer 1965
8.882 (6)	5.619 (2)	10.158 (7)	115.35 (4)	458.17 (67)	Hörmann and Raith 1971
8.886 (5)	5.608 (3)	10.155 (6)	115.49 (5)	456.80 (29)	Myer 1966
8.885 (1)	5.607 (2)	10.151 (1)	115.44 (1)	456.7 (2)	Bonazzi and Menchetti 1995
8.877 (1)	5.613 (1)	10.153 (1)	115.39 (1)	457.0	Carbonin and Molin 1980
8.887 (2)	5.615 (1)	10.161 (2)	115.46 (2)	457.80 (11)	Myer 1966
8.886 (9)	5.620 (3)	10.159 (10)	115.31 (7)	458.26	Hörmann and Raith 1971
8.884 (3)	5.613 (2)	10.155 (3)	115.42 (3)	457.40 (17)	Myer 1966
8.882 (1)	5.613 (1)	10.151 (1)	115.43 (1)	457.0	Carbonin and Molin 1980
8.889 (4)	5.621 (2)	10.161 (6)	115.450 (43)	458.44 (41)	Myer 1965
8.88 (1)	5.61 (1)	10.17 (1)	115.42 (3)	457.6 (1)	Seki 1959
8.876 (4)	5.613 (2)	10.160 (5)	115.40 (4)	457.30 (51)	Holdaway 1972
8.893 (7)	5.624 (2)	10.165 (8)	115.39 (5)	459.25 (82)	Hörmann and Raith 1971
8.885 (3)	5.625 (1)	10.153 (3)	115.41 (3)	458.30 (16)	Myer 1966
8.886 (2)	5.620 (1)	10.159 (3)	115.44 (3)	458.10 (15)	Myer 1966
8.893 (3)	5.640 (1)	10.185 (1)	115.34 (2)	461.70 (1)	Stergiou et al. 1987
8.889 (2)	5.625 (1)	10.154 (2)	115.41 (2)	458.60 (11)	Myer 1966
8.891 (2)	5.622 (1)	10.156 (2)	115.44 (2)	458.40 (11)	Myer 1966
8.896 (6)	5.628 (3)	10.166 (7)	115.50 (7)	459.4 (3)	Myer 1966
8.888 (1)	5.623 (1)	10.157 (1)	115.41 (1)	458.5	Carbonin and Molin 1980
8.888 (4)	5.629 (2)	10.161 (5)	115.43 (5)	459.10 (25)	Myer 1966
8.892 (2)	5.625 (1)	10.157 (3)	115.42 (2)	458.80 (41)	Myer 1966
8.892 (1)	5.622 (1)	10.159 (1)	115.40 (1)	458.8 (1)	Bonazzi and Menchetti 1995
8.886 (2)	5.621 (1)	10.157 (2)	115.45 (2)	458.10 (11)	Myer 1966
8.899 (5)	5.635 (2)	10.164 (6)	115.36 (4)	460.54 (62)	Hörmann and Raith 1971
8.884 (1)	5.621 (1)	10.154 (1)	115.39 (1)	458.1 (1)	Bonazzi and Menchetti 1995
8.893 (2)	5.634 (1)	10.159 (2)	115.415 (18)	459.73 (17)	Myer 1965
8.893 (3)	5.626 (2)	10.157 (3)	115.42 (3)	459.00 (17)	Myer 1966
8.896 (2)	5.627 (1)	10.159 (3)	115.408 (23)	459.32 (20)	Myer 1965
8.898 (2)	5.635 (1)	10.164 (2)	115.425 (23)	460.22 (18)	Myer 1965

Appendix A continued.

Composition	Sample
Al-Fe Epidotes (continued from previous page)	
$(Ca_{1.989}Pb_{0.017})(Al_{2.059}Fe_{0.724}Mn_{0.2})[Si_{3.011}O_{11}(O/OH)]$	Nat.
$(Ca_{1.985}Fe^{2+}_{0.015})(Al_{2.12}Fe^{3+}_{0.73}Ti_{0.015})[Si_{3.095}O_{11}(O/OH)]$	Nat.
$Ca_{1.99-2.005}(Al_{2.22-2.43}Fe^{3+}_{0.67-0.80})[Si_{2.93-2.985}O_{11}(O/OH)]$	Synth.
$(Ca_{1.975}Fe^{2+}_{0.035}Na_{0.005}K_{0.005}Mn^{2+}_{0.015}Mg_{0.01})(Al_{2.24}Fe^{3+}_{0.735}Ti_{0.005})[Si_{2.98}Al_{0.02}O_{11}(O/OH)]$	Nat.
$(Ca_{1.979}Fe^{2+}_{0.004}Mn^{2+}_{0.015}Mg_{0.003})(Al_{2.225}Fe^{3+}_{0.74}Ti_{0.01})[Si_{2.999}Al_{0.001}O_{11}(O/OH)]$	Nat.
$Ca_{1.961}(Al_{2.34}Fe_{0.741})[Si_{2.958}O_{11}(O/OH)]$	Nat.
$X_{Ep} \sim 0.75$ (composition determined from X-ray data)	Synth.
$(Ca_{2.025}Fe^{2+}_{0.005}K_{0.02})(Al_{2.14}Fe^{3+}_{0.775}Mg_{0.01}Mn^{2+}_{0.01}Ti_{0.005})[Si_{3.08}O_{11}(O/OH)]$	Nat.
$Ca_{1.978}(Al_{2.247}Fe_{0.777}Mn_{0.012})[Si_{2.986}O_{11}(O/OH)]$	Nat.
$(Ca_{1.99}Mn^{2+}_{0.007}Mg_{0.011})(Al_{2.192}Fe^{3+}_{0.779}Ti_{0.022})[Si_{2.995}Al_{0.005}O_{11}(O/OH)]$	Nat.
$Ca_2(Al_{2.22}Fe^{3+}_{0.78})[Si_3O_{11}(O/OH)]$? (composition from Rietveld refinment)	Nat.
$Ca_{1.99-2.025}(Al_{2.135-2.32}Fe^{3+}_{0.71-0.855})[Si_{2.985-3.00}O_{11}(O/OH)]$	Synth.
$Ca_2(Al_{2.21}Fe^{3+}_{0.79})[Si_3O_{11}(O/OH)]$	Nat.
$(Ca_{1.985}Fe^{2+}_{0.005}Na_{0.01}K_{0.02})(Al_{2.125}Fe^{3+}_{0.80}Mn^{2+}_{0.01})[Si_{3.04}P_{0.005}O_{11}(O/OH)]$	Nat.
$Ca_2(Al_{2.15}Fe^{3+}_{0.81}Ti_{0.02}Mn_{0.02})[Si_3O_{11}(O/OH)]$	Nat.
$(Ca_{1.948}Fe^{2+}_{0.019}Mn^{2+}_{0.03}Mg_{0.003})(Al_{2.169}Fe^{3+}_{0.824}Ti_{0.007})[Si_{2.982}Al_{0.018}O_{11}(O/OH)]$	Nat.
$Ca_{1.93-2.00}(Al_{2.145-2.34}Fe^{3+}_{0.78-0.87})[Si_{2.945-2.99}O_{11}(O/OH)]$	Synth.
$(Ca_{1.935}Fe^{2+}_{0.055}Na_{0.055}K_{0.005})(Al_{2.075}Fe^{3+}_{0.83}Mg_{0.07}Mn^{2+}_{0.015}Ti_{0.015})[Si_3O_{11}(O/OH)]$	Nat.
$Ca_2(Al_{2.16}Fe^{3+}_{0.84})[Si_3O_{11}(O/OH)]$	Nat.
$(Ca_{1.985}Fe^{2+}_{0.035}Mn^{2+}_{0.015}Mg_{0.015})(Al_{2.12}Fe^{3+}_{0.855}Ti_{0.005})[Si_{2.955}Al_{0.045}O_{11}(O/OH)]$	Nat.
$(Ca_{1.98}Na_{0.015})(Al_{1.985}Fe^{3+}_{0.86}Fe^{2+}_{0.08}Mn^{2+}_{0.02}Mg_{0.025})[Si_{3.06}O_{11}(O/OH)]$	Nat.
$Ca_2(Al_{2.14}Fe^{3+}_{0.86})[Si_3O_{11}(O/OH)]$	Nat.
$(Ca_{1.96}Fe^{2+}_{0.03}Na_{0.005}K_{0.005}Mn^{2+}_{0.01}Mg_{0.025})(Al_{2.085}Fe^{3+}_{0.865}Ti_{0.025})[Si_{2.97}Al_{0.03}O_{11}(O/OH)]$	Nat.
$(Ca_{1.935}Fe^{2+}_{0.05}Na_{0.005}K_{0.005}Mn^{2+}_{0.005}Mg_{0.01})(Al_{2.12}Fe^{3+}_{0.89}Ti_{0.005})[Si_{2.985}Al_{0.015}O_{11}(O/OH)]$	Nat.
$Ca_{1.976}(Al_{2.13}Fe_{0.923})[Si_{2.971}O_{11}(O/OH)]$	Nat.
$Ca_{1.968}(Al_{2.098}Fe_{0.942}Mn_{0.007})[Si_{2.985}O_{11}(O/OH)]$	Nat.
$Ca_2(Al_{2.04}Fe^{3+}_{0.96})[Si_3O_{11}(O/OH)]$? (no complete analysis)	Nat.
$Ca_{1.996}(Al_{2.001}Fe^{3+}_{0.961}Fe^{2+}_{0.017}Mn^{2+}_{0.004}Cr^{3+}_{0.006}Ti_{0.002})[Si_{3.013}O_{11}(O/OH)]$	Nat.
$Ca_2(Al_{2.053}Fe_{0.965}Ti_{0.012})[Si_{2.971}O_{11}(O/OH)]$	Nat.
$(Ca_{1.995}Fe^{2+}_{0.01})(Al_{1.935}Fe^{3+}_{0.985})[Si_{3.055}O_{11}(O/OH)]$	Nat.
$(Ca_{1.996}Mn^{2+}_{0.012}Mg_{0.012})(Al_{1.985}Fe^{3+}_{0.990}Ti_{0.004})[Si_{2.984}Al_{0.016}O_{11}(O/OH)]$	Nat.
$Ca_2(Al_2Fe^{3+})[Si_3O_{11}(O/OH)]$? (no complete analysis)	Nat.
$Ca_{1.962}(Al_{2.029}Fe_{1.006}Mn_{0.016}Ti_{0.011})[Si_{2.976}O_{11}(O/OH)]$	Nat.
$(Ca_{2.005}Sr_{0.036})(Al_{1.982}Fe_{1.015}Ti_{0.015})[Si_{2.948}O_{11}(O/OH)]$	Nat.
$Ca_{1.96}(Al_{2.063}Fe_{1.022})[Si_{2.954}O_{11}(O/OH)]$	Nat.
$Ca_{2.05-2.06}(Al_{1.90-2.04}Fe^{3+}_{0.955-1.115})[Si_{2.96-2.98}O_{11}(O/OH)]$	Synth.
$(Ca_{1.99}Fe^{2+}_{0.03})(Al_{1.935}Fe^{3+}_{1.045})[Si_{2.945}Al_{0.055}O_{11}(O/OH)]$	Nat.
$Ca_{2.02-2.035}(Al_{1.93-2.01}Fe^{3+}_{0.98-1.12})[Si_{2.955-2.99}O_{11}(O/OH)]$	Synth.
$Ca_{1.959}(Al_{1.957}Fe_{1.105}Mn_{0.015})[Si_{2.963}O_{11}(O/OH)]$	Nat.
$Ca_{2.03}(Al_{1.80}Fe^{3+}_{1.105}Fe^{2+}_{0.025}Mn^{2+}_{0.02})[Si_{3.03}O_{11}(O/OH)]$	Nat.
Pb-bearing Epidote	
$(Ca_{1.17}Mn^{2+}_{0.17}Pb_{0.47}Sr_{0.21})(Al_{1.95}Fe_{0.88}Mn_{0.10}Mg_{0.07})[Si_{2.95}Al_{0.05}O_{11}(O/OH)]$	Nat.
Sr-bearing Al-Fe-Mn Epidotes	
$(Ca_{1.84}Sr_{0.16})(Al_{1.87}Fe^{3+}_{0.35}Mn^{3+}_{0.78})[Si_3O_{11}(O/OH)]$	Nat.
$(Ca_{1.80}Sr_{0.20})(Al_{1.91}Fe^{3+}_{0.33}Mn^{3+}_{0.82})[Si_3O_{11}(O/OH)]$	Nat.
$(Ca_{1.82}Sr_{0.06})(Al_{1.86}Fe^{3+}_{0.35}Mn^{3+}_{0.82})[Si_{3.03}O_{11}(O/OH)]$	Nat.
$(Ca_{1.88}Sr_{0.08})(Al_{1.88}Fe^{3+}_{0.13}Mn^{3+}_{0.98})[Si_{2.98}O_{11}(O/OH)]$	Nat.
$(Ca_{1.74}Sr_{0.16})(Al_{1.83}Fe^{3+}_{0.06}Mn^{3+}_{1.15})[Si_{3.01}O_{11}(O/OH)]$	Nat.
$(Ca_{1.62}Sr_{0.35})(Al_{1.57}Fe^{3+}_{0.31}Mn^{3+}_{1.12})[Si_{3.01}O_{11}(O/OH)]$	Nat.
$(Ca_{1.05}Mn^{2+}_{0.22}Sr_{0.73})(Al_{1.80}M^{3+}_{1.20})[Si_3O_{11}(O/OH)]$; M = Fe⁺Mn	Nat.
$(Ca_{1.38}Sr_{0.62})(Al_{1.74}M^{3+}_{1.26})[Si_3O_{11}(O/OH)]$; M = Fe⁺Mn	Nat.
$(Ca_{1.87}Sr_{0.13})(Al_{1.97}Fe^{3+}_{0.309}Mn^{3+}_{0.721})[Si_3O_{11}(O/OH)]$	Nat.
Al-Fe-Mn Epidotes	
$(Ca_{1.92}Mg_{0.02}Mn^{2+}_{0.05}Na_{0.01})(Al_{1.96}Fe^{3+}_{0.66}Mn^{3+}_{0.38})[Si_{2.97}Al_{0.03}O_{11}(O/OH)]$	Nat.
$(Ca_{1.96}Mg_{0.03}Mn^{2+}_{0.01})(Al_{1.87}Fe^{3+}_{0.07}Mn^{3+}_{1.04}Ti_{0.02})[Si_{2.97}Al_{0.03}O_{11}(O/OH)]$	Nat.
$(Ca_{1.92}Mg_{0.02}Na_{0.01})(Al_{1.81}Fe^{3+}_{0.28}Mn^{3+}_{0.88})[Si_{3.04}O_{11}(O/OH)]$	Nat.
$(Ca_{1.92}Mg_{0.04})(Al_{1.75}Fe^{3+}_{0.14}Mn^{3+}_{1.08})[Si_{3.04}O_{11}(O/OH)]$	Nat.
$(Ca_{1.93}Mg_{0.02})(Al_{1.70}Fe^{3+}_{0.45}Mn^{3+}_{0.82})[Si_{3.05}O_{11}(O/OH)]$	Nat.
$(Ca_{1.98}Mg_{<0.01}Sr_{<0.01}Zn_{0.01})(Al_{2.43}Fe^{3+}_{0.43}Mn^{3+}_{0.14}Cu_{0.01})[Si_{2.99}O_{11}(O/OH)]$	Nat.
$Ca_2(Al_{1.87}Fe^{3+}_{0.51}Mn^{3+}_{0.66})[Si_{2.97}O_{11}(O/OH)]$	Nat.
$(Ca_{1.802}Mn^{2+}_{0.178}Mg_{0.025})(Al_{1.825}Fe^{3+}_{0.346}Mn^{3+}_{0.829})[Si_{2.992}Al_{0.008}O_{11}(O/OH)]$	Nat.

a [Å]	*b* [Å]	*c* [Å]	β [°]	*V* [Å³]	Source
8.894 (1)	5.647 (1)	10.162 (1)	115.41 (1)	461.0 (1)	Bonazzi and Menchetti 1995
8.898 (4)	5.631 (2)	10.163 (5)	115.423 (43)	459.94 (36)	Myer 1965
8.908 (3)	5.628 (2)	10.176 (4)	115.52 (5)	460.4 (3)	Liou 1973
8.898 (5)	5.635 (2)	10.161 (6)	115.32 (4)	460.53 (61)	Hörmann and Raith 1971
8.888 (4)	5.630 (2)	10.151 (5)	115.34 (4)	459.10 (51)	Holdaway 1972
8.890 (2)	5.623 (1)	10.156 (1)	115.41 (1)	458.6 (1)	Bonazzi and Menchetti 1995
8.900 (6)	5.639 (3)	10.165 (3)	115.75 (7)	459.5 (5)	Schiffman and Liou 1983
8.902 (2)	5.635 (1)	10.164 (2)	115.43 (2)	460.50 (11)	Myer 1966
8.894 (1)	5.630 (1)	10.157 (1)	115.41 (1)	459.4 (1)	Bonazzi and Menchetti 1995
8.893 (4)	5.631 (2)	10.145 (5)	115.34 (4)	459.10 (51)	Holdaway 1972
8.913 (1)	5.643 (1)	10.179 (1)	115.7 (1)	461.3	Nozik et al. 1978
8.891 (3)	5.625 (2)	10.177 (4)	115.50 (5)	459.4 (3)	Liou 1973
8.896 (1)	5.634 (1)	10.162 (1)	115.41 (1)	460.0	Carbonin and Molin 1980
8.901 (3)	5.643 (1)	10.166 (3)	115.41 (3)	461.20 (15)	Myer 1966
8.914 (9)	5.640 (3)	10.162 (9)	115.4 (2)	461.5	Dollase 1971
8.903 (4)	5.617 (2)	10.169 (5)	115.50 (4)	459.00 (51)	Holdaway 1972
8.893 (3)	5.624 (2)	10.175 (4)	115.48 (5)	459.4 (3)	Liou 1973
8.899 (1)	5.639 (1)	10.166 (2)	115.38 (2)	460.90 (9)	Myer 1966
8.8877 (14)	5.6275 (8)	10.1517 (12)	115.383 (14)	458.7	Gabe et al. 1973
8.911 (9)	5.640 (5)	10.171 (11)	115.44 (7)	461.6 (11)	Hörmann and Raith 1971
8.89 (1)	5.63 (1)	10.19 (1)	115.40 (3)	460.7 (1)	Seki 1959
8.894 (1)	5.637 (1)	10.158 (1)	115.36 (1)	460.2	Carbonin and Molin 1980
8.913 (10)	5.640 (4)	10.169 (11)	115.44 (6)	461.85 (103)	Hörmann and Raith 1971
8.915 (7)	5.650 (3)	10.178 (9)	115.40 (5)	462.75 (81)	Hörmann and Raith 1971
8.899 (1)	5.639 (1)	10.166 (1)	115.42 (1)	460.8 (1)	Bonazzi and Menchetti 1995
8.902 (1)	5.641 (1)	10.165 (1)	115.39 (1)	461.1 (1)	Bonazzi and Menchetti 1995
8.96 (1)	5.36 (1)	10.3 (1)	115.40 (2)	446.8	Paesano et al. 1983
8.890 (5)	5.641 (3)	10.164 (6)	115.55 (7)	459.9 (3)	Holland et al. 1996
8.903 (2)	5.649 (1)	10.163 (1)	115.39 (1)	461.8 (1)	Bonazzi and Menchetti 1995
8.904 (5)	5.649 (3)	10.173 (8)	115.440 (57)	462.04 (46)	Myer 1965
8.894 (4)	5.651 (2)	10.161 (5)	115.35 (4)	461.50 (51)	Holdaway 1972
8.96 (1)	5.63 (1)	10.3 (1)	115.40 (2)	469.4	Ito et al. 1954
8.901 (1)	5.649 (1)	10.173 (1)	115.41 (1)	462.0 (1)	Bonazzi and Menchetti 1995
8.901 (1)	5.645 (1)	10.168 (1)	115.37 (1)	461.6 (1)	Bonazzi and Menchetti 1995
8.901 (1)	5.646 (1)	10.167 (1)	115.41 (1)	461.5 (1)	Bonazzi and Menchetti 1995
8.911 (3)	5.643 (2)	10.180 (4)	115.52 (5)	462.0 (3)	Liou 1973
8.907 (1)	5.660 (1)	10.180 (1)	115.40 (1)	463.60 (6)	Myer 1966
8.922 (3)	5.648 (2)	10.194 (4)	115.57 (5)	463.4 (3)	Liou 1973
8.908 (1)	5.663 (1)	10.175 (2)	115.35 (1)	463.9 (1)	Bonazzi and Menchetti 1995
8.9 (1)	5.63 (1)	10.2 (1)	115.40 (3)	461.7 (1)	Seki 1959
8.958 (20)	5.665 (10)	10.304 (20)	114.4 (4)	476.2	Dollase 1971
8.884 (3)	5.684 (1)	10.202 (3)	115.23 (2)	466.0	Ferraris et al. (1989)
8.884 (2)	5.684 (1)	10.202 (3)	115.23 (2)	466.0	Catti et al. 1988
8.879 (2)	5.687 (1)	10.187 (3)	115.35 (2)	464.9	Catti et al. 1989
8.880 (3)	5.6829 (9)	10.187 (3)	115.36 (2)	464.5	Catti et al. 1989
8.870 (4)	5.699 (1)	10.201 (4)	115.30 (2)	466.2	Catti et al. 1989
8.897 (4)	5.702 (2)	10.232 (5)	115.07 (4)	470.2	Catti et al. 1989
8.849 (2)	5.671 (2)	10.203 (2)	114.63 (2)	465.4 (2)	Bonazzi et al. 1990
8.870 (2)	5.681 (1)	10.209 (2)	114.88 (2)	466.7 (2)	Bonazzi et al. 1990
8.878 (10)	5.692 (5)	10.201 (10)	115.4 (2)	465.7	Dollase 1969
8.85 (1)	5.660 (6)	10.18 (2)	115.6 (1)	459.9 (10)	Akasaka et al. 1988
8.881 (7)	5.687 (5)	10.180 (8)	115.53 (3)	464.0 (6)	Akasaka et al. 1988
8.864 (6)	5.690 (3)	10.189 (8)	115.4 (1)	464.2 (5)	Akasaka et al. 1988
8.877 (1)	5.696 (1)	10.198 (1)	115.61 (1)	465.0 (19)	Akasaka et al. 1988
8.881 (7)	5.697 (6)	10.194 (7)	115.54 (3)	465.4 (6)	Akasaka et al. 1988
8.8739 (11)	5.6156 (8)	10.1484 (13)	115.49 (1)	456.5 (1)	Langer et al. 2002
8.8756 (11)	5.6734 (7)	10.1686 (13)	115.5 (1)	462.2 (1)	Langer et al. 2002
8.847 (3)	5.677 (2)	10.159 (3)	115.35 (7)	461.1 (4)	Smith et al. 1982

Appendix A continued.

Composition	Sample
Al-Fe-Mn Epidotes (continued from previous page)	
$(Fe_{0.61};Mn_{0.08})$	
$(Fe_{0.61};Mn_{0.13})$	
$(Fe_{0.39};Mn_{0.38})$	
$(Fe_{0.21};Mn_{0.59})$	
$(Fe_{0.54};Mn_{0.31})$	
$(Fe_{0.71};Mn_{0.24})$	
$(Fe_{0.30};Mn_{0.73})$	
$(Fe_{0.64};Mn_{0.45})$	
$(Fe_{0.40};Mn_{0.70})$	
$(Fe_{0.41};Mn_{0.72})$	
$(Fe_{0.41};Mn_{0.72})$	
$(Fe_{0.62};Mn_{0.63})$	
$(Fe_{0.68};Mn_{0.75})$	
$(Fe_{0.66};Mn_{0.78})$	
Al-Mn Epidotes	
$(Ca_{1.92}Mn^{2+}_{0.11})(Al_{2.26}Mn^{3+}_{0.73})[Si_{2.97}O_{11}(O/OH)]$	Synth.
$Ca_{1.95}(Al_{2.05}Mn^{3+}_{0.975})[Si_{3.005}O_{11}(O/OH)]$	Synth.
$Ca_{1.97}(Al_{1.57}Mn^{3+}_{1.465})[Si_{2.985}O_{11}(O/OH)]$	Synth.
$Ca_2(Al_{2.5}Mn^{3+}_{0.5})[Si_3O_{11}(O/OH)]$	Synth.
$Ca_2(Al_{2.25}Mn^{3+}_{0.75})[Si_3O_{11}(O/OH)]$	Synth.
$Ca_2(Al_2Mn^{3+}_1)[Si_3O_{11}(O/OH)]$	Synth.
$Ca_2(Al_{1.75}Mn^{3+}_{1.25})[Si_3O_{11}(O/OH)]$	Synth.
$Ca_2(Al_{1.5}Mn^{3+}_{1.5})[Si_3O_{11}(O/OH)]$	Synth.
$Ca_2(Al_{1.25}Mn^{3+}_{1.75})[Si_3O_{11}(O/OH)]$	Synth.
$Ca_2(Al_1Mn^{3+}_{2.0})[Si_3O_{11}(O/OH)]$	Synth.
$Ca_2(Al_{0.5}Mn^{3+}_{2.5})[Si_3O_{11}(O/OH)]$	Synth.
REE bearing Epidotes	
$(Ca_{1.20}Y_{0.02}La_{0.23}Ce_{0.48}Nd_{0.07})(Al_{1.65}Fe_{1.20}Ti_{0.06}Mn_{0.04}Mg_{0.04})[Si_3O_{11}(O/OH)]$	Nat.
$(Ca_{1.08}Ce_{0.92})(Al_{0.66}Fe^{3+}_{1.24}Fe^{2+}_{0.93}Mn_{0.07}Ti_{0.14})[Si_{2.94}Al_{0.06}O_{11}(O/OH)]$	Nat.
$(Ca_{1.186}REE_{0.7})(Al_{1.921}Fe_{0.953}Mg_{0.167}Mn_{0.016}Ti_{0.045})[Si_{3.012}O_{11}(O/OH/F_{0.038})]$	Nat.
$(Ca_{1.271}REE_{0.7}Y_{0.021})(Al_{1.968}Fe_{0.944}Mg_{0.033}Ti_{0.051})[Si_{3.003}O_{11}(O/OH/F_{0.041})]$	Nat.
$(Ca_{1.05}Ce_{0.57}La_{0.33}Nd_{0.07}Pr_{0.03})(Al_{1.91}Fe_{0.14}Mg_{0.93}Ti_{0.06})[Si_{2.94}O_{11}(O/OH_{0.94}/F_{0.06})]$	Nat.
$(Ca_{1.05}Ce_{0.57}La_{0.33}Nd_{0.07}Pr_{0.03})(Al_{1.91}Fe_{0.14}Mg_{0.93}Ti_{0.06})[Si_{2.94}O_{11}(O/OH_{0.94}/F_{0.06})]$	Nat.
$(Ca_{0.91}Ce_{0.45}La_{0.20}Nd_{0.20}Pr_{0.09}Sm_{0.08}Gd_{0.06})(Al_{0.97}Fe_{0.25}Mg_{1.81})[Si_3O_{10.99}(OH_{1.25}/F_{0.88})]$	Nat.
$(Ca_{1.639}REE_{0.323}Sr_{0.007})(Al_{2.009}Fe_{0.833}Mg_{0.083}Mn_{0.021}Ti_{0.012})[Si_{2.982}O_{11}(O/OH)]$	Nat.
$(Ca_{1.25}REE_{0.6}Th_{0.02})(Al_{2.036}Fe_{0.890}Mg_{0.137}Mn_{0.02}Ti_{0.025})[Si_{3.024}O_{11}(O/OH/F_{0.037})]$	Nat.
$(Ca_{1.47}Mn^{2+}_{0.22}REE_{0.28}Sr_{0.03})(Al_{1.69}M^{3+}_{1.03}M^{2+}_{0.20}Mg_{0.08})[Si_3O_{11}(O/OH)]$; M = Fe⁺Mn	Nat.
$(Ca_{1.71}Mn^{2+}_{0.20}REE_{0.05}Sr_{0.04})(Al_{1.77}M^{3+}_{1.18}M^{2+}_{0.04}Mg_{0.01})[Si_3O_{11}(O/OH)]$; M = Fe⁺Mn	Nat.
$(Ca_{0.96}Mn^{2+}_{0.33}REE_{0.50}Sr_{0.19}Th^{4+}_{0.02})(Al_{1.71}Fe^{3+}_{0.288}Mn^{3+}_{0.432}Fe^{2+}_{0.112}Mn^{2+}_{0.168}Mg_{0.16}Cu_{0.13})[Si_3O_{11}(O_{0.97}/F_{0.03}/OH)]$	Nat.
$(Ca_{0.64}Mn^{2+}_{0.60}REE_{0.72}Sr_{0.04})(Al_1Fe^{3+}_{0.064}Mn^{3+}_{1.216}Fe^{2+}_{0.035}Mn^{2+}_{0.675}Cu_{0.01})[Si_3O_{11}(O_{0.97}/F_{0.03}/OH)]$	Nat.

a [Å]	*b* [Å]	*c* [Å]	β [°]	*V* [Å^3]	Source
	5.632				Strens 1966
	5.632				Strens 1966
	5.650				Strens 1966
	5.679				Strens 1966
8.870	5.650	10.170	115.5	460.4	Strens 1966; aus Ernst. 1964
8.87	5.650	10.150	115.4	459.5	Strens 1966
8.885	5.687				Strens 1966
8.87	5.660	10.150	115.4	459.9	Strens 1966; aus Marmo et al. 1959
8.89	5.670	10.220	115.6	464.8	Strens 1966; aus Marmo et al. 1959
8.86	5.681	10.156	115.4	461.8	Strens 1966
8.88	5.69	10.167	115.4	463.6	Strens 1966
8.89	5.67	10.170	115.5	461.9	Strens 1966; aus Marmo et al. 1959
8.88	5.66	10.160	115.5	460.9	Strens 1966; aus Nayak & Neuvonen. 1964
8.885	5.69	10.160	115.4	464.0	Strens 1966
8.847 (2)	5.674 (1)	10.170 (1)	115.56 (1)	460.6 (1)	Langer et al. 2002
8.844 (1)	5.677 (1)	10.167 (1)	115.54 (1)	460.6 (1)	Langer et al. 2002
8.855 (1)	5.713 (1)	10.208 (1)	115.62 (1)	465.6 (1)	Langer et al. 2002
8.857 (3)	5.636 (3)	10.163 (4)	115.65 (3)	457.3 (4)	Anastasiou and Langer 1977
8.839 (3)	5.651 (3)	10.163 (4)	115.58 (3)	457.9 (4)	Anastasiou and Langer 1977
8.839 (3)	5.664 (2)	10.166 (4)	115.61 (3)	459.0 (4)	Anastasiou and Langer 1977
8.846 (2)	5.688 (2)	10.187 (2)	115.63 (2)	462.1 (3)	Anastasiou and Langer 1977
8.853 (3)	5.702 (3)	10.200 (4)	115.69 (3)	464.0 (5)	Anastasiou and Langer 1977
8.859 (3)	5.712 (3)	10.200 (4)	115.66 (3)	465.2 (5)	Anastasiou and Langer 1977
8.861 (7)	5.726 (7)	10.194 (9)	115.71 (6)	466.0 (9)	Anastasiou and Langer 1977
8.864 (7)	5.732 (6)	10.197 (8)	115.67 (5)	467.0 (9)	Anastasiou and Langer 1977
8.927 (8)	5.761 (6)	10.150 (9)	114.77 (5)	474.0	Dollase 1971
8.962 (2)	5.836 (2)	10.182 (2)	115.02 (1)	482.6	Kartashov et al. 2002
8.902 (1)	5.713 (1)	10.127 (1)	114.86 (1)	467.3 (1)	Bonazzi and Menchetti 1995
8.883 (1)	5.710 (1)	10.092 (1)	114.96 (1)	464.1 (2)	Bonazzi and Menchetti 1995
8.916 (2)	5.700 (8)	10.140 (25)	114.72 (14)	468.1 (1)	Grew et al. 1991
8.905 (18)	5.684 (1)	10.113 (1)	114.62 (2)	465.3	Rouse and Peacor (1993)
8.934 (1)	5.721 (7)	10.176 (22)	114.31 (12)	474.0	Peacor and Dunn 1988
8.891 (1)	5.662 (1)	10.130 (2)	115.20 (1)	461.4 (1)	Bonazzi and Menchetti 1995
8.902 (1)	5.702 (1)	10.132 (1)	114.94 (1)	466.3 (1)	Bonazzi and Menchetti 1995
8.881 (1)	5.683 (1)	10.150 (2)	114.99 (2)	464.3 (2)	Bonazzi et al. 1992
8.857 (1)	5.671 (1)	10.156 (1)	115.29 (1)	461.2 (1)	Bonazzi et al. 1992
8.890 (2)	5.690 (1)	10.135 (2)	114.44 (2)	466.7 (2)	Bonazzi et al. 1996
8.896 (1)	5.706 (1)	10.083 (1)	113.88 (1)	468.0 (1)	Bonazzi et al. 1996

APPENDIX B

(on following 5 pages)

Bond lengths [Å], polyhedra volumes [Å^3], selected interatomic distances [Å] and angles [°], and distortion parameters in natural and synthetic monoclinic Al-Fe^{3+} solid solutions. Calculated from the data of Dollase 1968, 1971 (D68, D71); Gabe et al. 1973 (G); Carbonin and Molin 1980 (C80); Stergiou et al. 1987 (S); Kvick et al. 1988 (K); Bonazzi and Menchetti 1995 (B&M); Comodi and Zanazzi 1997 (C&Z); Giuli et al. 1999 (G99). The distortion parameters are calculated according to Robinson et al. (1971).

Composition [X_{Ep}]	0.03	0.22	0.24	0.30	0.34	0.38	0.40	0.40
Sample	Nat.	Nat.	Nat.	Nat.	Nat.	Nat.	Nat.	Nat.
Source	D68	C&Z	B&M	C80	C80	B&M	C80	G
Sample-Nr.			CH			LP		LEP
A-Positions								
A1 - O1 (2×)	2.490	2.485	2.485	2.4762	2.4758	2.478	2.4722	2.4780
A1 - O3 (2×)	2.369	2.355	2.354	2.3492	2.3497	2.353	2.3461	2.3449
A1 - O5	2.522	2.526	2.526	2.5317	2.5389	2.535	2.5393	2.5343
A1 - O6	2.745	2.764	2.766	2.7894	2.7998	2.786	2.8092	2.7893
A1 - O7	2.282	2.277	2.282	2.2752	2.2836	2.286	2.2825	2.2841
A1 - O9 (2×)	2.9524	2.963	2.965	2.9694	2.9779	2.973	2.9797	2.9746
Mean A1 - O	2.575	2.575	2.576	2.576	2.581	2.580	2.581	2.5781
A2 - O2 (2×)	2.543	2.537	2.537	2.5369	2.5380	2.534	2.4661	2.5359
A2 - O2′ (2×)	2.819	2.814	2.816	2.8039	2.8070	2.813	2.7918	2.8097
A2 - O3 (2×)	2.531	2.552	2.555	2.5729	2.5807	2.572	2.6440	2.5754
A2 - O7	2.267	2.263	2.262	2.2556	2.2539	2.260	2.3423	2.2616
A2 - O8 (2×)	3.0445	3.038	3.038	3.0324	3.0358	3.034	3.0569	3.0294
A2 - O10	2.575	2.554	2.560	2.5511	2.5501	2.554	2.5373	2.5509
Mean A2 - O	2.672	2.670	2.671	2.670	2.673	2.672	2.680	2.6713
M-Positions								
M1 – O1 (2×)	1.930	1.928	1.927	1.9311	1.9322	1.930	1.9329	1.9316
M1 – O4 (2×)	1.850	1.848	1.847	1.8451	1.8482	1.845	1.8471	1.8466
M1 – O5 (2×)	1.937	1.936	1.939	1.9413	1.9419	1.944	1.9463	1.9433
Mean M1 – O	1.906	1.904	1.904	1.906	1.907	1.906	1.909	1.9072
Volume M1	9.146	9.130	9.12	9.146	9.169	9.15	9.191	9.168
λ M1	1.0064	1.0058	1.0069	1.0066	1.0066	1.0069	1.0064	1.0064
σ^2 M1	19.6	19.6	19.7	19.6	19.7	19.1	18.7	18.9
Inclination to (100)	76.9	76.8	76.8	76.5	76.5	76.5	76.4	76.5
O1 – O1	3.8609	3.8579	3.8532	3.8622	3.8644	3.8592	3.8659	3.8633
M2 – O3 (2×)	1.859	1.854	1.854	1.8530	1.8552	1.854	1.8535	1.8582
M2 – O6 (2×)	1.923	1.926	1.927	1.9259	1.9268	1.928	1.9275	1.9262
M2 – O10 (2×)	1.852	1.859	1.858	1.8630	1.8659	1.861	1.8651	1.8642
Mean M2 – O	1.878	1.880	1.880	1.881	1.883	1.881	1.882	1.8829
Volume M2	8.773	8.807	8.80	8.818	8.845	8.82	8.837	8.848
λ M2	1.0047	1.0039	1.0045	1.0041	1.0042	1.0044	1.0042	1.0042
σ^2 M2	14.0	13.2	12.9	12.7	13.0	13.2	12.8	13.1
Inclination to (100)	66.5	65.6	65.6	65.0	64.9	65.1	64.5	64.9
M3 - O1 (2×)	2.184	2.190	2.191	2.1994	2.2035	2.200	2.2085	2.2000
M3 - O2 (2×)	1.927	1.944	1.944	1.9485	1.9541	1.954	1.9574	1.9563
M3 - O4	1.862	1.882	1.882	1.8906	1.8957	1.899	1.9004	1.9027
M3 - O8	1.781	1.788	1.790	1.7993	1.8043	1.803	1.8138	1.8100
Mean M3 - O	1.978	1.990	1.990	1.998	2.003	2.002	2.008	2.0042
Volume M3	10.009	10.193	10.19	10.295	10.369	10.36	10.443	10.396
λ M3	1.0262	1.0260	1.0269	1.0273	1.0274	1.0270	1.0277	1.0271
σ^2 M3	58.1	62.0	62.6	65.1	65.6	65.7	67.5	66.4
O4 – O8	3.638	3.6694	3.6692	3.687	3.6976	3.700	3.7125	3.7109
T-Positions								
T1 - O1 (2×)	1.652	1.650	1.651	1.6492	1.6527	1.652	1.6483	1.6523
T1 - O7	1.566	1.564	1.564	1.5688	1.5676	1.565	1.5664	1.5619
T1 - O9	1.628	1.634	1.630	1.6274	1.6335	1.633	1.6352	1.6327
Mean T1 – O	1.625	1.625	1.624	1.624	1.627	1.626	1.625	1.6248
Volume T1	2.190	2.193	2.19	2.187	2.199	2.20	2.191	2.192
T2 - O3 (2×)	1.620	1.619	1.620	1.6195	1.6203	1.619	1.6197	1.6190
T2 - O8	1.593	1.591	1.591	1.5887	1.5887	1.591	1.5913	1.5916
T2 - O9	1.627	1.622	1.628	1.6260	1.6276	1.627	1.6244	1.6272
Mean T2 – O	1.615	1.613	1.615	1.613	1.614	1.614	1.614	1.6142
Volume T2	2.157	2.151	2.16	2.152	2.156	2.16	2.154	2.155
T3 - O2 (2×)	1.629	1.624	1.624	1.6256	1.6280	1.627	1.6279	1.6253
T3 - O5	1.661	1.667	1.664	1.6675	1.6686	1.663	1.6661	1.6669
T3 - O6	1.657	1.646	1.643	1.6439	1.6451	1.643	1.6410	1.6479
Mean T3 – O	1.644	1.640	1.639	1.641	1.642	1.640	1.641	1.6414
Volume T3	2.261	2.248	2.24	2.248	2.257	2.25	2.250	2.251
T1T2O$_7$ group								
O7 – O9 – O8	127.084	128.834	129.175	130.231	130.929	130.393	131.719	130.811
T1 – O9 – T2	164.382	161.898	161.529	160.275	159.433	160.196	158.609	159.870
Proton environment								
H – O10	0.7689	0.6829	0.9611			0.8562		0.8872
O10 – O4	2.8922	2.8916	2.8930	2.8995	2.9024	2.9031	2.9052	2.8999
O10 – H ... O4	2.9253	2.9135	2.9032			2.9546		2.9037
O10 – H – O4	160.405	163.377	169.772			156.358		173.675

Composition [X_{Ep}]	0.42	0.46	0.47	0.50	0.60	0.63	0.66	0.70
Sample	Nat.	Nat.	Nat.	Nat.	Nat.	Nat.	Synth.	Nat.
Source	B&M	B&M	C80	C80	S	C80	G99	B&M
Sample-Nr.	VO	DF			/		CC11c	GI2
A-Positions								
A1 - O1 (2×)	2.473	2.472	2.4680	2.4649	2.4705	2.4658	2.4610	2.464
A1 - O3 (2×)	2.353	2.346	2.3414	2.3388	2.3412	2.3336	2.3430	2.338
A1 - O5	2.538	2.536	2.5401	2.5451	2.5538	2.5506	2.5591	2.549
A1 - O6	2.794	2.798	2.8232	2.8243	2.8543	2.8416	2.8479	2.838
A1 - O7	2.291	2.289	2.2840	2.2893	2.3152	2.2945	2.3079	2.295
A1 - O9 (2×)	2.979	2.977	2.9840	2.9851	3.0110	2.9938	2.9939	2.991
Mean A1 - O	2.581	2.579	2.582	2.582	2.597	2.586	2.590	2.585
A2 - O2 (2×)	2.535	2.535	2.5360	2.5341	2.5400	2.5366	2.5416	2.530
A2 - O2′ (2×)	2.811	2.807	2.7977	2.7978	2.7966	2.7891	2.7951	2.794
A2 - O3 (2×)	2.584	2.587	2.6030	2.6108	2.6466	2.6338	2.6291	2.624
A2 - O7	2.259	2.259	2.2547	2.2511	2.2647	2.2437	2.2485	2.251
A2 - O8 (2×)	3.031	3.027	3.0268	3.0228	3.30331	3.0195	3.0190	3.020
A2 - O10	2.554	2.548	2.5436	2.5405	2.5391	2.5398	2.5542	2.536
Mean A2 - O	2.673	2.672	2.673	2.672	2.684	2.674	2.677	2.672
M-Positions								
M1 – O1 (2×)	1.928	1.932	1.9336	1.9352	1.9265	1.9387	1.9415	1.933
M1 – O4 (2×)	1.846	1.844	1.8460	1.8450	1.8442	1.8478	1.8453	1.842
M1 – O5 (2×)	1.945	1.945	1.9495	1.9500	1.9637	1.9350	1.9529	1.953
Mean M1 – O	1.906	1.907	1.910	1.910	1.911	1.907	1.913	1.909
Volume M1	9.16	9.16	9.206	9.211	9.233	9.259	9.259	9.20
λ M1	1.0061	1.0069	1.0064	1.0064	1.0064	0.9998	1.0063	1.0065
σ^2 M1	19.3	18.8	18.4	18.3	17.5	17.5	17.0	18.2
Inclination to (100)	76.4	76.4	76.3	76.1	76.0	76.1	75.9	76.1
O1 – O1	3.8560	3.8635	3.8672	3.8704	3.8531	3.8775	3.8830	3.8657
M2 – O3 (2×)	1.850	1.854	1.8550	1.8530	1.8596	1.8541	1.8492	1.852
M2 – O6 (2×)	1.929	1.927	1.9242	1.9266	1.9312	1.9275	1.9278	1.926
M2 – O10 (2×)	1.862	1.862	1.8654	1.8694	1.8733	1.8704	1.8693	1.865
Mean M2 – O	1.880	1.881	1.882	1.883	1.888	1.884	1.882	1.881
Volume M2	8.81	8.82	8.827	8.851	8.919	8.863	8.836	8.82
λ M2	1.0044	1.0044	1.0044	1.0041	1.0043	1.0043	1.0043	1.0044
σ^2 M2	13.3	13.4	13.8	12.7	13.5	13.3	13.3	14.6
Inclination to (100)	64.9	64.7	64.1	63.9	63.0	63.4	63.7	63.6
M3 - O1 (2×)	2.206	2.206	2.2122	2.2151	2.2362	2.2205	2.2291	2.222
M3 - O2 (2×)	1.961	1.958	1.9648	1.9657	1.9847	1.9764	1.9777	1.978
M3 - O4	1.900	1.905	1.9108	1.9120	1.9378	1.9264	1.9323	1.927
M3 - O8	1.809	1.813	1.8199	1.8274	1.8404	1.8470	1.8423	1.840
Mean M3 - O	2.007	2.008	2.014	2.017	2.037	2.028	2.031	2.028
Volume M3	10.43	10.44	10.534	10.575	10.864	10.749	10.796	10.74
λ M3	1.0280	1.0278	1.0282	1.0283	1.0299	1.0279	1.0287	1.0286
σ^2 M3	68.2	68.2	70.0	70.7	76.4	71.9	73.4	73.6
O4 – O8	3.707	3.7158	3.7291	3.7380	3.7768	3.7724	3.7736	3.7658
T-Positions								
T1 - O1 (2×)	1.654	1.652	1.6505	1.6497	1.6573	1.6469	1.6430	1.649
T1 - O7	1.567	1.566	1.5681	1.5658	1.5509	1.5725	1.5697	1.566
T1 - O9	1.631	1.632	1.6343	1.6377	1.6463	1.6319	1.6306	1.631
Mean T1 – O	1.627	1.626	1.626	1.626	1.628	1.625	1.622	1.624
Volume T1	2.20	2.19	2.196	2.196	2.206	2.191	2.180	2.19
T2 - O3 (2×)	1.623	1.620	1.6187	1.6185	1.6125	1.6178	1.6240	1.617
T2 - O8	1.592	1.593	1.5926	1.5906	1.5867	1.5868	1.5944	1.591
T2 - O9	1.628	1.628	1.6254	1.6225	1.6440	1.6339	1.6277	1.633
Mean T2 – O	1.617	1.615	1.614	1.613	1.614	1.614	1.618	1.615
Volume T2	2.16	2.16	2.155	2.149	2.155	2.156	2.170	2.16
T3 - O2 (2×)	1.624	1.626	1.6260	1.6262	1.6317	1.6250	1.6162	1.626
T3 - O5	1.663	1.667	1.6664	1.6647	1.6600	1.6686	1.6688	1.666
T3 - O6	1.641	1.645	1.6447	1.6413	1.6405	1.6409	1.6381	1.641
Mean T3 – O	1.638	1.641	1.641	1.640	1.641	1.640	1.635	1.640
Volume T3	2.24	2.25	2.250	2.245	2.254	2.247	2.228	2.25
$T1T2O_7$ group								
O7 – O9 – O8	131.199	131.400	132.388	132.890	135.222	134.217	134.640	133.758
T1 – O9 – T2	159.198	159.018	157.768	157.407	154.724	155.902	155.517	156.445
Proton environment								
H – O10	0.8486	0.8616			1.0547			0.9108
O10 – O4	2.9090	2.9159	2.9144	2.9107	2.9432	2.9174	2.9199	2.9339
O10 – H ... O4	2.9410	2.9206			2.9548			2.9418
O10 – H – O4	161.296	172.832			169.369			170.995

Composition [X_{Ep}]	0.70	0.71	0.73	0.79	0.81	0.81	0.82	0.84
Sample	Nat.	Synth.	Nat.	Nat.	Nat.	Nat.	Nat.	Nat.
Source	B&M	G99	B&M	C80	K	D71	B&M	G
Sample-Nr.	PS	CC11b	GI1		/	/	MRV	HEP
A-Positions								
A1 - O1 (2×)	2.464	2.4695	2.463	2.4592	2.4608	2.4647	2.458	2.4585
A1 - O3 (2×)	2.338	2.3343	2.336	2.3282	2.3272	2.3250	2.329	2.3227
A1 - O5	2.551	2.5526	2.549	2.5594	2.5519	2.5622	2.556	2.5556
A1 - O6	2.836	2.8512	2.838	2.8633	2.8590	2.8847	2.858	2.8612
A1 - O7	2.295	2.3043	2.294	2.2967	2.2957	2.2932	2.296	2.2949
A1 - O9 (2×)	2.992	2.9933	2.994	3.0030	3.0019	3.0074	3.000	2.9999
Mean A1 - O	2.586	2.589	2.585	2.589	2.5874	2.593	2.587	2.5860
A2 - O2 (2×)	2.535	2.5435	2.531	2.5315	2.5193	2.5340	2.528	2.5270
A2 - O2′ (2×)	2.794	2.7877	2.794	2.7819	2.8007	2.7824	2.788	2.7842
A2 - O3 (2×)	2.627	2.6441	2.628	2.6557	2.6412	2.6817	2.648	2.6528
A2 - O7	2.255	2.2455	2.253	2.2477	2.2508	2.2342	2.249	2.2480
A2 - O8 (2×)	3.022	3.0217	3.021	3.0164	3.0177	3.0140	3.017	3.0146
A2 - O10	2.541	2.5242	2.536	2.5310	2.5206	2.5292	2.525	2.5307
Mean A2 - O	2.675	2.676	2.674	2.675	2.6729	2.679	2.674	2.6736
M-Positions								
M1 – O1 (2×)	1.936	1.9400	1.936	1.9377	1.9407	1.9436	1.937	1.9393
M1 – O4 (2×)	1.844	1.8470	1.844	1.8444	1.8454	1.8460	1.844	1.8434
M1 – O5 (2×)	1.952	1.9521	1.955	1.9606	1.9566	1.9708	1.959	1.9559
Mean M1 – O	1.911	1.913	1.912	1.914	1.9142	1.920	1.913	1.9129
Volume M1	9.22	9.248	9.23	9.274	9.274	9.364	9.26	9.252
λ M1	1.0064	1.0069	1.0068	1.0063	1.0063	1.0061	1.0064	1.0065
σ^2 M1	18.4	19.7	17.8	17.2	17.3	15.9	17.2	17.9
Inclination to (100)	76.1	76.1	76.0	75.8	76.1	75.8	75.8	75.9
O1 – O1	3.8721	3.8800	3.8715	3.8753	3.8811	3.887	3.8747	3.8787
M2 – O3 (2×)	1.853	1.8523	1.854	1.8546	1.8533	1.8597	1.852	1.8539
M2 – O6 (2×)	1.926	1.9312	1.926	1.9270	1.9249	1.9303	1.927	1.9269
M2 – O10 (2×)	1.865	1.8657	1.866	1.8729	1.9726	1.8741	1.869	1.8696
Mean M2 – O	1.881	1.883	1.882	1.885	1.8836	1.888	1.883	1.8835
Volume M2	8.82	8.844	8.83	8.872	8.855	8.917	8.84	8.853
λ M2	1.0047	1.0048	1.0046	1.0045	1.0044	1.0045	1.0046	1.0045
σ^2 M2	14.6	14.7	14.7	14.2	14.1	14.0	14.7	14.0
Inclination to (100)	63.6	63.2	63.5	62.8	63.0	62.3	62.9	62.7
M3 - O1 (2×)	2.218	2.2253	2.222	2.2309	2.2164	2.2398	2.227	2.2241
M3 - O2 (2×)	1.977	1.9835	1.980	1.9902	1.9871	1.9961	1.989	1.9855
M3 - O4	1.926	1.9180	1.928	1.9402	1.9435	1.9475	1.937	1.9352
M3 - O8	1.840	1.8516	1.843	1.8596	1.8601	1.8804	1.856	1.8600
Mean M3 - O	2.026	2.031	2.029	2.040	2.0351	2.050	2.038	2.0357
Volume M3	10.72	10.794	10.76	10.927	10.731	11.085	10.89	10.863
λ M3	1.0279	1.0285	1.0286	1.0291	1.0358	1.0287	1.0285	1.0283
σ^2 M3	72.7	72.9	73.1	76.7	74.7	76.6	75.4	74.7
O4 – O8	3.7648	3.7682	3.7706	3.7992	3.8031	3.8273	3.7927	3.7945
T-Positions								
T1 - O1 (2×)	1.653	1.6468	1.651	1.6520	1.6536	1.6455	1.651	1.6499
T1 - O7	1.567	1.5645	1.567	1.5676	1.5684	1.5855	1.567	1.5635
T1 - O9	1.636	1.6336	1.634	1.6373	1.6409	1.6392	1.636	1.6343
Mean T1 – O	1.627	1.623	1.626	1.627	1.6291	1.629	1.626	1.6244
Volume T1	2.20	2.186	2.19	2.202	2.209	2.211	2.20	2.190
T2 - O3 (2×)	1.619	1.6168	1.617	1.6175	1.6209	1.6117	1.619	1.6184
T2 - O8	1.592	1.5758	1.589	1.5936	1.5924	1.5880	1.594	1.5876
T2 - O9	1.630	1.6247	1.632	1.6309	1.6322	1.6282	1.632	1.6315
Mean T2 – O	1.615	1.609	1.614	1.615	1.6169	1.610	1.616	1.6140
Volume T2	2.16	2.133	2.16	2.159	2.167	2.139	2.16	2.155
T3 - O2 (2×)	1.627	1.6160	1.626	1.6275	1.6283	1.6220	1.627	1.6274
T3 - O5	1.667	1.6760	1.666	1.6653	1.6695	1.6616	1.665	1.6676
T3 - O6	1.643	1.6354	1.643	1.6418	1.6408	1.6399	1.639	1.6383
Mean T3 – O	1.641	1.636	1.640	1.641	1.6417	1.636	1.640	1.6402
Volume T3	2.25	2.231	2.25	2.250	2.255	2.232	2.25	2.249
T1T2O$_7$ group								
O7 – O9 – O8	133.517	134.178	133.916	135.431	135.327	136.104	135.001	135.392
T1 – O9 – T2	156.649	156.570	156.175	154.515	154.791	153.568	154.935	154.574
Proton environment								
H – O10	0.8525		0.7491		0.9753		0.8479	0.9548
O10 – O4	2.9329	2.9480	2.9331	2.9369	2.9222	2.9447	2.9391	2.9334
O10 – H ... O4	2.9482		2.9489		2.9393		2.9610	2.9790
O10 – H – O4	167.145		166.722		166.872		164.604	158.457

Composition [X_{Ep}]	0.85	0.85	0.86	0.91	0.95	1.00	1.0	1.02
Sample	Synth.	Synth.	Nat.	Nat.	Nat.	Nat.	Synth.	Nat.
Source	G99	G99	C80	B&M	B&M	B&M	G99	B&M
Sample-Nr.	CC9e	16b		TRV	IG	MBN	20c	CC
A-Positions								
A1 - O1 (2×)	2.4570	2.4547	2.4526	2.454	2.456	2.455	2.4564	2.454
A1 - O3 (2×)	2.3311	2.3248	2.3237	2.328	2.327	2.327	2.3265	2.327
A1 - O5	2.5583	2.5555	2.5583	2.558	2.559	2.564	2.5664	2.560
A1 - O6	2.8629	2.8758	2.8786	2.870	2.879	2.888	2.8730	2.882
A1 - O7	2.3010	2.2900	2.2993	2.297	2.300	2.301	2.2876	2.298
A1 - O9 (2×)	3.0022	2.9960	3.0076	3.009	3.009	3.013	3.0108	3.012
Mean A1 - O	2.589	2.586	2.589	2.590	2.591	2.593	2.590	2.592
A2 - O2 (2×)	2.5424	2.5263	2.5292	2.530	2.529	2.531	2.5420	2.531
A2 - O2′ (2×)	2.7872	2.7860	2.7793	2.783	2.782	2.781	2.7782	2.779
A2 - O3 (2×)	2.6570	2.6544	2.6687	2.669	2.671	2.678	2.6777	2.677
A2 - O7	2.2440	2.2418	2.2417	2.246	2.249	2.246	2.2479	2.245
A2 - O8 (2×)	3.0223	3.0147	3.0120	3.016	3.015	3.019	3.0202	3.016
A2 - O10	2.5213	2.5210	2.5254	2.525	2.524	2.519	2.5138	2.524
Mean A2 - O	2.678	2.673	2.675	2.677	2.677	2.678	2.680	2.678
M-Positions								
M1 – O1 (2×)	1.9478	1.9412	1.9395	1.942	1.942	1.945	1.9432	1.945
M1 – O4 (2×)	1.8493	1.8476	1.8456	1.847	1.847	1.848	1.8592	1.850
M1 – O5 (2×)	1.9677	1.9587	1.9625	1.963	1.966	1.967	1.9677	1.967
Mean M1 – O	1.922	1.916	1.916	1.917	1.918	1.920	1.923	1.921
Volume M1	9.381	9.299	9.300	9.32	9.34	9.36	9.417	9.37
λ M1	1.0064	1.0062	1.0062	1.0063	1.0059	1.0062	1.0055	1.0062
σ^2 M1	17.2	17.1	16.7	16.6	16.4	17.0	15.3	16.2
Inclination to (100)	75.7	75.8	75.7	75.7	75.7	75.7	75.7	75.7
O1 – O1	3.8955	3.8825	3.8789	3.8832	3.8846	3.8898	3.8863	3.8901
M2 – O3 (2×)	1.8548	1.8597	1.8532	1.853	1.853	1.852	1.8584	1.854
M2 – O6 (2×)	1.9271	1.9323	1.9241	1.926	1.929	1.930	1.9238	1.927
M2 – O10 (2×)	1.8671	1.8696	1.8719	1.869	1.873	1.874	1.8762	1.872
Mean M2 – O	1.883	1.887	1.883	1.883	1.885	1.885	1.886	1.884
Volume M2	8.840	8.908	8.848	8.84	8.87	8.88	8.888	8.86
λ M2	1.0050	1.0043	1.0044	1.0046	1.0048	1.0044	1.0046	1.0049
σ^2 M2	15.7	13.3	14.9	15.6	14.8	15.2	14.9	15.6
Inclination to (100)	62.8	62.7	62.3	62.5	62.4	62.2	62.2	62.3
M3 - O1 (2×)	2.2367	2.2291	2.2346	2.236	2.236	2.236	2.2401	2.239
M3 - O2 (2×)	1.9861	1.9771	1.9947	1.994	1.997	1.997	1.9858	1.998
M3 - O4	1.9240	1.9304	1.9454	1.944	1.947	1.949	1.9333	1.946
M3 - O8	1.8532	1.8532	1.8759	1.864	1.872	1.872	1.8497	1.871
Mean M3 - O	2.037	2.033	2.047	2.045	2.048	2.048	2.039	2.049
Volume M3	10.882	10.814	11.026	10.99	11.04	11.05	10.906	11.06
λ M3	1.0292	1.0287	1.0290	1.0295	1.0291	1.0288	1.0297	1.0289
σ^2 M3	74.3	74.5	78.0	76.7	77.1	77.0	76.2	76.6
O4 – O8	3.7761	3.7828	3.8208	3.8074	3.8193	3.8205	3.7824	3.8160
T-Positions								
T1 - O1 (2×)	1.6454	1.6516	1.6515	1.651	1.652	1.653	1.6538	1.651
T1 - O7	1.5660	1.5710	1.5694	1.573	1.568	1.567	1.5705	1.569
T1 - O9	1.6352	1.6304	1.6356	1.639	1.635	1.635	1.6412	1.637
Mean T1 – O	1.623	1.626	1.627	1.628	1.627	1.627	1.630	1.627
Volume T1	2.185	2.198	2.201	2.21	2.20	2.20	2.212	2.20
T2 - O3 (2×)	1.6161	1.6131	1.6188	1.618	1.619	1.621	1.6142	1.617
T2 - O8	1.5874	1.5900	1.5876	1.594	1.594	1.594	1.6013	1.594
T2 - O9	1.6262	1.6247	1.6346	1.634	1.635	1.635	1.6268	1.634
Mean T2 – O	1.611	1.610	1.615	1.616	1.617	1.618	1.614	1.616
Volume T2	2.145	2.140	2.160	2.16	2.16	2.17	2.156	2.16
T3 - O2 (2×)	1.6209	1.6315	1.6266	1.627	1.628	1.630	1.6281	2.626
T3 - O5	1.6600	1.6681	1.6676	1.667	1.664	1.664	1.6635	1.666
T3 - O6	1.6405	1.6293	1.6421	1.644	1.641	1.639	1.6528	1.644
Mean T3 – O	1.636	1.640	1.641	1.641	1.640	1.641	1.643	1.641
Volume T3	2.229	2.251	2.252	2.25	2.25	2.25	2.261	2.25
$T1T2O_7$ group								
O7 – O9 – O8	135.320	135.034	136.409	136.008	136.059	136.274	135.066	136.292
T1 – O9 – T2	154.778	155.131	153.521	153.646	153.793	153.522	153.720	153.474
Proton environment								
H – O10				0.8536	0.8885	0.8658		0.8781
O10 – O4	2.9494	2.9390	2.9409	2.9483	2.9459	2.9488	2.9348	2.9480
O10 – H ... O4				2.9512	2.9775	2.9776		2.9542
O10 – H – O4				174.313	161.711	162.430		171.965

Composition [X_{Ep}]	1.04	1.04	1.09	1.14
Sample	Nat.	Nat.	Synth.	Nat.
Source	B&M	B&M	G99	B&M
Sample-Nr.	NI	CZ	12a	FC
A-Positions				
A1 - O1 (2×)	2.455	2.454	2.4463	2.455
A1 - O3 (2×)	2.328	2.326	2.3333	2.325
A1 - O5	2.557	2.563	2.5569	2.560
A1 - O6	2.884	2.892	2.8842	2.902
A1 - O7	2.298	2.299	2.2950	2.299
A1 - O9 (2×)	3.011	3.015	3.0227	3.023
Mean A1 - O	2.592	2.594	2.593	2.596
A2 - O2 (2×)	2.534	2.533	2.5624	2.536
A2 - O2′ (2×)	2.777	2.774	2.9880	2.773
A2 - O3 (2×)	2.681	2.684	2.5030	2.700
A2 - O7	2.251	2.244	2.2189	2.244
A2 - O8 (2×)	3.016	3.020	3.0498	3.019
A2 - O10	2.526	2.518	2.3279	2.521
Mean A2 - O	2.679	2.678	2.675	2.682
M-Positions				
M1 – O1 (2×)	1.949	1.950	1.9464	1.954
M1 – O4 (2×)	1.849	1.853	1.8508	1.855
M1 – O5 (2×)	1.968	1.970	1.9766	1.976
Mean M1 – O	1.922	1.924	1.925	1.928
Volume M1	9.39	9.42	9.432	9.48
λ M1	1.0062	1.0064	1.0059	1.0064
σ^2 M1	16.6	16.5	15.5	16.5
Inclination to (100)	75.7	75.7	75.7	75.7
O1 – O1	3.8980	3.8989	3.8927	3.9082
M2 – O3 (2×)	1.853	1.858	1.8592	1.855
M2 – O6 (2×)	1.927	1.932	1.9249	1.930
M2 – O10 (2×)	1.871	1.874	1.8788	1.876
Mean M2 – O	1.884	1.888	1.888	1.887
Volume M2	8.85	8.92	8.910	8.90
λ M2	1.0049	1.0043	1.0045	1.0047
σ^2 M2	15.7	15.0	14.8	16.2
Inclination to (100)	62.2	62.1	62.1	61.7
M3 - O1 (2×)	2.239	2.242	2.2486	2.245
M3 - O2 (2×)	1.998	1.995	1.9943	2.003
M3 - O4	1.945	1.943	1.9437	1.951
M3 - O8	1.872	1.861	1.8560	1.881
Mean M3 - O	2.049	2.046	2.048	2.055
Volume M3	11.06	11.02	11.044	11.15
λ M3	1.0289	1.0295	1.0296	1.0295
σ^2 M3	75.6	75.6	75.9	76.6
O4 – O8	3.8175	3.8037	3.7988	3.8312
T-Positions				
T1 - O1 (2×)	1.651	1.652	1.6512	1.654
T1 - O7	1.564	1.566	1.5800	1.570
T1 - O9	1.637	1.637	1.6461	1.638
Mean T1 – O	1.626	1.627	1.632	1.629
Volume T1	2.19	2.20	2.221	2.21
T2 - O3 (2×)	1.616	1.617	1.6154	1.621
T2 - O8	1.593	1.599	1.5811	1.597
T2 - O9	1.633	1.636	1.6355	1.634
Mean T2 – O	1.615	1.617	1.612	1.618
Volume T2	2.16	2.17	2.147	2.17
T3 - O2 (2×)	2.626	2.628	1.6249	1.630
T3 - O5	1.667	1.669	1.6544	1.668
T3 - O6	1.644	1.642	1.6528	1.644
Mean T3 – O	1.641	1.642	1.639	1.643
Volume T3	2.25	2.26	2.245	2.26
$T1T2O_7$ group				
O7 – O9 – O8	136.244	136.571	136.896	137.054
T1 – O9 – T2	153.631	153.151	152.112	152.693
Proton environment				
H – O10	0.7330	0.9465		0.8622
O10 – O4	2.9522	2.9509	2.9404	2.9569
O10 – H ... O4	2.9914	2.9549		2.9673
O10 – H – O4	158.394	173.633		169.429

APPENDIX C

Lattice constants of natural and synthetic zoisite at room temperature and pressure.

Composition	Sample
$Ca_2Al_2Al[Si_3O_{11}(O/OH)]$	Synth.
$Ca_2Al_2Al[Si_3O_{11}(O/OH)]$	Synth
$Ca_2Al_2Al[Si_3O_{11}(O/OH)]$	Synth.
$Ca_2Al_2(Al_{0.957\text{-}0.977}Fe^{3+}_{0.023\text{-}0.043})[Si_3O_{11}(O/OH)]$	Nat.
$Ca_2Al_2(Al_{0.957\text{-}0.977}Fe^{3+}_{0.023\text{-}0.043})[Si_3O_{11}(O/OH)]$	Nat.
$Ca_2Al_2Al[Si_3O_{11}(O/OH)]$	Synth.
$Ca_2Al_2(Al_{0.953\text{-}0.977}Fe^{3+}_{0.023\text{-}0.047})[Si_3O_{11}(O/OH)]$	Synth.
$Ca_2Al_2(Al_{0.915\text{-}0.961}Fe^{3+}_{0.039\text{-}0.085})[Si_3O_{11}(O/OH)]$	Synth.
$Ca_2Al_2(Al_{0.881\text{-}0.927}Fe^{3+}_{0.073\text{-}0.119})[Si_3O_{11}(O/OH)]$	Synth.
$Ca_2Al_2(Al_{0.865\text{-}0.903}Fe^{3+}_{0.097\text{-}0.135})[Si_3O_{11}(O/OH)]$	Synth.
$(Ca_{2.025}Fe^{2+}_{0.01}Na_{0.005}K_{0.02})Al_2(Al_{0.94}Fe^{3+}_{0.015}Mg_{0.005}Ti_{0.005})[Si_{2.995}P_{0.005}O_{11}(O/OH)]$	Nat.
$(Ca_{1.995}Fe^{2+}_{0.02}Na_{0.005}K_{0.02})Al_2(Al_{0.935}Fe^{3+}_{0.035}Mg_{0.005}Ti_{0.005})[Si_{2.955}P_{0.005}Al_{0.03}O_{11}(O/OH)]$	Nat.
$(Ca_{2.07}Fe^{2+}_{0.015}Na_{0.005}K_{0.02})Al_2(Al_{0.815}Fe^{3+}_{0.105}Mg_{0.005}Ti_{0.005}Mn_{0.005})[Si_{2.985}P_{0.005}Al_{0.01}O_{11}(O/OH)]$	Nat.
$(Ca_{2.005}Fe^{2+}_{0.015}Na_{0.005}K_{0.02})Al_2(Al_{0.85}Fe^{3+}_{0.105}Mg_{0.005}Ti_{0.01})\ [Si_{2.98}P_{0.01}Al_{0.01}O_{11}(O/OH)]$	Nat.
$(Ca_{2.00}Fe^{2+}_{0.02}Na_{0.005}K_{0.02})Al_2(Al_{0.81}Fe^{3+}_{0.14}Mg_{0.005})\ [Si_{3.005}P_{0.005}O_{11}(O/OH)]$	Nat.
$Ca_2Al_2Al[Si_3O_{11}(O/OH)]$	Synth.
$Ca_2Al_2(Al_{0.9}Fe^{3+}_{0.1})[Si_3O_{11}(O/OH)]$	Nat.
$Ca_2Al_2Al[Si_3O_{11}(O/OH)]$	Synth.
$Ca_2Al_2Al[Si_3O_{11}(O/OH)]$	Synth.
$Ca_2Al_2Al[Si_3O_{11}(O/OD)]$	Synth.
$Ca_2Al_2Al[Si_3O_{11}(O/OH)]$	Synth.
$Ca_2Al_2(Al_{0.89\text{-}0.92}Fe^{3+}_{0.08\text{-}0.11})[Si_3O_{11}(O/OH)]$	Nat.
$Ca_2Al_2Al[Si_3O_{11}(O/OH)]$	/
$Ca_2Al_2(Al_{0.925}Fe^{3+}_{0.075})[Si_3O_{11}(O/OH)]$	Nat.
$Ca_2Al_2Al[Si_3O_{11}(O/OH)]$	Synth.
$Ca_2Al_2Al[Si_3O_{11}(O/OH)]$	Synth.
$Ca_{2.02}Al_2(Al_{0.92}Fe^{3+}_{0.075}Mn_{0.005})[Si_{2.89}Al_{0.11}O_{11}(O/OH)]$	Nat.
$Ca_2Al_2Al[Si_3O_{11}(O/OH)]$	Synth.
$(Ca_{1.97}Sr_{<0.01}Mg_{<0.01}Zn_{0.01})Al_2(Al_{0.86}Fe^{3+}_{0.10}Mn^{3+}_{0.03}Cu_{0.01})[Si_{3.02}O_{11}(O/OH)]$	Nat.
$Ca_2Al_2(Al_{0.75}Mn^{3+}_{0.25})[Si_3O_{11}(O/OH)]$	Synth.
$Ca_2Al_2(Al_{0.88}Fe^{3+}_{0.01}Mn^{3+}_{0.11})[Si_{2.99}O_{11}(O/OH)]$	Nat.
$Ca_2Al_2(Al_{0.83}Fe^{3+}_{0.03}Mn^{3+}_{0.14})[Si_3O_{11}(O/OH)]$	Nat.
$Ca_{1.99}Al_2(Al_{0.86}Mn^{3+}_{0.14})[Si_{2.99}O_{11}(O/OH)]$	Nat.
$(Ca_{1.98}Sr_{0.02})Al_2(Al_{0.85}Fe^{3+}_{<0.01}Mn^{3+}_{0.14})[Si_{2.99}O_{11}(O/OH)]$	Nat.
$Ca_2Al_2(Al_{0.82}Fe^{3+}_{<0.01}Mn^{3+}_{0.17})[Si_{3.01}O_{11}(O/OH)]$	Nat.
$Ca_2Al_2(Al_{0.77}Fe^{3+}_{0.12}Mn^{3+}_{0.11})[Si_3O_{11}(O/OH)]$	Nat.
$(Ca_{1.98}Sr_{<0.01}Mg_{0.01})Al_2(Al_{0.96}Fe^{3+}_{<0.01}V^{3+}_{0.01})[Si_3O_{11}(O/OH)]$	Nat.
Tanzanite	Nat.

a [Å]	*b* [Å]	*c* [Å]	*V* [Å^3]	Source
16.188 (6)	5.550 (2)	10.034 (4)	901.5 (6)	Grevel et al. 2000
16.178 (6)	5.547 (2)	10.029 (5)	900.0 (7)	Grevel et al. 2000
16.186 (7)	5.548 (3)	10.039 (6)	901.5 (8)	Grevel et al. 2000
16.219 (9)	5.566 (3)	10.05 (1)	907 (1)	Pawley et al. 1998
16.210 (2)	5.5552 (8)	10.041 (1)	904.2 (2)	Pawley et al. 1996
16.1913 (4)	5.5488 (1)	10.0320 (3)	901.30 (5)	Liebscher et al. 2002
16.1900 (6)	5.5511 (2)	10.0332 (3)	901.70 (7)	Liebscher et al. 2002
16.2009 (5)	5.5536 (2)	10.0336 (3)	902.76 (6)	Liebscher et al. 2002
16.1983 (8)	5.5564 (2)	10.0376 (5)	903.43 (10)	Liebscher et al. 2002
16.1964 (11)	5.5580 (3)	10.0400 (6)	903.8 (11)	Liebscher et al. 2002
16.205 (2)	5.551 (1)	10.035 (1)	902.64 (18)	Myer 1966
16.205 (1)	5.554 (1)	10.038 (1)	903.38 (16)	Myer 1966
16.213 (2)	5.558 (1)	10.037 (2)	904.34 (23)	Myer 1966
16.214 (2)	5.557 (1)	10.037 (2)	904.26 (22)	Myer 1966
16.224 (2)	5.563 (21)	10.044 (3)	906.51 (27)	Myer 1966
/	/	/	901.86 (32)	Schmidt and Poli 1994
16.212 (3)	5.555 (1)	10.034 (2)	903.6 (4)	Comodi and Zanazzi 1997
16.1903 (15)	5.5487 (7)	10.0337 (11)	901.37 (13)	Chatterjee et al. 1984
16.193 (2)	5.549 (1)	10.036 (2)	901.8 (1)	Langer and Lattard 1980
16.194 (2)	5.550 (1)	10.036 (2)	902.0 (1)	Langer and Lattard 1980
16.15 (1)	5.581 (5)	10.06 (1)	906.2 (24)	Pistorius 1961
16.212 (8)	5.559 (6)	10.036 (4)	904.5 (15)	Dollase 1968
16.23	5.51	10.16	909	Fesenko et al. 1955
16.20	5.54	10.07	904	Newton 1965
16.188 (6)	5.581 (3)	10.043 (5)	904.2 (6)	Storre et al. 1982
16.190 (14)	5.559 (4)	10.035 (10)	903.2 (14)	Storre et al. 1982
16.20	5.56	10.04	904	Seki 1959
16.188 (6)	5.581 (3)	10.043 (5)	904.2 (6)	Johannes and Ziegenbein 1980
16.2051 (37)	5.5488 (12)	10.0229 (18)	902.1	Langer et al. 2002
16.177 (6)	5.575 (2)	10.045 (3)	905.8 (4)	Anastasiou and Langer 1977
16.194 (3)	5.559 (1)	10.041 (2)	903.9 (0.2)	Reinecke 1986
16.199 (2)	5.565 (1)	10.038 (2)	904.8 (0.2)	Reinecke 1986
16.189 (2)	5.562 (1)	10.039 (1)	904.0 (0.2)	Reinecke 1986
16.188 (4)	5.562 (2)	10.039 (3)	903.9 (0.3)	Reinecke 1986
16.190 (4)	5.563 (1)	10.038 (2)	904.1 (0.2)	Reinecke 1986
16.204 (2)	5.560 (1)	10.035 (1)	904.1 (0.2)	Reinecke 1986
16.20 (1)	5.55 (1)	10.00 (1)	899 (3)	Hurlbut 1969
16.1909 (15)	5.5466 (5)	10.0323 (6)	900.9 (9)	Smith et al. 1987

APPENDIX D

Bond lengths [Å], polyhedra volumes [Å^3], selected interatomic distances [Å] and angles [°] in natural and synthetic Al-Fe^{3+} zoisite solid solutions. Calculated from the data of Dollase 1968 (D68); Brunsmann 2000 (B); Liebscher et al. 2002 (L).

Composition [X_{Fe}]	0.0 (0)	0.035 (12)	0.062 (23)	0.096 (23)	0.095 (15)	0.116 (19)
Sample	synth.	synth.	synth.	synth.	nat.	synth.
Source	B, L	B, L	B, L	B, L	D68	B, L
A-Positions						
A1 - O1 (2×)	2.475 (12)	2.457 (16)	2.468 (14)	2.46 (2)	2.51 (1)	2.40 (3)
A1 - O3 (2×)	2.415 (12)	2.405 (18)	2.409 (16)	2.39 (2)	2.42 (1)	2.39 (4)
A1 - O5	2.598 (16)	2.61 (2)	2.62 (2)	2.63 (3)	2.59 (1)	2.62 (6)
A1 - O6	2.565 (16)	2.57 (2)	2.57 (2)	2.60 (3)	2.55 (1)	2.57 (5)
A1 - O7	2.229 (18)	2.27 (2)	2.26 (2)	2.32 (3)	2.25 (1)	2.45 (6)
A1 - O9 * (2×)	2.902 (5)	2.906 (7)	2.908 (6)	2.915 (10)	2.916	2.933 (18)
Mean A1 - O (without *)	2.453 (14)	2.453 (18)	2.458 (17)	2.46 (2)	2.47 (1)	2.46 (4)
A2 - O2 (2×)	2.505 (12)	2.504 (16)	2.486 (16)	2.45 (2)	2.52 (1)	2.50 (4)
A2 - O2′ (2×)	2.794 (12)	2.824 (16)	2.819 (14)	2.83 (2)	2.79 (1)	2.84 (4)
A2 - O3 (2×)	2.448 (12)	2.437 (18)	2.445 (16)	2.47 (2)	2.47 (1)	2.49 (4)
A2 - O7	2.321 (16)	2.33 (2)	2.32 (2)	2.31 (3)	2.31 (1)	2.26 (5)
A2 - O8 * (2×)	3.015 (8)	3.004 (10)	3.018 (10)	2.990 (14)	3.007	2.96 (2)
A2 - O10 *	3.013 (18)	3.03 (3)	3.00 (2)	2.98 (4)	3.01 (1)	3.01 (6)
Mean A2 - O (without *)	2.545 (13)	2.551 (17)	2.546 (16)	2.54 (2)	2.55 (1)	2.56 (4)
M-Positions						
M1,2 – O1	1.991 (12)	1.979 (16)	1.997 (14)	1.96 (2)	1.96 (1)	1.93 (3)
M1,2 – O3	1.864 (12)	1.850 (16)	1.859 (14)	1.83 (2)	1.85 (1)	1.84 (3)
M1,2 – O4	1.827 (12)	1.835 (14)	1.839 (14)	1.85 (2)	1.84 (1)	1.84 (3)
M1,2 – O5	1.893 (12)	1.917 (16)	1.920 (14)	1.90 (2)	1.90 (1)	1.88 (4)
M1,2 - O6	1.932 (12)	1.900 (16)	1.911 (14)	1.92 (2)	1.93 (1)	1.91 (4)
M1,2 - O10	1.848 (10)	1.871 (14)	1.857 (12)	1.86 (2)	1.85 (1)	1.90 (3)
Mean M1,2 – O	1.893 (12)	1.892 (15)	1.897 (14)	1.89 (2)	1.89 (1)	1.88 (3)
Volume	9.0 (2)	9.0 (2)	9.0 (2)	8.9 (3)	8.9	8.8 (4)
M3 - O1 (2×)	2.129 (12)	2.142 (16)	2.126 (16)	2.10 (2)	2.13 (1)	2.07 (4)
M3 - O2 (2×)	1.934 (12)	1.938 (16)	1.939 (14)	1.94 (2)	1.96 (1)	1.90 (3)
M3 - O4	1.871 (18)	1.90 (3)	1.87 (2)	1.87 (4)	1.82 (1)	1.92 (6)
M3 - O8	1.74 (2)	1.75 (3)	1.74 (2)	1.82 (4)	1.78 (1)	1.95 (6)
Mean M3 - O	1.956 (14)	1.97 (2)	1.957 (17)	1.96 (3)	1.97 (1)	1.97 (4)
Volume	9.7 (2)	9.8 (2)	9.7 (2)	9.7 (3)	9.9	9.8 (5)
O4 – O8	3.61 (3)	3.65 (4)	3.61 (3)	3.69 (3)	3.61	3.87 (6)
T-Positions						
T1 - O1 (2×)	1.659 (12)	1.686 (16)	1.672 (14)	1.75 (2)	1.66 (1)	1.83 (4)
T1 - O7	1.607 (16)	1.58 (2)	1.57 (2)	1.60 (3)	1.59 (1)	1.57 (5)
T1 - O9	1.634 (18)	1.66 (3)	1.68 (2)	1.66 (4)	1.65 (1)	1.67 (6)
Mean T1 – O	1.640 (15)	1.65 (2)	1.649 (17)	1.69 (3)	1.64 (1)	1.73 (5)
Volume	2.24 (5)	2.30 (8)	2.28 (8)	2.46 (11)	2.23	2.60 (17)
T2 - O3 (2×)	1.614 (12)	1.639 (18)	1.630 (16)	1.65 (2)	1.62 (1)	1.67 (4)
T2 - O8	1.63 (2)	1.61 (3)	1.61 (2)	1.56 (4)	1.58 (1)	1.47 (6)
T2 - O9	1.620 (18)	1.56 (2)	1.56 (2)	1.54 (3)	1.62 (1)	1.48 (5)
Mean T2 – O	1.620 (16)	1.61 (2)	1.608 (18)	1.60 (3)	1.61 (1)	1.57 (5)
Volume	2.17 (5)	2.14 (7)	2.12 (7)	2.09 (10)	2.14	1.97 (14)
T3 - O2 (2×)	1.632 (10)	1.620 (14)	1.637 (14)	1.651 (18)	1.62 (1)	1.64 (3)
T3 - O5	1.635 (18)	1.62 (2)	1.61 (2)	1.65 (3)	1.65 (1)	1.70 (6)
T3 - O6	1.660 (18)	1.67 (2)	1.68 (2)	1.62 (3)	1.67 (1)	1.65 (5)
Mean T3 – O	1.640 (14)	1.633 (17)	1.641 (17)	1.64 (2)	1.64 (1)	1.66 (4)
Volume	2.23 (5)	2.21 (7)	2.24 (8)	2.26 (10)	2.23	2.31 (15)
T1T2O$_7$ Group						
O7 – O8	4.62 (3)	4.66 (4)	4.62 (4)	4.73 (6)	4.61	4.80 (11)
T1 - O9 - T2	174.5 (12)	173.1 (16)	173.2 (14)	172 (2)	172.6 (8)	170 (4)
O7 – O9 – O8	118 (1)	121 (1)	120 (1)	123 (2)	120	130 (4)
Proton environment						
H – O10	/	/	/	/	1.2 (2)	/
O10 – H ... O4	2.74 (3)	2.69 (4)	2.72 (4)	2.70 (6)	2.76 (2)	2.63 (11)

APPENDIX E

Optical properties of natural and synthetic monoclinic epidote minerals.

Composition	Sample
Al-Fe Epidote	
$Fe^{3+} = 0$	
$Fe^{3+} = 0.10$	
$Ca_2(Al_{2.92}Fe^{3+}_{0.115})[Si_{2.97}O_{11}(O/OH)]$	Nat.
$(Ca_{1.975}Fe^{2+}_{0.01}Mn^{2+}_{0.01})(Al_{2.79}Fe^{3+}_{0.16})[Si_{3.04}O_{11}(O/OH)]$	Nat.
$Ca_{1.99}(Al_{2.865}Fe^{3+}_{0.185}Mg_{0.01}Mn_{0.005})[Si_{2.945}O_{11}(O/OH)]$	Nat.
$Fe^{3+} = 0.20$	
$(Ca_{1.975}Fe^{2+}_{0.04}Na_{0.005}K_{0.005}Mn^{2+}_{0.015}Mg_{0.005})(Al_{2.705}Fe^{3+}_{0.225}Ti_{0.003})[Si_{3.00}O_{11}(O/OH)]$	Nat.
$Ca_{1.98}(Al_{2.35}Fe^{3+}_{0.225})[Si_{2.945}O_{11}(O/OH)]$	Nat.
$Ca_{1.985}(Al_{2.73}Fe^{3+}_{0.235}Fe^{2+}_{0.02}Mn^{2+}_{0.04})[Si_{3.005}O_{11}(O/OH)]$	Nat.
$(Ca_{2.015}Na_{0.015})(Al_{2.725}Fe^{3+}_{0.24}Fe^{2+}_{0.04}Mn^{2+}_{0.01})[Si_{2.95}Al_{0.05}O_{11}(O/OH)]$	Nat.
$(Ca_{1.99}Fe^{2+}_{0.01}Na_{0.015}K_{0.02})(Al_{2.68}Fe^{3+}_{0.25}Mg_{0.015}Mn^{2+}_{0.02}Ti_{0.005})[Si_{3.00}P_{0.005}O_{11}(O/OH)]$	Nat.
$(Ca_{1.923}K_{0.023})(Al_{2.633}Fe^{3+}_{0.276}Ti_{0.004}Fe^{2+}_{0.038}Mg_{0.071})[Si_{3.028}O_{11}(O/OH)]$	Nat.
$(Ca_{1.925}Fe^{2+}_{0.04}Na_{0.005}K_{0.005}Mn^{2+}_{0.005}Mg_{0.035})(Al_{2.665}Fe^{3+}_{0.29}Ti_{0.025})[Si_{2.995}Al_{0.005}O_{11}(O/OH)]$	Nat.
$(Ca_{1.985}Fe^{2+}_{0.02}Mn^{2+}_{0.005})(Al_{2.465}Fe^{3+}_{0.305}Ti_{0.015})[Si_{2.915}O_{11}(O/OH)]$	Nat.
$(Ca_{1.965}Fe^{2+}_{0.045}Na_{0.015}K_{0.015}Mn^{2+}_{0.01}Mg_{0.035})(Al_{2.585}Fe^{3+}_{0.31}Ti_{0.055})[Si_{2.975}Al_{0.025}O_{11}(O/OH)]$	Nat.
$(Ca_{1.982}Fe^{2+}_{0.005}Mn^{2+}_{0.007}Mg_{0.03})(Al_{2.644}Fe^{3+}_{0.348}Ti_{0.008})[Si_{3.002}O_{11}(O/OH)]$	Nat.
$Fe^{3+} = 0.35$	
$(Ca_{1.975}Fe^{2+}_{0.04}Na_{0.005}K_{0.005}Mn^{2+}_{0.005}Mg_{0.005})(Al_{2.56}Fe^{3+}_{0.36}Ti_{0.05})[Si_{2.96}Al_{0.04}O_{11}(O/OH)]$	Nat.
$(Ca_2Fe^{2+}_{0.03}Na_{0.01}K_{0.02})(Al_{2.59}Fe^{3+}_{0.365}Mg_{0.01}Mn^{2+}_{0.005}Ti_{0.01})[Si_{2.995}O_{11}(O/OH)]$	Nat.
$(Ca_{1.955}Fe^{2+}_{0.04}Na_{0.005}K_{0.005}Mn^{2+}_{0.005}Mg_{0.005})(Al_{2.595}Fe^{3+}_{0.365}Ti_{0.03})[Si_{2.98}Al_{0.02}O_{11}(O/OH)]$	Nat.
$Ca_{1.98}(Al_{2.695}Fe^{3+}_{0.365}Mn_{0.015})[Si_{2.945}O_{11}(O/OH)]$	Nat.
$(Ca_{1.90}Fe^{2+}_{0.035}Na_{0.01}K_{0.005}Mn^{2+}_{0.01})(Al_{2.595}Fe^{3+}_{0.37}Mg_{0.045}Ti_{0.03})[Si_{2.97}Al_{0.025}P_{0.005}O_{11}(O/OH)]$	Nat.
$(Ca_{1.823}Sr_{0.08}Na_{0.01})(Al_{2.641}Fe^{3+}_{0.38}Ti_{0.011}Fe^{2+}_{0.051}Mg_{0.03})[Si_3O_{11}(O/OH)]$	Nat.
$(Ca_{1.955}Fe^{2+}_{0.035}Na_{0.005}K_{0.005}Mn^{2+}_{0.005})(Al_{2.595}Fe^{3+}_{0.38}Ti_{0.02})[Si_{2.995}Al_{0.005}O_{11}(O/OH)]$	Nat.
$(Ca_{1.999}Fe^{2+}_{0.027}Mg_{0.018})(Al_{2.57}Fe^{3+}_{0.385})[Si_{2.955}Al_{0.045}O_{11}(O/OH)]$	Nat.
$(Ca_{1.985}Fe^{2+}_{0.04}Na_{0.005}K_{0.005}Mn^{2+}_{0.005})(Al_{2.53}Fe^{3+}_{0.39}Ti_{0.05})[Si_{2.985}Al_{0.015}O_{11}(O/OH)]$	Nat.
$(Ca_{1.95}Fe^{2+}_{0.04}Na_{0.015}Mn^{2+}_{0.005})(Al_{2.93}Fe^{3+}_{0.395}Ti_{0.03})[Si_{3.04}O_{11}(O/OH)]$	Nat.
$(Ca_{2.00}Fe^{2+}_{0.015}Mn^{2+}_{0.005})(Al_{2.475}Fe^{3+}_{0.40}Ti_{0.01})[Si_{3.075}O_{11}(O/OH)]$	Nat.
$Ca_{1.965}(Al_{2.605}Fe^{3+}_{0.415})[Si_{3.015}O_{11}(O/OH)]$	Nat.
$(Ca_{1.925}Fe^{2+}_{0.045}Na_{0.005}K_{0.005}Mn^{2+}_{0.005})(Al_{2.48}Fe^{3+}_{0.44}Ti_{0.025})[Si_{3.05}O_{11}(O/OH)]$	Nat.
$(Ca_{1.955}Fe^{2+}_{0.01}Mn^{2+}_{0.005})(Al_{2.5}Fe^{3+}_{0.44}Ti_{0.01})[Si_{3.05}O_{11}(O/OH)]$	Nat.
$(Ca_{1.90}Fe^{2+}_{0.04}Na_{0.01}K_{0.005}Mn^{2+}_{0.005})(Al_{2.55}Fe^{3+}_{0.455}Mg_{0.055}Ti_{0.015})[Si_{2.91}Al_{0.08}P_{0.01}O_{11}(O/OH)]$	Nat.
$Ca_{2.04}(Al_{2.525}Fe^{3+}_{0.455}Mg_{0.035}Ti_{0.005}Mn_{0.005})[Si_{2.935}O_{11}(O/OH)]$	Nat.
$(Ca_{1.93}Fe^{2+}_{0.04}Na_{0.01}K_{0.005}Mn^{2+}_{0.005})(Al_{2.475}Fe^{3+}_{0.485}Mg_{0.04}Ti_{0.02})[Si_{2.96}Al_{0.035}P_{0.005}O_{11}(O/OH)]$	Nat.
$(Ca_{1.92}Fe^{2+}_{0.05}Na_{0.02}K_{0.01}Mn^{2+}_{0.005}Mg_{0.01})(Al_{2.465}Fe^{3+}_{0.485}Ti_{0.025})[Si_{3.015}O_{11}(O/OH)]$	Nat.
$(Ca_{1.975}Fe^{2+}_{0.02}Na_{0.01}K_{0.025})(Al_{2.41}Fe^{3+}_{0.49}Mg_{0.01}Mn^{2+}_{0.01}Ti_{0.005})[Si_{3.045}P_{0.005}O_{11}(O/OH)]$	Nat.
$(Ca_{1.95}Fe^{2+}_{0.02}Mn^{2+}_{0.01})(Al_{2.425}Fe^{3+}_{0.515})[Si_{3.05}O_{11}(O/OH)]$	Nat.
$Ca_{1.855}(Al_{2.51}Fe^{3+}_{0.525}Fe^{2+}_{0.065}Mn^{2+}_{0.01}Mg_{0.04})[Si_{2.98}Al_{0.02}O_{11}(O/OH)]$	Nat.
$(Ca_{1.981}Mn^{2+}_{0.018}Mg_{0.003})(Al_{2.461}Fe^{3+}_{0.53}Ti_{0.006})[Si_{2.997}Al_{0.003}O_{11}(O/OH)]$	Nat.
$(Ca_{1.93}Fe^{2+}_{0.05}Na_{0.025}K_{0.02}Mn^{2+}_{0.015})(Al_{2.425}Fe^{3+}_{0.53}Ti_{0.025})[Si_{3.005}O_{11}(O/OH)]$	Nat.
$(Ca_{1.905}Fe^{2+}_{0.045}Na_{0.01}K_{0.005}Mn^{2+}_{0.01})(Al_{2.40}Fe^{3+}_{0.535}Mg_{0.085}Ti_{0.02})[Si_{2.96}Al_{0.04}P_{0.01}O_{11}(O/OH)]$	Nat.
$Fe^{3+} = 0.54$	
$(Ca_{1.95}Fe^{2+}_{0.04}Sr_{0.015})(Al_{2.37}Fe^{3+}_{0.575}Mg_{0.015}Mn^{2+}_{0.005}Ti_{0.03}V_{0.005}Cr_{0.005})[Si_{3.005}O_{11}(O/OH)]$	Nat.
$Fe^{3+} = 0.59$	
$(Ca_{1.965}Fe^{2+}_{0.015}K_{0.02})(Al_{2.295}Fe^{3+}_{0.625}Mg_{0.015}Mn^{2+}_{0.005}Ti_{0.005})[Si_{3.045}P_{0.005}O_{11}(O/OH)]$	Nat.
$(Ca_{1.99}Fe^{2+}_{0.02}Na_{0.015}K_{0.02})(Al_{2.225}Fe^{3+}_{0.625}Mg_{0.04}Mn^{2+}_{0.005}Ti_{0.005})[Si_{3.07}O_{11}(O/OH)]$	Nat.
$(Ca_{1.98}Fe^{2+}_{0.025}Na_{0.01}K_{0.02})(Al_{2.265}Fe^{3+}_{0.625}Mg_{0.02}Ti_{0.005})[Si_{3.08}O_{11}(O/OH)]$	Nat.
$(Ca_{1.96}Fe^{2+}_{0.03}Na_{0.01}K_{0.015})(Al_{2.30}Fe^{3+}_{0.64}Mg_{0.005}Mn^{2+}_{0.01}Ti_{0.01})[Si_{3.025}O_{11}(O/OH)]$	Nat.
$(Ca_2Fe^{2+}_{0.02}Na_{0.01}K_{0.02})(Al_{2.295}Fe^{3+}_{0.645}Mg_{0.015}Mn^{2+}_{0.005}Ti_{0.005})[Si_{3.08}O_{11}(O/OH)]$	Nat.
$Fe^{3+} = 0.67$	
$(Ca_{1.93}Fe^{2+}_{0.05}Na_{0.03}K_{0.005}Mn^{2+}_{0.015})(Al_{2.24}Fe^{3+}_{0.675}Mg_{0.065}Ti_{0.035})[Si_{2.93}Al_{0.07}O_{11}(O/OH)]$	Nat.
$(Ca_{1.895}Fe^{2+}_{0.04}Na_{0.0025}K_{0.0025}Mn^{2+}_{0.015}Mg_{0.005})(Al_{2.17}Fe^{3+}_{0.675}Ti_{0.02})[Si_{2.96}Al_{0.04}O_{11}(O/OH)]$	Nat.
$Fe^{3+} = 0.69$	
$(Ca_{1.96}Fe^{2+}_{0.025}Mn^{2+}_{0.01})(Al_{2.185}Fe^{3+}_{0.70}Ti_{0.015})[Si_{3.07}O_{11}(O/OH)]$	Nat.
$Fe^{3+} = 0.70$	
$Fe^{3+} = 0.70$	
$(Ca_{1.845}Fe^{2+}_{0.035}Na_{0.015}Mn^{2+}_{0.025})(Al_{2.245}Fe^{3+}_{0.715}Mg_{0.045}Ti_{0.01})[Si_{3.055}O_{11}(O/OH)]$	Nat.
$(Ca_{1.945}Fe^{2+}_{0.02}Mn^{2+}_{0.005})(Al_{2.205}Fe^{3+}_{0.715}Ti_{0.01})[Si_{3.065}O_{11}(O/OH)]$	Nat.

n_α	n_β	n_γ	$n_\gamma - n_\alpha$	$2V_z$	Source
1.716	1.717	1.721	0.0052	66.2	Strens 1966
1.718	1.720	1.723	0.0056	81.7	Strens 1966
1.7176	1.7195	1.7232	0.0056	81	Johnston 1948
1.700	1.701	1.709	0.009	40	Myer 1965
1.706	1.709	1.712	0.006		Johnston 1948
1.724	1.729	1.734	0.0105	89.3	Strens 1966
1.710	1.711	1.714	0.0040	76	Hörmann and Raith 1971
1.7238	1.7291	1.7343	0.0105	89	Johnston 1948
1.710	1.713	1.719	0.009	65	Seki 1959
1.710	1.714	1.719	0.009	76 (2)	Seki 1959
1.709	1.711	1.717	0.008	60	Myer 1966
1.710		1.718	0.008	87.5 (15)	Kiseleva et al. 1974
1.712	1.715	1.719	0.0074	86	Hörmann and Raith 1971
1.713	1.717	1.726	0.013	70	Myer 1965
1.714	1.717	1.721	0.0070	87	Hörmann and Raith 1971
1.712	1.718	1.724	0.012	90	Holdaway 1972
1.723	1.734	1.744	0.0216	93.4	Strens 1966
1.717	1.722	1.727	0.0100	92	Hörmann and Raith 1971
1.713	1.718	1.725	0.012	76	Myer 1966
1.715	1.719	1.724	0.0088	93	Hörmann and Raith 1971
1.714	1.716	1.724	0.01	89	Johnston 1948
	1.726				Myer 1966
1.711	1.714	1.719	0.008	86 (1)	Kiseleva et al. 1974
1.717	1.722	1.727	0.0104	94	Hörmann and Raith 1971
1.713	1.720	1.727	0.014	90	Holdaway 1972
1.716	1.721	1.726	0.0102	94	Hörmann and Raith 1971
1.719	1.726	1.731	0.0123	95	Hörmann and Raith 1971
1.715	1.724	1.730	0.015	102	Myer 1965
1.714	1.7196	1.725	0.011	90	Johnston 1948
1.719	1.726	1.731	0.0122	96	Hörmann and Raith 1971
1.716	1.726	1.733	0.017	100	Myer 1965
	1.728				Myer 1966
1.712	1.723	1.735	0.023		Johnston 1948
	1.729				Myer 1966
1.720	1.728	1.734	0.0147	98	Hörmann and Raith 1971
1.716	1.729	1.739	0.023	98	Myer 1966
1.718	1.728	1.740	0.022	85	Myer 1965
1.726	1.735	1.741	0.015	< 130	Seki 1959
1.721	1.732	1.743	0.022	90	Holdaway 1972
1.723	1.733	1.741	0.0185	99	Hörmann and Raith 1971
	1.737				Myer 1966
1.753	1.781	1.812	0.059	90	Strens 1966
1.718	1.734	1.746	0.028	100	Myer 1966
1.728	1.746	1.766	0.038	80	Strens 1966
1.720	1.734	1.747	0.027	93	Myer 1966
1.718	1.735	1.750	0.032	95	Myer 1966
1.722	1.738	1.751	0.029	98	Myer 1966
1.720	1.735	1.748	0.028	95	Myer 1966
1.720	1.736	1.750	0.03	95	Myer 1966
1.735	1.754	1.775	0.040	75	Strens 1966
	1.741				Myer 1966
1.723	1.742	1.752	0.0280	105	Hörmann and Raith 1971
1.740	1.762	1.780	0.040		Strens 1966
1.721	1.741	1.756	0.035	100	Myer 1965
1.731	1.752	1.772	0.041	85	Strens 1966
1.739	1.760	1.779	0.040	80	Strens 1966
1.721	1.740	1.756	0.035	96	Myer 1966
1.721	1.741	1.756	0.035	100	Myer 1965

APPENDIX E. continued

Composition	Sample
Al-Fe Epidote (continued)	
$(Ca_{1.945}Fe^{2+}_{0.02}Mn^{2+}_{0.005})(Al_{2.185}Fe^{3+}_{0.715}Ti_{0.03})[Si_{3.06}O_{11}(O/OH)]$	Nat.
$Fe^{3+} = 0.72$	
$(Ca_{1.975}Fe^{2+}_{0.035}Na_{0.005}K_{0.005}Mn^{2+}_{0.015}Mg_{0.01})(Al_{2.24}Fe^{3+}_{0.735}Ti_{0.005})[Si_{2.98}Al_{0.02}O_{11}(O/OH)]$	Nat.
$(Ca_{1.979}Fe^{2+}_{0.004}Mn^{2+}_{0.015}Mg_{0.003})(Al_{2.25}Fe^{3+}_{0.74}Ti_{0.01})[Si_{2.999}Al_{0.001}O_{11}(O/OH)]$	Nat.
$Ca_{1.99\text{-}2.005}(Al_{2.22\text{-}2.43}Fe^{3+}_{0.67\text{-}0.80})[Si_{2.93\text{-}2.985}O_{11}(O/OH)]$	Synth.
$(Ca_{2.025}Fe^{2+}_{0.005}K_{0.02})(Al_{2.14}Fe^{3+}_{0.775}Mg_{0.01}Mn^{2+}_{0.01}Ti_{0.005})[Si_{3.08}O_{11}(O/OH)]$	Nat.
$(Ca_{1.99}Mn^{2+}_{0.007}Mg_{0.011})(Al_{2.192}Fe^{3+}_{0.779}Ti_{0.022})[Si_{2.995}Al_{0.005}O_{11}(O/OH)]$	Nat.
$Ca_{1.99\text{-}2.025}(Al_{2.135\text{-}2.32}Fe^{3+}_{0.71\text{-}0.855})[Si_{2.985\text{-}3.00}O_{11}(O/OH)]$	Synth.
$(Ca_{1.985}Fe^{2+}_{0.005}Na_{0.01}K_{0.02})(Al_{2.125}Fe^{3+}_{0.80}Mn^{2+}_{0.01})[Si_{3.04}P_{0.005}O_{11}(O/OH)]$	Nat.
$(Ca_{1.948}Fe^{2+}_{0.019}Mn^{2+}_{0.03}Mg_{0.003})(Al_{2.169}Fe^{3+}_{0.824}Ti_{0.007})[Si_{2.982}Al_{0.018}O_{11}(O/OH)]$	Nat.
$(Ca_{1.935}Fe^{2+}_{0.055}Na_{0.055}K_{0.005})(Al_{2.075}Fe^{3+}_{0.83}Mg_{0.07}Mn^{2+}_{0.015}Ti_{0.015})[Si_3O_{11}(O/OH)]$	Nat.
$Ca_{1.93\text{-}2.00}(Al_{2.145\text{-}2.34}Fe^{3+}_{0.78\text{-}0.87})[Si_{2.945\text{-}2.99}O_{11}(O/OH)]$	Synth.
$(Ca_{1.985}Fe^{2+}_{0.035}Mn^{2+}_{0.015}Mg_{0.015})(Al_{2.12}Fe^{3+}_{0.855}Ti_{0.005})[Si_{2.955}Al_{0.045}O_{11}(O/OH)]$	Nat.
$(Ca_{1.98}Na_{0.015})(Al_{1.985}Fe^{3+}_{0.86}Fe^{2+}_{0.08}Mn^{2+}_{0.02}Mg_{0.025})[Si_{3.06}O_{11}(O/OH)]$	Nat.
$(Ca_{1.96}Fe^{2+}_{0.03}Na_{0.005}K_{0.005}Mn^{2+}_{0.01}Mg_{0.025})(Al_{2.085}Fe^{3+}_{0.865}Ti_{0.025})[Si_{2.97}Al_{0.03}O_{11}(O/OH)]$	Nat.
$(Ca_{1.935}Fe^{2+}_{0.05}Na_{0.005}K_{0.005}Mn^{2+}_{0.005}Mg_{0.01})(Al_{2.12}Fe^{3+}_{0.89}Ti_{0.005})[Si_{2.985}Al_{0.015}O_{11}(O/OH)]$	Nat.
$Ca_{1.805}(Al_{2.183}Fe^{3+}_{0.936}Ti_{0.012}Fe^{2+}_{0.023}Mg_{0.018})[Si_{3.017}O_{11}(O/OH)]$	Nat.
$Ca_{1.944}(Al_{2.092}Fe_{0.981}Mn_{0.009})[Si_{2.969}O_{11}(O/OH)]$	Nat.
$(Ca_{1.995}Fe^{2+}_{0.01})(Al_{1.935}Fe^{3+}_{0.985})[Si_{3.055}O_{11}(O/OH)]$	Nat.
$Ca_{2.05\text{-}2.06}(Al_{1.90\text{-}2.04}Fe^{3+}_{0.955\text{-}1.115})[Si_{2.96\text{-}2.98}O_{11}(O/OH)]$	Synth.
$(Ca_{1.996}Mn^{2+}_{0.012}Mg_{0.012})(Al_{1.985}Fe^{3+}_{0.990}Ti_{0.004})[Si_{2.984}Al_{0.016}O_{11}(O/OH)]$	Nat.
$(Ca_{1.99}Fe^{2+}_{0.03})(Al_{1.935}Fe^{3+}_{1.045})[Si_{2.945}Al_{0.055}O_{11}(O/OH)]$	Nat.
$Ca_{2.02\text{-}2.035}(Al_{1.93\text{-}2.01}Fe^{3+}_{0.98\text{-}1.12})[Si_{2.955\text{-}2.99}O_{11}(O/OH)]$	Synth.
$Ca_{2.03}(Al_{1.80}Fe^{3+}_{1.105}Fe^{2+}_{0.025}Mn^{2+}_{0.02})[Si_{3.03}O_{11}(O/OH)]$	Nat.
Al-Fe-Mn Epidote	
$(Fe_{0.45};Mn_{0.17})$	
$(Fe_{0.67};Mn_{0.06})$	
$(Fe_{0.64};Mn_{0.21})$	
$(Fe_{0.67};Mn_{0.19})$	
$(Fe_{0.55};Mn_{0.38})$	
$(Fe_{0.23};Mn_{0.73})$	
$(Fe_{0.30};Mn_{0.71})$	
$(Fe_{0.28};Mn_{0.75})$	
$(Fe_{0.40};Mn_{0.70})$	
$(Fe_{0.64};Mn_{0.45})$	
$(Fe_{0.39};Mn_{0.71})$	
$(Fe_{0.59};Mn_{0.61})$	
$(Fe_{0.53};Mn_{0.68})$	
$(Fe_{0.92};Mn_{0.30})$	
$(Fe_{0.62};Mn_{0.63})$	
$(Fe_{0.51};Mn_{0.76})$	
$(Fe_{0.68};Mn_{0.75})$	
$(Fe_{0.66};Mn_{0.78})$	
Al-Mn Epidote	
$Ca_{1.92}Mn^{2+}_{0.11}(Al_{2.26}Fe_{0.981}Mn^{3+}_{0.73})[Si_{2.79}O_{11}(O/OH)]$	Synth.
$Ca_{1.98}(Al_{2.01}Mn^{3+}_{1.00})[Si_{3.00}O_{11}(O/OH)]$	Synth.
$Ca_{1.98}(Al_{1.93}Mn^{3+}_{1.11})[Si_{2.98}O_{11}(O/OH)]$	Synth.
$Ca_{1.96}(Al_{1.82}Mn^{3+}_{1.23})[Si_{2.99}O_{11}(O/OH)]$	Synth.
$Ca_{1.97}(Al_{1.59}Mn^{3+}_{1.45})[Si_{2.98}O_{11}(O/OH)]$	Synth.
REE Epidote	
$(Ca_{1.08}Ce_{0.92})(Al_{0.66}Fe^{3+}_{1.24}Fe^{2+}_{0.93}Mn_{0.07}Ti_{0.14})[Si_{2.94}Al_{0.06}O_{11}(O/OH)]$	Nat.
$(Ca_{1.05}Ce_{0.57}La_{0.33}Nd_{0.07}Pr_{0.03})(Al_{1.91}Fe_{0.14}Mg_{0.93}Ti_{0.06})[Si_{2.94}O_{11}(O/OH_{0.94}/F_{0.06})]$	Nat.

n_α	n_β	n_γ	$n_\gamma - n_\alpha$	$2V_z$	Source
1.721	1.741	1.757	0.036	98	Myer 1965
1.736	1.757	1.778	0.042	85	Strens 1966
1.726	1.746	1.758	0.0320	107	Hörmann and Raith 1971
1.728	1.746	1.763	0.035	93	Holdaway 1972
1.730		1.775	0.035		Liou 1973
1.729	1.749	1.764	0.035	100	Myer 1966
1.729	1.751	1.768	0.039	99	Holdaway 1972
1.738		1.770	0.032		Liou 1973
1.728	1.748	1.763	0.035	100	Myer 1966
1.730	1.753	1.772	0.042	97	Holdaway 1972
	1.763				Myer 1966
1.735		1.778	0.043		Liou 1973
1.731	1.756	1.770	0.0390	106	Hörmann and Raith 1971
1.729	1.754	1.776	0.047	106.5 (5)	Seki 1959
1.729	1.754	1.767	0.0377	108	Hörmann and Raith 1971
1.734	1.762	1.776	0.0423	109	Hörmann and Raith 1971
1.740	1.757	1.771	0.031	111.5 (15)	Kiseleva et al. 1974
1.755	1.768	1.781	0.026	107 (1)	Kiseleva et al. 1974
1.736	1.773	1.788	0.052	115	Myer 1965
1.748		1.785	0.037		Liou 1973
1.741	1.771	1.790	0.049	105	Holdaway 1972
1.751	1.784	1.797	0.046	116	Myer 1966
1.745		1.786	0.041		Liou 1973
1.740	1.768	1.787	0.047	106	Seki 1959
	1.730		0.028	73	Strens 1966
1.733	1.750	1.762	0.029	102	Strens 1966
1.730	1.746	1.765	0.035	98	Strens 1966
	1.749			104	Strens 1966
1.740	1.752	1.779	0.039	87	Strens 1966
1.732	1.750	1.778	0.046		Strens 1966
1.746	1.764	1.806	0.0604	68.2	Strens 1966
1.739	1.765	1.799	0.0600	69.5	Strens 1966
1.742	1.767	1.805	0.063	81	Strens 1966
1.751	1.781	1.812	0.061	86	Strens 1966
1.746	1.776	1.793	0.047	87	Strens 1966
1.754	1.772	1.795	0.041	85	Strens 1966
1.751	1.783	1.833	0.082	79.5	Strens 1966
1.743	1.779	1.808	0.065	97	Strens 1966
1.756	1.783	1.823	0.067	72	Strens 1966
1.750	1.782	1.832	0.0823	80.6	Strens 1966
1.768	1.803	1.843	0.075	88	Strens 1966
1.772	1.813	1.860	0.088	88	Strens 1966
1.729 (7)	1.746 (7)	1.778 (8)	0.049		Langer et al. 2002
1.731 (7)	1.759 (9)	1.794 (8)	0.063		Langer et al. 2002
1.738 (5)	1.767 (5)	1.799 (9)	0.061		Langer et al. 2002
1.746 (5)	1.783 (5)	1.823 (11)	0.077		Langer et al. 2002
1.757 (5)	1.805 (5)	1.852 (5)	0.095		Langer et al. 2002
1.825 (2)	1.855 (5)	1.880 (5)	0.055	97	Kartashov et al. 2002
1.735 (3)	1.741 (3)	1.758 (3)	0.023	64.2 (3)	Grew et al. 1991

APPENDIX F

Optical properties of natural zoisite.

Composition
$(Ca_{2.025}Fe^{2+}_{0.01}Na_{0.005}K_{0.02})Al_2(Al_{0.94}Fe^{3+}_{0.015}Mg_{0.005}Ti_{0.005})[Si_{2.995}P_{0.005}O_{11}(O/OH)]$
$(Ca_{1.995}Fe^{2+}_{0.02}Na_{0.005}K_{0.02})Al_2(Al_{0.935}Fe^{3+}_{0.035}Mg_{0.005}Ti_{0.005})[Si_{2.955}P_{0.005}Al_{0.03}O_{11}(O/OH)]$
$(Ca_{2.07}Fe^{2+}_{0.015}Na_{0.005}K_{0.02})Al_2(Al_{0.815}Fe^{3+}_{0.105}Mg_{0.005}Ti_{0.005}Mn^{3+}_{0.005})[Si_{2.985}P_{0.005}Al_{0.01}O_{11}(O/OH)]$
$(Ca_{2.005}Fe^{2+}_{0.015}Na_{0.005}K_{0.02})Al_2(Al_{0.85}Fe^{3+}_{0.105}Mg_{0.005}Ti_{0.01})$ $[Si_{2.98}P_{0.01}Al_{0.01}O_{11}(O/OH)]$
$(Ca_{2.00}Fe^{2+}_{0.02}Na_{0.005}K_{0.02})Al_2(Al_{0.81}Fe^{3+}_{0.14}Mg_{0.005})$ $[Si_{3.005}P_{0.005}O_{11}(O/OH)]$
$Ca_{2.02}Al_2(Al_{0.93}Fe^{3+}_{0.075}Mn^{3+}_{0.005})[Si_{2.89}Al_{0.11}O_{11}(O/OH)]$
$(Ca_{1.791}K_{0.011}Na_{0.018})(Al_{2.455}Fe^{3+}_{0.20}Ti_{0.011}Mg_{0.374})[Si_{3.129}O_{11}(O/OH)]$
$Ca_{2.07}Al_2(Al_{1.04}Fe^{3+}_{0.1}Cr^{3+}_{0.02})[Si_{3.02}O_{11}(O/OH)]$
$(Ca_{1.987}Mg_{0.008}Sr_{0.002})Al_2(Al_{0.985}Fe^{3+}_{0.002}V^{3+}_{0.012})[Si_3O_{11}(O/OH)]$
"tanzanite" (pure zoisite, no analysis given)

n_α	n_β	n_γ	n_γ - n_α	$2V_z$	Source
1.6911	1.6935	1.6991	0.0080	50 (1)	Myer 1966
1.6920	1.6933	1.6980	0.0060	35 (1)	Myer 1966
1.6976	1.6990	1.7027	0.0051	40 (1)	Myer 1966
1.6980	1.6990	1.7042	0.0062	37 (1)	Myer 1966
1.6990	1.7021	1.7070	0.0080	69 (2)	Myer 1966
1.694	1.698	1.707	0.013	44 (5)	Seki 1959
1.700	1.700	1.703	0.003	55 (2)	Kiseleva et al.1974
1.700	1.700	1.705	0.005	25 (8)	Game 1954
1.6925	1.6943	1.7015	0.009	53	Hurlbut 1969
1.6917	1.6927	1.7005	0.0088	n.d.	Anderson 1968